

1-1-2009

Experimental Study On The Flexural Behavior Of Structural Insulated Headers

Dana Benadova
Ryerson University

Follow this and additional works at: <http://digitalcommons.ryerson.ca/dissertations>



Part of the [Civil Engineering Commons](#)

Recommended Citation

Benadova, Dana, "Experimental Study On The Flexural Behavior Of Structural Insulated Headers" (2009). *Theses and dissertations*. Paper 1077.

EXPERIMENTAL STUDY ON THE FLEXURAL BEHAVIOR OF STRUCTURAL INSULATED HEADERS

T14
4819
P
1346
2009

By

DANA BENADOVA, Ing.

Technical University in Kosice, Slovakia, 1994

A Thesis
Presented to Ryerson University
In partial fulfillment of the
Requirement for the degree of
Master of Applied Science
In the program of
Civil Engineering
Toronto, Ontario, Canada, 2009
Dana Benadova 2009 ©

AUTHOR'S DECLARATION

I hereby declare that I am the sole author of this thesis.

I authorize Ryerson University to lend this document to other institutions or individuals for the purpose of scholarly research.

Dana Benadova

I further authorize the Ryerson University to reproduce the document by photocopying or by other means, in total or part, at the request of other institutions or individuals for the purpose of scholarly research.

Dana Benadova

EXPERIMENTAL STUDY ON THE FLEXURAL BEHAVIOR OF STRUCTURAL INSULATED HEADERS

By

Dana Benadova

Master of Applied Science in Civil Engineering

Department of Civil Engineering

Ryerson University, Toronto

2009

ABSTRACT

A series of flexural tests were conducted on 18 structural insulated header panels with timber flanges and Oriented Strand Board (OSB) webs to predict their behavior when subject to gravity loading when used in residential and low rise non-residential buildings. The experiments were designed and performed to test full-scale Structural Insulated Panels (SIPs) headers for exterior or interior wall residential construction. The structural adequacy of the header panels of various sizes is investigated in order to meet both strength and serviceability limit-state design requirements per Canadian Standards for timber design. Strength requirements included flexure and shear, while serviceability check included limiting deflection under operating conditions. Results from experimental testing were used to draw conclusions with respect to the structural qualifications for these SIP headers to be “as good as” the structural capacity of conventional wood-frame buildings.

ACKNOWLEDGEMENTS

I wish to express my deep appreciation to my advisor, Dr. Khaled Sennah, for his continuous support and valuable supervision during the development of this research. Dr. K. Sennah devoted his time and effort to make this study a success. His most helpful guidance is greatly appreciated.

The in-kind contribution from Thermapan Inc. of Fort Erie, Ontario and assistance from their representative Edward Jonus during the testing is greatly appreciated. The assistance from the technicians Mohamad Aldardari and Roger Smith at the Structural Laboratory of the Ryerson University is acknowledged. I would also like to acknowledge the financial support from Ryerson University in the form of graduate scholarship and research assistantship.

DEDICATION

*This thesis is dedicated to
my husband Erik, my children
Martin, Daniel, Barbora
and my mother.*

TABLE OF CONTENTS

	Page
AUTHOR'S DECLARATIONS	ii
BORROWERS PAGE	iii
ABSTRACT	iv
ACKNOWLEDGEMENTS	v
DEDICATION	vi
TABLE OF CONTENTS	vii
LIST OF SYMBOLS	xii
LIST OF TABLES	xiv
LIST OF FIGURES	xv
Chapter I INTRODUCTION	
1.1 General	1
1.2 Problem	3
1.3 Objective	4
1.4 Scope	5
1.5 Contents and Arrangement of the Thesis	5
Chapter II LITERATURE REVIEW	
2.1 General	7
2.2 Structural Insulated Panels (SIP)	7
2.2.1 General	7
2.2.2 History of Structural Insulated Panels	8
2.2.3 Advantages and Disadvantages of Structural Insulated	9
2.3.4 Fabrication and Erection Aspects	10
2.3.5 Joints and Splices	11
2.3.6 Structural Behavior of SIPs	11

2.3.7 Durability and Energy Efficiency of Structural Insulated Panels	12
2.3.8 Fire Resistance of SIP Systems	14
2.4 Plywood Web Beams	14
2.4.1 General	14
2.4.2 Material in Web Beams	15
2.4.2.1 Sawn Lumber	15
2.4.2.2 Oriented Strand Board (OSB)	15
2.4.3 Design Considerations	16
2.4.3.1 Calculation of Section Properties	16
2.4.3.2 Stiffeners	17
2.4.3.3 Joints and Splices	18
2.4.3.4 Lateral Stability	18
2.5 Structural Analysis and Design of plywood and OSB web beams	19
2.5.1 General	19
2.5.2 “Plywood Construction Manual” Design Procedure	19
2.5.2.1 Stresses	19
2.5.2.2 Deflection	23
2.6 Theoretical Investigation and Experimental Studies	24
2.6.1 Structural Insulated Panels (SIPs)	24
2.6.2 Web Beams and Composite Beams	27
2.6.2.1 Theoretical Background	27
2.6.2.2 Experimental Studies	29

Chapter III EXPERIMENTAL STUDY

3.1 General	33
3.2 SIP Header Panel Configuration	34
3.3 Description of Panel Groups	35
3.4 Material Properties	36
3.5 Test method for SIP Panels in Flexure	38
3.5.1 Flexure Load Test setup	40

3.5.2 Instrumentation for Flexure Load Test	41
3.5.3 Flexure Load Test Procedure	42

Chapter IV EXPERIMENTAL RESULTS

4.1 General	43
4.2 Panel Group A	43
4.3 Panel Group B	45
4.4 Panel Group C	47
4.5 Panel Group D	49
4.6 Panel Group E	52
4.7 Panel Group F	53

Chapter V ANALYSIS AND DISCUSSION

5.1 General	57
5.2 Experimental Findings	57
5.2.1 General	57
5.2.2 Header Group A	58
5.2.3 Header Group B	59
5.2.4 Header Group C	59
5.2.5 Header Group D	60
5.2.6 Header Group E	60
5.2.7 Header Group F	60
5.3 Proposed Design Tables	61
5.3.1 General	61
5.3.2 Code Requirements for the Structural Qualification of SIP Header Panels	62
5.3.3 Design Tables	62
5.4 General Design Procedure for Calculating Web Beam Resistance	65
According to CAN/CSA-O86-01	
5.4.1 General	65

5.4.2 Effective Stiffness	65
5.4.3 Bending Resistance	66
5.4.5 Web Shear-through Thickness	67
5.4.6 Flange -Web Shear	68
5.4.7 Deflection	69
5.5 Calculations of Flexural Resistance of Header Panels	69
5.5.1 General	69
5.5.2 Geometrical Characteristics and Other Specifications of Headers	70
5.5.3 Coefficients	71
5.6 Calculations of the Flexural Resistance of the 350-mm deep Headers (Groups A, C, and E)	72
5.6.1 Calculation the Moment Resistance of the Headers	72
5.6.2 Calculation the Shear Resistance of the Headers	74
5.6.3 Calculation of the Deflection of the Headers	75
5.7 Calculation of the Flexural Resistance of 660-mm deep Headers (Groups B, D, and F)	76
5.7.1 Calculation of the Moment Resistance of the Headers	76
5.7.2 Calculation of the Shear Resistance of the Headers	78
5.7.3 Calculation of the Deflection of the Headers	79
5.8 Comparison between CAN/CSA-O86-01 Calculations and Experimental Findings	80

Chapter VI SUMMARY, CONCLUSION AND RECOMMENDATION

6.1 General	83
6.2 Conclusions	83
6.3 Recommendations for Future Research	84
REFERENCES	86

TABLES	91
Tables of Chapter III	92
Tables of Chapter V	95
FIGURES	105
Figures of Chapter I	106
Figures of Chapter II	108
Figures of Chapter III	111
Figures of Chapter IV	124
4.2 Panel Group A	129
4.3 Panel Group B	137
4.4 Panel Group C	145
4.5 Panel Group D	153
4.6 Panel Group E	163
4.7 Panel Group F	179
Figures of Chapter V	189
APPENDIX A:	193
CAN/CSA O86-01 Design Tables	194

LIST OF SYMBOLS

Symbol	Meaning
c_c	Distance from neutral axis to outer fibre at compression flange
c_t	Distance from neutral axis to outer fibre at tension flange
C	Load coefficient to account for effect of distribution of total load
d	Header panel depth
d_c	Compression flange-web contact depth
d_t	Tension flange-web contact depth
d_l	Flange-web contact depth between the flange area and web under consideration
DL	Dead load
E	Modulus of Elasticity
f_y	Flexural Stress at any point of beam
F_c	Flexural Stress at the extreme fibre at compression flange
F_t	Flexural Stress at the extreme fibre at tension flange
G	Shear through thickness Rigidity
h	Height of beam
I	Moment of Inertia
I_g	Gross Moment of Inertia
I_n	Net Moment of Inertia
Q_g	First moment of beam area above neutral axis
Q_l	First moment of flange section under consideration
l	Total length of header panel
L	Clear length of header panel
L_H	Length of a header when calculating maximum supported length of roof
L_S	Maximum supported length roof member
LL	Live load
M	Bending Moment
M_r	Moment resistance of header panel

M_{rc}	Moment resistance at compression flange
M_{rt}	Moment resistance at tension flange
M_y	Bending Moment along y-axis
S_c	Section Moduli at compression flange
S_t	Section Moduli at tension flange
t	Web Thickness
U_c	Compression flange-web shear property
U_t	Tension flange-web shear property
U_w	Web shear property
v_c	Compression flange-web shear
v_r	Flange web shear stress on plane under consideration
v_t	Tension flange-web shear
v_w	Shear stress in the web at neutral axis
V	Shear force at any point of beam
V_r	Shear resistance of header panel at its neutral axis
w_d	Design ultimate jacking load capacity
w_M	Uniform load based on resisting moment
w_V	Uniform load based on shear resistance
w_Δ	Uniform load based on flexural stiffness
W	Total load
W_s	Jacking load capacity at deflection limit L/360 or L/180
Δ_s	Shear deflection at any location in the span of beam

LIST OF TABLES

Table 3.1	The main characteristic of standard SIPs as specified by Thermapan
Table 3.2	Allowable axial loads for header panels as specified by Thermapan
Table 3.3	Geometric characteristics of tested header panels
Table 3.4	Header configuration – dimensions as specified by Thermapan Inc. and as measured before testing
Table 5.1	Summary of experimental results for Applied Ultimate Jacking Load
Table 5.2	Summary of experimental results for Applied Jacking Load at Deflection Limit $L/360$
Table 5.3	Summary of experimental results for Applied Jacking Load at Deflection Limit $L/180$
Table 5.4	Design Table for Ultimate Limit State
Table 5.5	Design Table for Serviceability Limit State at Deflection Limit $L/360$
Table 5.6	Design Table for Serviceability Limit State at Deflection Limit $L/180$
Table 5.7	Summary of header panels flexural resistance, shear resistance and deflection
Table 5.8	Comparison summary of uniform load as per CAN/CSA-O86-01 calculations and uniform load determined from the experimental findings
Table 5.9	Design Table of maximum supported length of roof members

LIST OF FIGURES

- Figure 1.1 Sample of Structural Insulated Panels
- Figure 1.2 Layers in Structural Insulated Panel
- Figure 1.3 View of residential building construction using SIPs
- Figure 1.4 Typical SIP wall assemblage with a SIP header above the opening
- Figure 2.1 Components of typical plywood web beam
- Figure 2.2 Box section plywood web beam with flange covered or partially covered
- Figure 2.3 Tapered plywood web beam and beam with top flange arched
- Figure 2.4 I-section, double I and double box and spaced plywood web beams
- Figure 2.5 Typical Oriented strand board (OSB) lay-ups
- Figure 2.6 Examples of engineered components made of OSB
- Figure 2.7 Flange-web shear stress planes
- Figure 2.8 Plywood web beams with equal flange-web shear stress
- Figure 2.9 Panel web beam section
- Figure 3.1 Schematic view of a tested header panel
- Figure 3.2 Schematic view and dimensions of header panel group A
- Figure 3.3 Schematic view and dimensions of header panel group B
- Figure 3.4 Schematic view and dimensions of header panel group C
- Figure 3.5 Schematic view and dimensions of header panel group D
- Figure 3.6 Schematic view and dimensions of header panel group E
- Figure 3.7 Schematic view and dimensions of header panel group F
- Figure 3.8 Schematic diagram of arrangement of strain gauges for 14" deep header panels (Group A, C, and E)
- Figure 3.9 Schematic diagram of arrangement of strain gauges for 26" deep header panels (Group B, D, and F))
- Figure 3.10 Schematic diagram of test setup with steel rollers used for testing H-9 only
- Figure 3.11 Schematic diagram of test setup with flat surface used for testing all headers except the header H-9
- Figure 3.12 View of setup for header H-1 before testing
- Figure 3.13 View of setup for header H-2 before testing

- Figure 3.14 View of setup for header H-3 before testing
- Figure 3.15 View of setup for header H-4 before testing
- Figure 3.16 View of setup for header H-5 before testing
- Figure 3.17 View of setup for header H-6 before testing
- Figure 3.18 View of setup for header H-7 before testing
- Figure 3.19 View of setup for header H-8 before testing
- Figure 3.20 View of setup on steel rollers for header H-9 before testing
- Figure 3.21 View of setup for header H-10 before testing
- Figure 3.22 View of setup for header H-11 before testing
- Figure 3.23 View of setup for header H-12 before testing
- Figure 3.24 View of setup for header H-13 before testing
- Figure 3.25 View of setup for header H-14 before testing
- Figure 3.26 View of setup for header H-15 before testing
- Figure 3.27 View of setup for header H-16 before testing
- Figure 3.28 View of setup for header H-17 before testing
- Figure 3.29 View of setup for header H-18 before testing
- Figure 3.30 View of load cell assembly used in testing
- Figure 3.31 Schematic diagram of dial gauge and LVDT's
- Figure 3.32 View of deflection sensors used in testing
- Figure 4.1 View of header H-1 after failure
- Figure 4.2 Close-up view of the failure mode in the left side of header H-1
- Figure 4.3 Close-up view of the failure mode of the right side of header H-1
- Figure 4.4 Jacking load-deflection relationship for header H-1
- Figure 4.5 History of Jacking Load-Strain relationship for Header H-1
- Figure 4.6 Strains across the header section for Header H-1 at $F_{ULT}/3$
- Figure 4.7 View of header H-2 after failure
- Figure 4.8 Close-up view of the failure mode of header H-2
- Figure 4.9 Close-up view of the foam and header end after removing the deformed OSB web of header H-2
- Figure 4.10 Jacking load-deflection relationship for header H-2
- Figure 4.11 View of header H-3 after failure

- Figure 4.12 Close-up view of the failure mode of header H-3
- Figure 4.13 Close-up view of the failure mode of header H-3
- Figure 4.14 View of the foam at the location of failure of header H-3
- Figure 4.15 Jacking load-deflection relationship for header H-3
- Figure 4.16 View of header H-4 after failure
- Figure 4.17 Close-up view of the failure mode of the right side of header H-4
- Figure 4.18 Close-up view of the failure mode of the right side of header H-4
- Figure 4.19 Close-up view of the failure mode of the left side of header H-4
- Figure 4.20 Jacking load-deflection relationship for header H-4
- Figure 4.21 View of header H-5 after failure
- Figure 4.22 Close-up view of the failure mode of the right side of header H-5
- Figure 4.23 Close-up view of the failure mode of the left side of header H-5
- Figure 4.24 Jacking load-deflection relationship for header H-5
- Figure 4.25 View of header H-6 before testing
- Figure 4.26 View of header H-6 after failure
- Figure 4.27 Close-up view of the failure mode of the right side of header H-6
- Figure 4.28 Close-up view of the failure mode of the left side of header H-6
- Figure 4.29 Jacking load-deflection relationship for header H-6
- Figure 4.30 History of Jacking Load-Strain relationship for Header H-6
- Figure 4.31 Strains across the header section for Header H-6 at $F_{ULT}/3$
- Figure 4.32 View of header H-7 after failure
- Figure 4.33 Close-up view of the failure mode of the right side of header H-7
- Figure 4.34 Close-up view of the failure mode of left side of header H-7
- Figure 4.35 View of the foam at the location of failure of header H-7
- Figure 4.36 Close-up view of the of the tensile fracture of the OSB web of header H-7
- Figure 4.37 Jacking load-deflection relationship for header H-7
- Figure 4.38 View of header H-8 after failure
- Figure 4.39 Close-up view of the failure mode of the right side of header H-8
- Figure 4.40 Close-up view of the failure mode of the left side of header H-8
- Figure 4.41 Jacking load-deflection relationship for header H-8
- Figure 4.42 History of Jacking Load-Strain relationship for Header H-8

Figure 4.43	Strains across the header section for Header H-8 at $F_{ULT}/3$
Figure 4.44	View of header H-9 after failure
Figure 4.45	Other view of the failure mode of header H-9
Figure 4.46	Close up view of the failure mode of header H-9
Figure 4.47	Jacking load-deflection relationship for header H-9
Figure 4.48	View of header H-10 after failure
Figure 4.49	Close-up view of the failure mode of the left side of header H-10
Figure 4.50	Close-up view of the failure mode of the right side of header H-10
Figure 4.51	Jacking load-deflection relationship for header H-10
Figure 4.52	History of Jacking Load-Strain relationship for Header H-10
Figure 4.53	Strains across the header section for Header H-10 at $F_{ULT}/3$
Figure 4.54	View of header H-11 after failure
Figure 4.55	Views of the failure mode of header H-11
Figure 4.56	Jacking load-deflection relationship for header H-11
Figure 4.57	View of header H-12 after failure
Figure 4.58	Close-up views of the failure mode of header H-12
Figure 4.59	Jacking load-deflection relationship for header H-12
Figure 4.60	View of header H-13 after failure
Figure 4.61	View of header H-13 after failure
Figure 4.62	Close-up view of the failure mode at support of header H-13
Figure 4.63	Close-up view of the flexure failure mode at quarter point of header H-13
Figure 4.64	Close-up view of the flexure failure mode at quarter point of header H-13
Figure 4.65	Close-up view of the flexure failure mode at quarter point of header H-13
Figure 4.66	Close-up view of the flexure failure mode at quarter point of header H-13
Figure 4.67	Close-up view of the flexure failure mode at quarter point of header H-13
Figure 4.68	Close-up view of the flexure failure mode at quarter point of header H-13
Figure 4.69	Jacking load-deflection relationship for header H-13
Figure 4.70	View of header H-14 after failure
Figure 4.71	Close-up view of the failure mode at support of header H-14
Figure 4.72	Close-up view of the flexure failure mode near mid-span of header H-14

- Figure 4.73 Close-up view of the flexure failure mode between quarter point and mid-span of header H-14
- Figure 4.74 Jacking load-deflection relationship for header H-14
- Figure 4.75 History of Jacking Load-Strain relationship for Header H-14
- Figure 4.76 Strains across the header section for Header H-14 at $F_{ULT}/3$
- Figure 4.77 View of header H-15 after failure
- Figure 4.78 View of header H-15 showing flexure failure at mid-span
- Figure 4.79 Close-up view of flexure failure mode at front side of mid-span of header H-15
- Figure 4.80 Neutral axis after the flexure failure mode at back side of mid-span of header H-15
- Figure 4.81 Neutral axis after the flexure failure mode of header H-15 at loading point
- Figure 4.82 Close-up view of the failure mode at support of header H-15
- Figure 4.83 Jacking load-deflection relationship for header H-15
- Figure 4.84 View of header H-16 after failure
- Figure 4.85 Close-up views of the failure mode at supports of header H-16
- Figure 4.86 View of the foam at the location of failure of header H-16
- Figure 4.87 Jacking load-deflection relationship for header H-16
- Figure 4.88 View of header H-17 after failure
- Figure 4.89 Close-up views of the failure mode at right support of header H-17
- Figure 4.90 Close-up view of the failure mode at left support of header H-17
- Figure 4.91 Jacking load-deflection relationship for header H-17
- Figure 4.92 View of header H-18 after failure
- Figure 4.93 Close-up view of the failure mode of header H-18
- Figure 4.94 Close-up views of the failure mode of left side of header H-18
- Figure 4.95 Jacking load-deflection relationship for header H-18
- Figure 4.96 History of Jacking Load-Strain relationship for Header H-18
- Figure 4.97 Strains across the header section for Header H-18 at $F_{ULT}/3$
- Figure 5.1 Views of headers in different locations in several house cross sections
- Figure 5.2 View of header beams in a residential house
- Figure 5.3 View of snow load on a roof of a residential house

Figure 5.4	Geometrical characteristics of header panel section as shown in Clause 8.5 of CAN/CSA-O86-01
Figure 5.5	Geometrical characteristics of 356 mm deep header panels (Panel groups A, C, and E)
Figure 5.6	Geometrical characteristics of 660 mm deep header panels (Panel groups B, D, and F)
Figure A1	Table 4.3.2.2
Figure A2	Table 5.4.2
Figure A3	Table 5.4.3
Figure A4	Table 5.4.4
Figure A5	Table 5.4.5
Figure A6	Table 5.5.6.2.2
Figure A7	Table 5.3.1C
Figure A8	Table 7.3C
Figure A9	Table 7.3C (Concluded)
Figure A10	Table 7.4.4.1
Figure A11	Table 8.4.3.1
Figure A12	Figure 8.5.6

Chapter I

INTRODUCTION

1.1 General

Structural Insulated Panels (SIPs) are prefabricated large panels mostly used in residential and light commercial construction for exterior walls, roof, floors and foundation application. Formed from a thick layer of foam core laminated between two layers of sheathing, SIPs are a viable alternative to traditional wood stud-wall system. Developed in North America, SIPs satisfy building performance criteria while being both sustainable and cost effective (Kermani, 2006). Most structural insulated panels use either plywood or oriented strand board (OSB) for their facings while the most common foam core is expanded polystyrene (EPS). Figure 1.1 shows view of a structural insulated panel sample, while Figure 1.2 shows view of individual layers of the structural insulated panel. Figure 1.3 shows how the SIP panels are used while building a house or a small residential building.

One of the structural components of timber frame residential building is a header beam. Wall headers are used primary transfer roof live and dead loads over windows and doors to the full length wall studs. There are three common ways of providing a header in a structural insulated panel building envelope. One of the options is having no header with only lumber framing around the opening. Secondly, a structural insulated box beam is used with slightly increased thermal bridging and is shown in Figure 1.4. The last option is to use an insulated header beam that is the strongest and provides no thermal bridge (Malko, 2008). Few researchers have undertaken experimental studies to investigate the accuracy of design of

timber structural insulated panels. However, in regard to structural insulated panels functioning as headers, no test programs have been recorded so far.

In general, a SIP can be structurally compared to an I-beam and analogy of stressed skinned panels can be applied to structural insulated panel that is used as a wall, roof or floor structural element. In this case, the foam core acts as the web, while the facings are analogous to the I-beam's flanges. In case of flexural loading, all of the elements of a SIP are stressed; the skins are in tension and compression, while the core resists shear and buckling. Under in-plane loading, the facings of a SIP act as slender columns, and the core stabilizes the facings and resists forces that may cause local buckling of the facings.

However, in the case of structural insulated header panel that consists of lumber flanges and plywood or OSB web faces, the sandwich theory does not apply. Unlike the SIP wall, floor or roof panels, the foam core in insulated header panels provide only the thermal resistance and can not be considered as a structural component of the SIP header. Thus, the structural behavior of SIP header panel is best represented by analogy and design methods applicable to plywood web beams. Plywood web beams are built-up wood structural elements designed to resist flexural loads. The flanges are longitudinal members at the top and bottom of the beam and the webs are wood panel sheathing applied on both sides of the beam. For design purposes, as with many other types of non-prismatic beams, the flanges may be assumed to resist only flexural stresses and the webs may be assumed to resist only shear stresses. One of the most common types of the plywood web beams are box beams. Box beams provide high flexural strength and rigidity. As a result of their high torsional rigidity, box beams have excellent resistance to lateral buckling and are occasionally used as lintels above store windows or as floor or roof beams in residential construction.

1.2 The Problem

For 150 years, the traditional timber framing has gone unchallenged as the dominant structural system in low-rise residential construction. However, structurally insulated panels (SIPs) are gradually gaining popularity providing a viable solution. SIPs can provide residential and commercial structures with greater energy efficiency and quality. Energy efficiency in construction becomes appealing when one considers a growing world population and the realization that our energy resources are finite and subject to disruption (Gagnon and Adams, 1999). SIPs have the potential for greater quality compared to traditional framing. SIPs generally cost 2 to 10% more than an insulated and sheathed wood frame but provide 20 to 50% more insulation (Cathcart, 1998). Findings indicate that SIPs saved about two-thirds of the site framing labor for walls and roofs, with cycle time savings of similar magnitude (Mullens et al., 2006).

However, as with any other new product on the market, proof of testing is required to ensure compliance with industry standards. As each SIP product is unique to the manufacturer, and is dependent on the composite action of components parts and manufacturing techniques, structural behavior using linear elastic theory is considered to be appropriate only for estimating initial strength. Fully correlated tests on the products behavior are necessary to ensure that assumptions on material behavior are correct or adjusted. At the same time, one common way for structural components to be considered for approval by building code is through the practice of full-scale performance testing of the components. Acceptance criteria via performance tests are ordinarily based on deflection and ultimate load-carrying capacity. Clause 8.5 of Canadian Standard for Engineering Design of Wood, CAN/CSA-O86-01 (2001) specifies the effective stiffness, bending resistance, shear resistance

and deflection of plywood or OSB web beams. However, current timber codes are not directly applicable for the design of SIP products and require correlation with product experimental tests. As such, it is felt necessary to conduct experimental testing to-collapse on these panels to determine the structural capacity and serviceability performance of the structural insulated header beams. To address the need for testing of these developed panels, Canadian Construction Materials Commission (CCMC) and National Research Council Canada (NRC) developed technical guide for stressed skin panels for walls and roof. This guide formed the basis for the experimental testing conducted in this thesis for flexure, with the ultimate goal of providing enough technical data for strength and serviceability of such panel. With this database, Thermapan, Inc., the manufacturer of SIPs and provider of the SIP samples for the experimental testing, can certify these panels for use in the Canadian market.

1.3 Objective

The main objectives of this research work can be stated as follows:

1. To contribute to the efficient design of structural insulated timber header panels by developing experimentally calibrated models capable of predicting accurately their response when subjected to flexural loading.
2. The developed panel system provides builders and homeowners with energy efficient, structurally superior, environmentally friendly and easy to install building system.
3. The proposed research fosters new industry-university interaction in the field of materials and manufacturing research and development that produces a specific benefit to the Canadian economy.

1.4 Scope

The scope of this study includes:

1. A literature review on previous research work and codes of practice related to the structural behavior of Structural insulated timber header panels when subjected to transverse loading.
2. Perform experiments up-to-collapse on 18 actual-size timber panels according to ASTM standards to determine their ultimate load carrying capacity and deflection at service load level.
3. Correlate the experimental findings with code requirements at ultimate and serviceability limit states requirements for possible qualification for building construction.
4. Draw conclusion with respect to the structural adequacy of the tested sandwich header panels for possible use in residential construction.

1.5 Contents and Arrangement of the Thesis

Chapter II of the thesis presents a literature review of previous research on all type of structural insulated timber panels and plywood or OSB web beams. Chapter III discusses the experimental program conducted on selected panel sizes, including panel sizes and material properties, and the ASTM Standard test procedure for flexure. Chapter IV presents the experimental results in the form of graphs and photo documentation, while Chapter V summarizes the experimental findings and their correlations with theoretical results. Chapter

VI presents the conclusion of this research work and recommendations for future research.

Appendix A provides the CAN/CSAO86-01 tables that were used for the headers calculations.

Chapter II

LITERATURE REVIEW

2.1 General

In the past, a significant amount of research was conducted to predict the behavior of sandwich panels. However, only very few researchers have undertaken experimental studies to investigate the accuracy of design of timber sandwich panels. Building panels come in many configurations, known variously as foam-core panels, stressed-skin panels, nail-base panels, sandwich panels, and curtain-wall panels, among others. Many of these building panels are nonstructural, while some have no insulation. The structural insulated timber sandwich panels structurally act as stressed-skin panels, while the structural insulated timber header panels can be structurally compared to plywood or OSB web beams. The literature review conducted is presented in the following manner:

1. Structural insulated panels
2. Plywood web beams
3. Structural analysis and design method of plywood web beams
4. Experimental studies

2.2 Structural Insulated Panels (SIP)

2.2.1 General

Structural insulated panels (SIPs) are engineered composite load-carrying panel products consisting of a rigid insulating foam core sandwich between two structural faces that

are used primarily in residential and light commercial applications. The SIP panels replace conventional studs-wall system and provide insulated, finish-ready surfaces. Figure 2.1 shows detail views of Structural Insulated Panels while Figure 2.2 shows SIPs in a construction process. The material used to produce these building components can vary greatly in both the structural sheathing and the inner insulation core. Butt (2008) describes several types of common Structural Insulated Sandwich panels with materials such as oriented strand board (OSB), plywood, sheet rock, cement board, and sheet metal that are used as panel facing. Materials commonly used for timber structural insulated panels are OSB or plywood combined with a variety of plastic foams including expanded polystyrene (EPS), extruded polystyrene, urethane and other similar insulation cores.

2.2.2 History of Structural Insulated Panels

SIPs are not a new concept to researchers. In the 1930s, the Forest Products Laboratory began researching honey-comb paper-core and plywood-skinned panels in structural applications. These paper-core panels were the predecessors of today's OSB-skinned foam-core building panels. In the 1950s, trial SIP homes were built and one larger building product company attempted SIP manufacturing but stopped due to lack of demand. Since that time, smaller SIP manufactures have continued to develop the manufacturing process and the product (Gagnon and Adams, 1999) and the SIPs became readily available on the construction market. In 1990, The Structural Insulated Panel Association (SIPA) was founded in USA to provide support and visibility for those manufacturing and building with this emerging construction technology. In response to the need for the industry to develop product documentation, SIPA has cooperated with the American Society for Testing Materials

(ASTM) task group to define a standard test method to determine structural capacities of Insulated panels (ASTM, 2002). The ASTM standard defines a testing protocol to be followed by all manufactures to document the strength and stiffness properties of their product to code agencies for product certification (Butt, 2008).

2.2.3 Advantages and Disadvantages of Structural Insulated

A SIP-based system offers superior insulation, exceptional strength and fast installation. One of the superior advantages of SIP panels is a great time saving over conventional stud wall construction. SIP panels replace several components of a building, including studs and joists, insulation, vapor barrier and air barrier and thus SIP framing requires substantially less site labor than traditional stud-and-butt framing. With wood framing, additional insulation requires deeper lumber dimensions or double framing. SIP insulation, in contrast, gets less expensive as the panels get thicker, since the skins and manufacturing and installation process remains the same. SIPs have the potential for greater quality compared to traditional framing. They are assembled in a controlled factory environment versus the variable “on-site” environment. Panelization, in general, simplifies the construction process, making it more controllable, systematic, and faster (Gagnon and Adams, 1999).

Despite their rapid growth, SIPs are only used in about 1% of new homes. Mullens et al. (2006) states that several factors limit SIPs growth. Probably the most important factor is that the SIP construction is more expensive than comparable wood-frame construction. Material costs were generally cited as the largest driver of the cost premium, however Mullens et al. found that the erection costs could also be higher for SIPs, not to mention that panels did

require a lift truck and construction crane. Factors contributing to the lack of SIP acceptance by builders are risk and uncertainty about local building code official approval, long-term durability, impacts on the supply chain or impacts on the construction process. Gagnon and Adams (1997) concluded that based on the survey results, builders need more information about SIPs before they would consider their use.

^{2.2.4} **2.3.4 Fabrication and Erection Aspects**

SIPs are factory-produced, pre-fabricated building materials used as wall, roof and floor components on all types of residential and commercial buildings. Panel manufacturers supply splines, connectors, adhesives, and fasteners to erect their systems. When engineered and assembled properly, a structure built with these panels needs no frame or skeleton to support it. Thus, the greatest benefit of using SIP panels system is that structural support and the insulation are incorporated into a single system during manufacture. Kermani (2006) states that there are two main fabrication techniques: an industrial adhesive is applied to pre-cut foam core and then the core is cold pressed between two pieces of facing (panel boards) until the adhesive is cured or the foam cures to bond to the facings. Either method produces a single solid building element that provides both structural and insulation qualities. The panels are produced in varying sizes and thickness depending on application and thermal/structural requirements.

The manufacturing process has a major influence on the panel's strength and stiffness, and high quality bonding through is essential. For a SIP to function robustly there must be no slip between the outer skins and the core material. To achieve this, adhesive technology is used. The adhesive used must be capable of transferring shear and tensile forces across the

interface and not deteriorate over time or under the effect of moisture (Milner 2003). Similarly, the method of erection and connection has a large influence on the finished strength of the components.

2.2.5

2.3.5 Joints and Splices

SIP floors and roofs are installed by placing the panels side by side. The connections between the panels in the span direction can be either foam-spline or solid lumber spline. The foam-spline connection is preferred for roof construction to assist in energy efficiency. Butt (2008) describes solid lumber spline connection that is used for floor construction. The foam-spline connection is constructed by providing a recess in the foam core at the long edges of the panels. A foam block with two OSB facings glued to it is inserted at the edge of one panel. Then, the adjacent panel is slide over spline. The block OSB facings are then nailed to the OSB of the connected panels to provide structural integrity of the floor/roof. In a solid lumber spline, a recess is formed in the foam core before gluing it to the OSB facings. The width of the insert is usually half the width of the solid sawn lumber. After placing a panel over the walls, a sawn lumber is inserted in the recess along the panel length. Then, the adjacent panel slides over the sawn lumber, followed by nailing their OSB facings to the solid lumber.

2.2.6

2.3.6 Structural Behavior of SIPs

In conventional construction, loads are distributed or carried along studs and joists. In case of SIP panels, loads are evenly distributed across the entire panel, allowing greater loads. The insulating core and the two skins of a SIP are nonstructural and insubstantial components in themselves, but when pressure-laminated together under strictly controlled conditions, these

materials act synergistically to form a composite that is much stronger than the sum of its parts. SIPs utilize a stressed-skin principle where the overall strength of the panel is much greater than the strength of the components, thus reducing the need for structural framing. The foam panel is structurally analogous to an I-beam with the facing acting as the flange and the foam as the web. In case of flexural loading, all of the elements of a SIP are stressed; the skins are in tension and compression, while the core resists shear and buckling. Under in-plane loading, the facings of a SIP act as slender columns, and the core stabilizes the facings and resists forces that may cause local buckling of the facings. SIPs are predominantly subjected to the three major load components that are

1. Vertical loads (direct compression)
2. Transverse wind loads (combined bending and axial compression), and
3. In plane lateral forces imposed by wind and/or seismic loading (racking loading)

^{2.2.7}**2.3.7 Durability and Energy Efficiency of Structural Insulated Panels**

Kermani (2006) stated that in regard to durability no long-term test program was recorded. However he pointed out that there are examples of SIP buildings in the United States that have been in service for 50 years. Milner (2003) reasoned that a SIP panel, a quality-manufactured panel itself should not deteriorate or degrade unless it is incorrectly built, exposed to ultra-violet light, rodents or insects.

The interesting pilot project was launched by Structural Insulated Panel Association (SIPA) in partnership with Oak Ridge National Laboratory (ORNL) when building four “net-zero energy” research homes in order to confirm the super airtight and energy efficiency of homes built with SIP products. As mentioned in the paper presented by SIPA (2003),

airtightness relates directly to durability. An integral part of the SIP building system is properly sealed joints. When panel joints are sealed properly to prevent air infiltration and exfiltration, moisture is prevented from entering the building envelope and long-term durability is ensured. In the project, under blower door testing, a room with SIP walls, a SIP ceiling, a window, a door, pre-routed wiring chases and electrical outlets showed 90% less air leakage than an otherwise identical room built with 2 by 6 studs, OSB sheathing, fiberglass insulation and drywall. As stated in the report by SIPA, one reason for the high performance of the SIP test room was that the joints were properly sealed.

Compared with standard frame construction, SIPs can be inherently more energy efficient. Part of the efficiency improvement is also attributed to the insulating properties of the foam. A substantial improvement is also associated with the reduced need for framing members, which can operate as “thermal bridging” (Lee 1997; Waters 2003). SIP panels are highly energy efficient as they create a continuous whole-wall system with no thermal bridging, breaks, or air infiltration, which results in significantly less heating and cooling fuel consumption and lower energy costs. The main characteristic of energy efficiency of a material is its R-value, which is defined as a measure of the capacity of a material, such as insulation, to resist heat flow. The higher is the R-value of a material, the greater is its insulating capacity. R-values of SIP panels depend on the type of foam core and its thickness. Eventually, the R-values for a building envelopes built of the SIP panels are much higher than in conventional constructions. Kosny and Christian (1999) performed hot-box testing and finite difference computer modeling to analyze thermal performance of the clear wall area and wall interface details of the SIP building system. The objective of the project that was was to demonstrate the impact of real-world construction techniques on the reported R-value of

construction systems. The analysis performed at ORNL showed that for most wall systems, construction detail reduce R-values stated for clear wall configuration. However, test results and the computer modeling proved that in SIP systems such reductions are small and SIPs are considered as thermally efficient.

2.2.8

2.3.8 Fire Resistance of SIP Systems

In regard to fire, manufactures across North America have proven the performance of SIP system through some of the most extensive fire assembly testing in construction industry. The results of this destructive testing allow documentation of SIP performance under rigorous test standards. American national standards like ASTM E 119 and ASTM E 84 have been met by protecting SIPs in a similar fashion to other wood-based structures (Kermani, 2006). However, most buildings higher than three stories are subject to a different set of building regulations due to the loads applied to the walls and floor systems. While neither EPS nor urethane foams (the main core materials) are particularly flammable, they will burn when exposed to flame, so their use in high-rise or large public buildings without extensive fire suppression technology is limited.

2.3

2.4 Plywood Web Beams

2.3.1

2.4.1 General

A plywood web beam consists of one or more plywood webs to which sawn lumber or glued laminated timber flanges are attached along opposite edges. At intervals along the beam, lumber stiffeners are used to separate the flanges and control web buckling. Components of a typical plywood web beam are shown in Figure 1.1. There are several types of plywood web

beams among which the most common are box and double box beams, I- and double I-beams, spaced, tapered and arched beams. The different types of plywood web beams are shown in Figures 2.2, 2.3, and 2.4.

2.3.2

2.4.2 Material in Web Beams

2.4.2.1 Sawn Lumber

Lumber products are manufactured in accordance with CSA O141, Softwood Lumber. Sawn lumber commonly used have thicknesses from 38 to 89 mm and depths from 89 to 286 mm. The selection tables in Wood Design Manual include three thicknesses (38, 64 and 89 mm), three visual grade categories (Select Structural, No.1 and No.2 grade) and several Machine Stress-Rated grades. In 38 mm thickness, the most readily obtainable material is No.1 or No.2 grade.

2.4.2.2 Oriented Strand Board (OSB)

Due to its low cost and high strength, oriented strand board (OSB) is a popular choice for subfloors, wall and roof sheathing, and wood web beams in light wood frame construction. OSB is layered wood composite panel material composed of wood wafers that are bonded under heat and pressure with a waterproof resin. The outer layers of wood wafers are aligned in the long panel direction, while the inner layers have random or cross alignment. The Figure 2.5 shows typical OSB lay-ups. OSB was first commercially produced in the early 1980's but is now well established in the building industry and is recognized in the National Building Code of Canada (Wang, 1994).

The general product standard for OSB is *CSA O437, OSB and Waferboard*. The product standard contains three designations: O-1 and O-2 indicate the alignment of the strands as in OSB; while R-1 indicates random alignment, and is less common. OSB can be certified specifically for engineered design applications, in accordance with CSA Standard O452, Design Rated OSB. This standard contains certification and grade-marking requirements for three types of design-rated OSB panels:

- Type 1 (Standard) – products consisting of three different rating grades (A, B or C)
- Type 2 (Plus) – products exceeding Type 1 rating grade levels by 10% or more
- Type 3 (Proprietary) – products for which a certification organization certifies specified design capacities, different from Standard or Plus capacities.

OSB is extensively used for the webs of prefabricated wood I-joists. Proprietary OSB could also be used for manufacture of box beams and stress-skin panels where panel properties can be tailored to suit the product. Stress-skin panels are constructed by gluing sheathing to lumber joists to form a composite panel. Structural insulated panels are another application of OSB. Figure 2.6 shows the examples of structural engineered components made of OSB.

³2.4.3 Design Considerations

³2.4.3.1 Calculation of Section Properties

The plywood webs and lumber flanges of a plywood web beam need not have equal values of modulus of elasticity in flexure. Calculation of the section properties of such beams is conveniently handled by use of the transformed section method which considers a hypothetical section with all materials having the same E value. It is optional which of the materials transformed. If, for example, the plywood webs are transformed into an equivalent

amount of material with the same E value as the lumber flanges, then the dimensions of the stressed web plies will be changed by the ratio $n = E_w/E_f$. It should be noted that only the wood fibres parallel to the span of the beam are assumed to contribute to the section properties of plywood web beams. The small contribution of the web plies perpendicular to the beam span can be ignored. If a beam is unsymmetrical about its X-X axis, it is necessary to calculate the location of the neutral axis.

³2.4.3.2 Stiffeners

Plywood web beams usually require several stiffeners fastened to the webs between the inner surfaces of the flanges. The function of these stiffeners is to distribute concentrated loads into the beam, stabilize the web against buckling, separate the flanges under loading, and space the flanges accurately during fabrication. For design purposes stiffeners may be divided into two classes: bearing stiffeners and intermediate stiffeners. The location of bearing stiffeners will be determined by the location of reactions and heavy concentrated loads. Such stiffeners are designed using allowable compression stress perpendicular to the grain of the flange lumber. The main purpose of the intermediate stiffeners is to stabilize the web. In general, the cross-sectional areas of intermediate stiffeners should provide adequate column strength to resist any compressive forces from the flanges and to provide sufficient bearing area. They should also be thick enough to allow adequate fastening of the web to prevent the web from buckling.

³2.4.3.3 Joints and Splices

Where lumber or plywood of full beam length is not available and joints become necessary, the most desirable method of splicing longitudinally, both in plywood and lumber, is with a glued scarf joint. Tests show that a glued scarf joint will develop varying percentage of the full strength of clear wood depending on the slope of the scarf with respect to the grain of the lumber and the species of wood. A slope often used for softwood lumber is 1 in 12. This value will develop most of the clear wood strength and the full strength of a piece of structural lumber containing the normal growth characteristics. Scarf joints in lumber are usually made by a fabricator when the beam is built; in plywood they are generally made at mills where they are equipped for such an operation.

³2.4.3.4 Lateral Stability

Plywood web beams are usually deep relative to their overall width consequently some means of controlling lateral buckling of the compression flange may be required. Plywood box beams however are laterally stiffer than plywood I beams of the same width and depth. It is good design practice to provide lateral support to beams and have some method of gauging its effectiveness. One method assumes that the upper flange acts as a column that tends to deflect sideways between points of support. The allowable stress in a wood column is varied with its length / minimum depth ratio to provide an adequate factor of safety against buckling failure. The method goes beyond the scope of this text and is not further discussed.

⁴2.5 Structural Analysis and Design of plywood and OSB web beams

⁴2.5.1 General

Several box beam design manuals are available in North America (Lewicke, 1992). For further comparison with his experimental results, Lewicke (1992) briefly describes design methods that are presented in CAN/CSA-O86.01 (Canadian Standard Association), Wood Handbook (Forest Products Laboratory, 1987), Plywood Design Specification, Supplement Two, Design and Fabrication of Plywood Lumber Beams (American Plywood Association, 1990) and Design of Glued and Nailed Plywood Web Beams (Council of Forest Industries of British Columbia, 1989). In this thesis two methods for analyzing and designing of plywood web beams are described. The first method for preliminary design of web beams is the design procedure as described in the "Plywood Construction Manual" (edited by Payne, 1971) and is presented in this chapter. The second design approach for plywood or OSB web beams as specified in Clause 8.5 of Canadian Standard for Engineering Design of Wood, CSA/CAN-O86-01 will be presented in Chapter V along with the sample calculation of the flexure resistance of a header panel.

⁴2.5.2 "Plywood Construction Manual" Design Procedure

⁴2.5.2.1 Stresses

Stresses in a plywood web beam at service load are calculated using standard engineering formulae. These formulae are derived assuming elastic behavior of homogeneous beam materials. A plywood web beam must satisfy three basic criteria:

1. Flange stress
2. Web shear stress at neutral axis

3. Flange – web shear stress

(a) **Flange Stress**

The basic formula for flexural stress at any point in a beam is

$$f_y = \frac{My}{I} \quad (2.1)$$

Using the appropriate form of this formula, the flexural stress in critical locations of a plywood web beam can be calculated and compared with the allowable stress published in the governing code or specification. Because allowable tension and compression stresses for wood are not equal, plywood web beams are often designed with unequal flange areas. In this case, the flexural stress at the extreme outer fibre of both the tension and compression flanges must be calculated as:

$$F_t = \frac{Mc_t}{I_n} \quad (2.2) \quad \text{and} \quad F_c = \frac{Mc_c}{I_n}. \quad (2.3)$$

The computed stresses can then be compared to the allowable stresses.

Since $S_t = \frac{I_n}{c_t}$ and $S_c = \frac{I_n}{c_c}$ are geometrical properties of the beam section, they are termed as

section moduli and are often calculated separately as follows:

$$S_t = \frac{I_n}{c_t} \quad (2.4) \quad \text{and} \quad S_c = \frac{I_n}{c_c} \quad (2.5)$$

The flexural stress formulae are then modified and used in the form

$$F_t = \frac{M}{S_t} \quad (2.6) \quad \text{and} \quad F_c = \frac{M}{S_c} \quad (2.7)$$

It should be noted that I_n is *Net Moment of Inertia* in which local discontinuities are not assumed to contribute to the cross section.

Web Shear Stress at Neutral Axis

The basic formula for the shear stress in the webs at the neutral axis is

$$\frac{VQ_g}{I_g \sum t} \quad (2.8)$$

The computed shear stress can be compared with the allowable shear-through-thickness stress published in the governing code or specification.

Since $\frac{I_g \sum t}{Q_g}$ is a geometrical property of the beam section it is often calculated separately.

This property is called the web shear property and is expressed as

$$U_w = \frac{I_g \sum t}{Q_g} \quad (2.9)$$

The web shear stress formula is then modified and used as follows:

$$v_w = \frac{V}{U_w} \quad (2.10)$$

(b) Flange – Web Shear Stress

Where flanges and webs are joined by glue, the joint is parallel with the plane of plies of the plywood webs and its strength is limited by rolling shear in the plane of the plies of the plywood webs. The shear stresses on planes between the webs and flanges of plywood web beams are illustrated in Figure 2.7 and can be calculated using the basic horizontal shear stress formula

$$v_r = \frac{VQ_1}{I_g d_1} \quad (2.11)$$

where v_r = flange web shear stress on plane under consideration

Q_1 = first moment of flange section under consideration

d_l = flange-web contact depth between the flange area and web under consideration

These calculations assume that the horizontal shear stress is equal in all webs and that they receive load from the flanges in proportion to their thickness. Generally, the difficulty in using the shear stress equation will be in the determination of the value of Q_l which will be related to the web thickness and the flange shape, size and location. In practice, several standard cross sections are used for which the value of Q_l is readily calculated. The Figure 2.8 shows number of such beam sections which have equal flange-web shear stress at each contact face in the compression or tension flanges.

The equations for flange-web shear for these cases will be

$$v_c = \frac{VQ_c}{I_g \sum d_c} \quad (2.12) \quad \text{and} \quad v_t = \frac{VQ_t}{I_g \sum d_t} \quad (2.13)$$

The expressions $\frac{I_g \sum d_c}{Q_c}$ and $\frac{I_g \sum d_t}{Q_t}$ are geometrical properties of the beam section and are often calculated separately. They are called flange-web shear properties and are expressed as

$$U_c = \frac{I_g \sum d_c}{Q_c} \quad (2.14) \quad \text{and} \quad U_t = \frac{I_g \sum d_t}{Q_t} \quad (2.15)$$

The flange-web shear stress formula is then modified and used as follows:

$$v_c = \frac{V}{U_c} \quad (2.16) \quad \text{and} \quad v_t = \frac{V}{U_t} \quad (2.17)$$

It should be noted that I_g is *Gross Moment of Inertia* in which local discontinuities of the flanges and webs are ignored in the calculations.

⁴ 2.5.2.2 Deflection

In the service load range, correctly designed and fabricated plywood web beams deflect according to elastic theory. Standard deflection formulae may therefore be employed to calculate the portion of the total deflection that is caused by bending deformations. Since wood has a modulus of elasticity in shear that is low relative to the modulus of elasticity in flexure, shear deflection may be a significant part of the total deflection. Separate calculations should be made for bending and shear deflection. Simplified rules may be used for shear deflection if the actual calculation of shear deflection is considered too complex.

(a) *Bending Deflection*

The bending deflection of a prismatic plywood web beam is easily calculated using standard formulae for the applicable load configuration. It is important to note that the published moduli of elasticity in flexure of the sawn lumber flange material and the plywood web material can be increased by 5% and 10% respectively. It is done because the published E values of sawn lumber and plywood are based on test procedures which produce beam deflections due to both shearing and bending deformations. It has been found that the true moduli of elasticity in flexure, based on bending deformation only, for lumber and plywood are respectively 5% and 10% greater than E values derived from such tests. For this reason the published E values of sawn lumber and plywood used for the flanges of plywood web beams can be increased accordingly. As a result, if this is done, a separate calculation must be made for shear deflection.

Shear Deflection

The shear deflection at any location in the span of a beam is found from the formula

$$\Delta_s = \frac{E_w C W L h^2 K}{G E I} \quad (2.18)$$

The computed shear and bending deflection are then added to obtain the total load deflection. The load coefficient C modifies the term WL to account for the effect of distribution of the total load W as well as location on the span L where the value of deflection due to shear is desired. The section shear constant K is a section property that depends on the shape of the cross section and arises because of non-uniform distribution of shearing stresses across the section. It should be noted that it is difficult to calculate for all but the simplest cases. Because of this, several approximate rules for estimating the deflection due to shearing forces have been presented.

2.6 Theoretical Investigation and Experimental Studies

2.6.1 Structural Insulated Panels (SIPs)

Although SIPs have been used extensively as an alternative structural system to conventional framing for residential and light commercial buildings, to date little independent data are available on their structural performance and behavior. Kermani (2006) informs that there are no current SIPs design standards. The American Plywood Association supplement No.4 is the only standard dealing with wood-based sandwich panels and provides some limited design information on the uniform transverse or combined loading cases. A draft European code prEN 14509 CEN/TC 128: "Self supporting double skin metal faced insulated sandwich panels" is considered partly appropriate for the design of SIPs. Currently, a

European technical approval guideline (ETAG) for product certification for “prefabricated wood-based load bearing stressed skin panels is being drafted but no formal acceptance of this is as yet released.

Kermani (2006) conducted comprehensive research study on SIPs at Napier University in the United Kingdom and subsequently published several papers in which he presented the experimental program and its results. The performance under combined bending and axial compression and the effects of medium-loading on panel integrity for use as load-bearing walls and columns was studied in the series of tests. Panels of different lengths 600 mm and 400 mm wide with OSB facing 11 mm thick and insulating core of 95 mm were subjected to uniform axial compression in the first test series and to combined bending and axial compression in the second series of tests. To determine the effects of medium-term loading on the deformation characteristics (creep effect) of SIPs under axial compression and to examine the possibility of de-bonding/bulging within the sandwich panel tests were carried out using universal testing machine. Based on the results, Kermani (2006) presented design charts for estimating compressive strength with respect of wall height and also for combined bending and direct compression for 2400 mm high walls.

Another experimental research program conducted by Kermani (2006) studied the structural performance of wall diaphragms with and without openings, for doors and windows, under the action of racking loads. Nineteen walls of 2400 mm × 2400 mm were tested to evaluate the racking resistance of the SIP walls under vertical load applied along the header and to determine the effects of size and position of openings (for windows and doors) on the racking strength and stiffness of SIP walls. Kermani demonstrated that walls constructed of SIPs provide superior racking resistance to a comparable traditional stud wall. However, the

racking resistance of SIP wall is directly related to the size of the openings; with an increase in opening size the racking resistance of the wall decreases sharply. The reduction in racking strength and stiffness with respect to the level of opening has also been reported in previous studies by Johnson and Dolan (1996) and Enjily and Griffiths (1996).

Since the structural integrity of SIPs depends entirely upon the glue bonds between the skins and the core, Kermani (2006) also conducted a series of supplementary tests that were conducted to determine the effect of tensile loading. The results showed that when subjected to tensile loading (perpendicular to the plane of a panel) and also skewed/eccentric loading (in-plane shear) all failures occurred in the polystyrene and the glue lines remained intact demonstrating that suitability robust bonding techniques are available.

Butt (2008) performed an extensive experimental program on flexural and creep behavior when tested 53 full-size structural insulated panels with the aim to evaluate their potential use in low-rise residential building acting as a floor or roof member. The panels were divided into 15 groups that generally differed in sizes of the panels, thickness of the OSB sheathing and panel connections. The panel width was 1200 mm, the OSB thickness was in most of the panel samples 11 mm and the thickness of the EPS foam core was constant for all the panels. Butt's research work was focused on structural performance of SIPs with respect to the effectiveness of the foam core in providing composite action of the SIP member. Except of flexural behavior of the panels under static four points loading, Butt also studied the creep behavior of the SIP panels by testing four sample panels under long term uniform loading. He also compared the behavior of the panels with respect to different connections of the adjacent panels that could have either lumber connection or foam-spline connection. Butt (2008) presented the discussion on adequacy of the tested floor/roof SIP panels for their use in

residential construction with emphasis on code requirements for ultimate and serviceability limit states.

The correct design of the details of sandwich panels is at least as important as the analysis of deflections, stresses and backing loads. These details include nature of the edge members, splices and joints in the cores and faces, stiffeners and inserts to distributed concentrated load, type of adhesive, method of fabrication and so fourth. If the temperatures of the two faces differ, or if the moisture contents differ the differential expansion of the faces may lead to substantial transverse deflections (Butt, 2008).

Very few experimental studies were conducted on connections in SIPs. Kermani (2006) carried out the experimental study to evaluate the strength of a glue bonded polystyrene insulated core to OSB manufactured under normal conditions. In order to examine the possible effects of discontinuity in the core material, a number of panel specimens were tested with an unglued joint between the polystyrene core blocks at the mid-height of the panel. In these panels failure was initiated predominantly at that joint where up to 20% reduction in strength was noted. This highlighted the importance of continuity of the core material in providing an adequate composite action over the full loading range.

⁵2.6.2 Web Beams and Composite Beams

⁵2.6.2.1 Theoretical Background

Beam members are predominantly subjected to bending, coexisting with shear, bearing and buckling. Besides having sufficient strength capabilities to resist these effects, it is important that the beams have adequate stiffness to avoid excessive deflection or local buckling of the cross-section. Traditionally, only the deflection component of a beam owing to

bending is considered since the shear modulus for materials such as steel, is considerably higher as a percentage of the true elastic modulus than in timber. The shear deformation is however, a significant proportion of the overall deflection of a timber beam or an engineered timber beam. A number of factors, such as the geometrical configuration, the shear modulus of the web materials and the loading type and position, influence the shear deformation of a beam (Kermani, 2006).

Very little has been published on box beams with wood panel webs (Lewicke, 1992). Most of the published material consists of design manuals produced by government, regulatory agencies or industry groups. Publications on the theory behind wood box beams and results of box beam tests are limited to a series of reports. Nearly all available material on wood panel web box beams deals with thin webs, less than 6 mm that have low bending stiffness. No results involving wood box beams using web materials commonly used in North America wood frame construction, such as softwood plywood or OSB 9.5 mm or more in thickness, appear to have been published (Lewicke, 1992). The early research work on wood box beams recognized that web buckling was a problem but the means of critical loads were not available (Trayer and March, 1930). Saydel (1933) presented a method of predicting the critical shear stress in rectangular orthotropic plates and reported the experimental results that confirmed the method. The Saydel's work was based on analytical methods developed by Timoshenko (1921) and Bergmann and Reissner (1932). The Forest Product Laboratory (FPL) used Saydel's (1933) work as a basis for extensive experiments which investigated the behavior of plywood plates loaded in shear and/or compression that resulted in publishing the FPL report series. In another series of reports, researches of FPL investigated behavior of plywood web box beams. The purpose of both series of FPL was to examine the use of

plywood web box beams as aircraft components. Later work on shear buckling in plates (Kuhn, 1952) is based on thin aluminum plates with a negligible stiffness and its methods are not applicable to wood. Post-buckling behavior of metallic beam webs and tension field action based on membrane theory (negligible bending stiffness) was published by Timoshenko and Gere (1961). Based on the theories mentioned above, Lewicke (1992) explains two phenomena related to the behavior of buckling of web beams – behavior of plates subjected to shear forces and box beam action.

⁵2.6.2.2 Experimental Studies

There have been several experimental studies conducted on behavior of composite beams with wood based web. Lewicke (1992) studied the behavior and strength of wood composite box beams webs in the areas of critical shear buckling load, ultimate post-buckling strength and shear deflection. Three types of beams with 6.35 mm thick OSB webs. The beams used 38mm×89 Paralam parallel strand lumber flanges and dimension lumber stiffeners. The entire depth was 610 mm and the length of the beams was 2440 mm. The beams were constructed and tested to obtain data on out-of-plane web deflection, vertical deflection and ultimate shear strength. The investigation focused on web panel aspect ratio and face grain orientation. Each type of beam used OSB panels from different production runs. The beams also differed in location of web stiffeners and the point of load application or different orientation of the web panels face grain. The beams were 610 mm deep and 2440 mm long and were tested under quarter point load or one third point load. Lewicke (1992) presented several box beam design methods that are available in North America. He concluded that the main differences between the methods are notation, the method of

converting basic beam dimensions into section properties and the assumptions regarding which beam elements resist normal stresses. Lewicke attempted to develop a method of predicting the ultimate shear strength of OSB box beam webs. He compared various design methods of estimating shear deflection in wood composite box beams to determine which method predicts box beam shear deflection most accurately.

Prefabricated wood I-beam with OSB webs is another type of plywood web beams that is widely used in North America. Wang (1994) investigated the effects of web openings on the shear strength of OSB web I-beams and identified a possible failure mechanism. His experimental program consisted of testing 610 mm, 406 mm and 241 mm deep simply supported beams with different hole geometries under a single point load. Wang (1994) identified four modes of failure that occurred in one or in combination of four modes. The first mode was observed at the specimens with a hole depth equal to the full height of the web that exhibited failure with the web pulling out of the flange. The second model exhibited Vierendeel truss action causing failure at the corners of the hole. The third mode was due to a cross section shear failure and the last mode exhibited buckling of web. Wang concluded that the shear strength of a beam with an opening was reduced by as much as 79% when compared to a reference beam without holes. Among the other conclusions, Wang found out that web buckling mode was observed in deeper beams (610 mm) with or without holes, that specimens with web openings failed suddenly and that longer shear spans corresponding to greater bending moments at the location of the hole resulted in an increase in shear strength. Wang suggested a design procedure using a Vierendeel analysis and a cross section check to predict the shear strength of OSB webbed I-beams with a rectangular opening.

Application of composite beam is often limited by the shear strength of the web. Hunt (1974) performed a pilot testing of a composite beam with a structural particleboard as a web material and found that the in-plane shear modulus was 2.5 times greater than for plywood. Hunt thus suggested that structural particleboard has potential advantages as web material in composite beams. In another study of composite beams, Hunt (1976) investigated the feasibility of using 2 by 4 lumber and structural lumber in combination with particleboard as acting as a web in 16-foot garage headers. In this experimental program, Hunt compared the structural performance of each tested beam type with a double 2 by 12 header, a beam that time commonly used in a wood framing house construction for framing a garage opening.

Composite beams made of other materials than wood was also the objective of researches. Li (2005) studied cold form steel sections used in composite configuration with 38×89 mm lumber, 38×184 mm and 19 mm thick oriented strand board (OSB). The study showed that combining cold-formed steel sections with wood members is effective and results in increased flexural rigidity, strength, ductility and stability above that of either material performing separately.

Milner (2001) studied analytically thin-web box beams made by nailing plywood or other webs to solid timber flanges as their analysis presents problems related to the significant shear and nail distortions that result in increased deflection. Milner presented an engineering method and demonstrated how to model nailed box beams for any load distribution in any type of structure using commercially available structural analysis software.

Racher (2005) states that the design of timber I-beams with OSB web is currently based on simplified analytical models and experimental works. In his work, the effect of the slenderness of the web is analyzed through experimental program and a finite element model.

The effective stiffness and the bending capacity of the tested I-beams was evaluated and compared to the theoretical evaluation taking into account the shear deformation of the web. Racher showed that for highest heights of the cross-section, the ultimate capacity of the I-web beams is governed by the plate behavior of the web, resulting in the failure of the glued joint. Based on the experimental data and the observed failure modes, Rachel concluded that the combination of shear stress in the glued joint is the most likely cause of failure for slender I-beams.

Kermani (2006) investigated the strength and deformation characteristics of lightweight timber composite beams manufactured with six different cross-sectional profiles in comparison with readily available laminated veneer lumber (LVL) and glued-laminated (Glulam) beams. All engineered profiles comprised solid timber or LVL flanges and three-ply plywood webs. The number of webs varied from one to four. The beams had an overall 290 mm and were either 88 mm or 106 mm wide. The beam span varied between 2100 mm to 4350 mm. Kermani showed that the addition of extra webs to the I-beam profile significantly enhanced the bending and shear capacity of the beam while maintaining a high strength to weight ratio. The boxed I-beam proved to be the most efficient to manufacture and displayed superior structural performance compared with the rest of the profiles in terms of flexural stiffness and bending and shear capacity. The experimental results confirmed the significant contribution of the shear deflection to the total deflection of the I-beams, box beams and even solid section beams. Kermani concluded that, in most cases, it is possible to predict the failure mode by comparing the theoretical stresses with the characteristic values of the component.

Chapter III

EXPERIMENTAL STUDY

3.1 General

In order to develop a better understanding of the structural behavior of structural insulated timber header panels at service and ultimate loading conditions, an experimental research program was performed at the structures laboratory of Ryerson University. Eighteen flexural tests to-collapse were performed on selected sizes of structural insulated header panels to provide experimental data that was further evaluated for building code compliance. The experimental data was correlated to the predicted results obtained from available analytical method in CAN/CSA-O86-01 for box beam design. This chapter summarises the geometrical and material properties of the tested header panels, the setup for flexural test and the test procedure.

Structural Insulated Panels (SIPs) have many applications, such as exterior walls, floors, roofs, flat ceilings, vaulted ceilings, foundation, log homes, additions, and renovations. The structural insulated header panels tested at Ryerson University were manufactured and provided for the experimental program by Thermapan Industries Inc., a Canadian-based company that has been manufacturing Structural Insulated Panels (SIPs) for residential and commercial building applications since 1980. The most common panel configuration manufactured by Thermapan Inc. is the "Standard" panel which consists of 7/16" Oriented Strand Board (OSB) on both sides and expanded polystyrene foam core (EPS). Thermapan SIP panels are available in the following standard sizes: 4x8, 4x9, 4x10, 4x12, 4x14 and 4x16

square feet. The main characteristics of the Standard SIP panels manufactured by Thermapan Inc. are shown in Table 3.1.

3.2 SIP Header Panel Configuration

The main function of the SIP panels that were experimentally tested and are described in this chapter - if used in a building application – is to support vertical load above a window or a door opening in either external or internal SIP wall. For the purpose of this study, those SIP panels will be further in the text called as “header panels” or “headers” as per their function in a building envelope. The SIP header panels manufactured by Thermapan Industries Inc. are available in different standard sizes. Table 3.2 shows allowable axial loads for SIP headers 6 ½” deep for different standard lengths, as specified by Thermapan Inc. considering the superseded allowable stress design method. From that table, it is apparent that headers are available with clear length 4, 6, 8, 10, 12, and 16 feet. Header height can vary as 13.5, 16, 20, 24 and 48 inches. The panel width can be either 4-1/2 or 6-1/2 inches, depending on the flange dimensions that is either 2×4 or 2×6 lumber. According to the Thermapan Specifications, SIP header panels are made of two equal layers of APA rated sheathing, 7/16" (11 mm) O.S.B. or 5-ply plywood. The core is 1.18 pcf density EPS adhered to the sheathing with adhesive and set under pressure. All flanges are SPF No.1 lumber.

The SIP header panels are installed by placing next to interior or exterior SIP wall panel. The connection between the header panel and adjacent wall panels is made as solid lumber spline. Figure 3.1 illustrates how the header panel configuration is made and details the header-wall connection. For the purpose of the experimental testing, adjacent SIP walls are represented by two SIP posts, as shown in the Figure 3.1. The header flanges are made of two

2×6 lumber wood connected with lumber blocking at the edges of the header as it shown Figure 3.1. The header-posts connection is made by overlapping top and bottom flange onto the SIP posts. From the dimensions of the header panels described later in this chapter, it is obvious that overlapping of the top lumber flange is about 12 inches long, while the bottom flange exceeds only about one inch into the post. The OSB facing is not connected in the joint spline of the header and the posts. It was observed the gap between the OSB facing was about ¼” to ½” wide. After the connection of the headers and walls was made, the OSB facings were nailed to the solid wood.

3.3 Description of Panel Groups

The experimental program included 18 header panels for flexure testing under static four-point loading. As shown in Figure 3.1, the tested header panels consisted of 2”×6” sawn lumber, Oriented Strand Board (OSB) of thickness 7/16”(11mm) and Expanded Polystyrene (EPS) insulation foam core. The width of all panels is 6 ½”. The foam core width is the difference between the total depth and the thickness of the two OSB facings. The total length and depth of panels varies as well as varies their clear length and clear depth. Table 3.3 summarizes the geometric characteristics of the panels.

The tested panels were divided into 6 groups based on the length and depth of the panel. The schematic views and panel dimensions are illustrated in Figures 3.2 to 3.7. Group A (panels H-1, H-2 and H3) consisted of 3 panels of total length 1219.20 mm (48”) and total depth 355.60 mm (14”). The jacking load-strain relationships were recorded only for panel H-3. Group B (panels H-4, H-5 and H-6) consisted of 3 panels of total length 1219.20 mm (48”) and total depth 660.40 mm (26”). The jacking load-strain relationships were recorded only for

panel H-6. Group C (panels H-7, H-8 and H-9) consisted of 3 panels of total length 1828.80 mm (72") and total depth 355.60 mm (14") and the jacking load-strains relationships were recorded for only panel H-8. Group D (panels H-10, H-11 and H-12) consisted of 3 panels of total length 1828.80 mm (72") and total depth 660.40 mm (26"). The jacking load-strain relationships were recorded for only panel H-10. Group E (panels H-13, H-14 and H-15) consisted of 3 panels of total length 2438.40 mm (72") and total depth 355.60 mm (14"). The jacking load-strain relationships were recorded for only panel H-14. Group F (panels H-16, H-17 and H-18) consisted of 3 panels of total length 2438.40 mm (72") and total depth 660.40 mm (26"). The jacking load-strain relationships were recorded for only panel H-18. The strain gauges for all panels were installed at nine different locations at header's mid-span except the header H-14 where only three strain gauges were placed. Figure 3.8 shows schematic diagram of arrangement for headers of 14 inches depth (panel groups A, C, and E), while Figure 3.9 shows the arrangement of strain gauges for the 26 inches deep header panels (panel groups B, D, and F). It should be mentioned that there were some discrepancies between the actual dimensions of the headers and dimensions as specified by the manufacturer. The actual dimensions of header panels were thoroughly measured before each testing and are summarized in Table 3.4.

3.4 Material Properties

The Therman SIPs as manufactured by Therman Industries Inc. consists of three elements, factory crafted in a computer assisted lamination assembly line. The exterior faces are oriented strand board (OSB) manufactured and grade stamped as per APA (1990). The OSB board used to fabricate the panels had 1R24/EF16/W24 panel mark with 10.5 mm

thickness construction sheathing. The minimum material properties for OBS boards, as supplied by the SIP manufacturer are specified as follows:

Modulus of rupture: 28.955 MPa (4200 psi) in the span direction

12.409 MPa (1800 psi) in the direction normal to the span direction

Modulus of elasticity: 5515 MPa (800,000 psi) in the span direction

1551 MPa (225,000 psi) in the direction normal to the span direction

However, material characteristics as specified in the OSB Design Manual (2004) for the 1R24/EF16/W24 panel are listed below.

Bending resistance, M_r = 228 N.mm/mm

Axial tensile resistance, T_r = 57 N.mm/mm

Axial compressive resistance, P_r = 67 N.mm/mm

Shear through thickness resistance, V_r = 44 N/mm

Bending stiffness, EI = 730,000 N.mm²/mm

Axial stiffness, EA = 38,000 N/mm

Shear through thickness rigidity, G = 11,000 N/mm

Expanded Polystyrene is a polymer impregnated with a foaming agent with, when exposed to steam, creates a uniform closed cell structures highly resistant to heat flow and moisture penetration. This in-plant expansion process is fused into blocks which are cured for dimensional stability and cut into boards. The expanded polystyrene (EPS) core used to fabricate the panels was Type 1. Thermapan Industries Inc. specifies a priority density that demonstrates a load failure of 25 psi when tested as per ASTM C297. EPS core material must meet the minimum standard CAN/ULC-S701 and demonstrate the following minimum strength characteristics:

Nominal density	16 kg/m ³ (1.0 lbs/ft ³)
Shear strength:	83 kPa (12 psi)
Shear modulus:	2758 kPa (400 psi)
Flexural strength:	172 kPa (25 psi)
Tensile strength:	103 kPa (15 psi)
Compressive strength:	70 kPa (10 psi)

The urethane adhesive must meet the following standards:

ASTM D-2294: 7 Day High Temperature Creep Test

ASTM D-905: Block Shear Test Using Plywood

ASTM C-297: Tension Test of Flat Sandwich Construction in a Flatwise Plane

ASTM D-1877: Resistance of Adhesive to Cyclic Laboratory Aging Conditions

ASTM D-1002: Strength Properties of Adhesive Bonds in Shear by Tension Loading

3.5 Test method for SIP Panels in Flexure

In 2007, the National Research Council Canada (NRC) prepared a technical guide (IRC, 2007) that describe the technical requirements and performance criteria for the assessment of stressed skin panels (with lumber 1200 mm o.c. and EPS core) for walls and roofs for the purpose of obtaining a CCMC (Canadian Construction Materials Commission) evaluation report. The requirements and criteria referenced in this guide were developed to evaluate the performance of stressed skin panels for walls and roofs with respect to their performance as an alternative solution established with respect to Part 4, Structural Design, and Part 9, Housing and Small Buildings, of the National Building Code of Canada (NBCC,

2005). The Technical Guide focuses on the structural qualification of stressed skin composite panels as being “as good as” the structural capacity of the conventional wood-frame buildings. A successful evaluation conforming to this Technical Guide will result in a published CCMC Evaluation Report that is applicable only to products bearing the proper identification number of CCMC’s evaluation number. This NRC/IRC/CCMC Technical Guide specifies test methods for SIPs similar to those specified in ASTM E 72-02, *Standard Test Methods for Conducting Strength Tests of Panels for Building Construction*, (ASTM, 2002) as well as ICC AC04, *Acceptance Criteria for Sandwich Panels*, (2004). It should be noted that ICC AC04 acceptance criteria is based on ASTM E 72 standard test methods. As such, bending qualification tests on the panels were conducted in accordance with the method described in the ASTM E 72-02, *Transverse Load Test*. ASTM E 72-02 specifies at least three identical specimens for each test. This condition is reflected in the tested panel groups shown in Tables 3.3 and 3.4. The other applicable Codes and Standards that are listed in NRC/IRC/CCMC Technical Guide for Stressed Skinned Panels for Walls and Roofs are as follows:

ASTM D 905-03	Standard Test Method for Strength Properties of Adhesive Bonds in Shear by Compression Loading
ASTM D 1037-99	Standard Test Methods for Evaluating Properties of Wood-Base Fiber and Particle Panel Materials
ASTM D 1761-88(2000)	Standard Test Methods for Mechanical Fasteners in Wood
ASTM E 96-02	Standard Test Methods for Water Vapor Transmission of Materials
ASTM E 529-94 (1998)	Standard Guide for Conducting Flexural Tests on Beams and Girders for Building Construction

3.5.1 Flexure Load Test setup

The setup for tested header panels was prepared as per ASTM E72-02 and is shown in Figure 3.10. In this load setup, the header panels are supported over two steel rollers of 25.4 mm diameter and 178 mm length. The rollers were inserted between two steel plates – PL. 178×152×12 mm and PL. 305×178×12 mm. Supported by steel pedestals, the whole assembly was resting on the laboratory strong floor. This setup was used only for the first test conducted on header panels when header H-9 was tested. For all other tests, the headers were supported over the flat surface. This setup is shown in Figure 3.11. Figure 3.12 shows view of the test setup for header H-1 before testing. Similarly, the test setups for all header panels (H-2 to H-18) were photographed before each testing and are shown in Figures 3.13 to 3.29.

The loading for all tested panels was applied at the quarter points of panel clear length, except of the first test with the roller support when the load was applied at the quarter points of the length between the supports. The load was applied from the jack using a spread beam HSS 152×152×8. The length of the spread beam varied, depending on length of a tested panel. In most cases (panels H-1 to H-12, H-16, H-17 and H-18), the HSS beam was approximately 1500 mm long. For testing of panels H-13, H-14 and H-15, the spread HSS beam of length 2400 mm was used. The spread beam rested on two steel rollers of the identical dimensions as the support steel rollers, two steel plates PL. 152×152×12 and two short HSS 152×152×8 beams 178 mm long. The weight of the described loading system is approximately 0.90 kN or 1.3 kN, depending on the length of the spread beam. Two universal flat load cells of 200 kN (45,045 lb) and of 50 kN (11,261 lb) capacity were used to measure the jacking loads applied on all header panels. The load cell used during the testing is shown in Figure 3.30.

3.5.2 Instrumentation for Flexure Load Test

Two sets of Linear Variable Displacement Transducers (LVDTs) were used to measure vertical displacement (deflection) in all panels at the mid-span location. Mechanical Dial gauge was used to measure the deflection for backup purpose. It was located 100 mm away from the centre line of the panel. Dial gauge readings were manually taken at each increment of loading (generally, at each 1 kN) throughout the test up to certain load increment based on the level of deformation in the panel during testing. Figure 3.31 shows schematic view of sensors for deflection reading, while Figure 3.32 shows the dial gauge and two LVDTs installed under the panel at mid-span location. To measure the flexural strain on the top and bottom flange, and on one side of the OSB web of the header panel, 9 strain gauges were used. They were placed at the mid-span location of a panel at different locations across the depth of the header panel. Two strain gauges were placed on the top and bottom lumber flanges of the header panel and 5 strain gauges were applied on the OSB face of the panel. The strain gauges that were used during the tests had a length of 50 mm, a resistance of 350 ohms and a sensitivity of 2000×10^{-6} strain/mm. The flexural strains were recorded on one header from each panel group. During testing, the data from the LVDTs, strain sensors and load cell were captured by a test control software (TCS) using a SYSTEM 5000 data acquisition unit. This powerful hardware/software simplifies the process of collecting, reducing and presenting data captured by strain gauges and LVDT's. The TCS was adjusted to sample the data at rate of one reading per second during the loading test.

3.5.3 Flexure Load Test Procedure

A test set-up was prepared for each test at the structural laboratory of Ryerson University. Both Linear Variable Displacement Transducers (LVDTs) and strain gauges were installed at predetermined locations in the panel to record deflection and normal strains. The available MTS system-5000 data-acquisition system was used to capture reading from sensors. For each panel, jacking load was applied in increments so that readings from dial gauge could be recorded. When significant panel deformation was noticed, the dial gauge was removed and the jacking load continued to be applied until the failure. Visual inspection was conducted at each load increment during the test to record any change in structural integrity of the sandwich panel. The test was terminated after specimen failure. Test stopped when the jacking load was not increasing while panel deflection was increasing by continuously pressing the pump handle. Test data were then used to draw the load-deflection and load-strain relationships for each panel. Mode of failure of each panel was also recorded.

Chapter IV

EXPERIMENTAL RESULTS

4.1 General

Experimental testing to-collapse on 18 actual-size timber panels according to ASTM standards was performed to determine their structural behavior at service and ultimate load levels. Discussion of the experimental results with respect to the failure modes of the tested headers, jacking load-deflection and jacking load-strains relationships are presented panels in this chapter. The summary of the experimental results presented in tables is included in Chapter V.

4.2 Panel Group A

In this group, three identical headers (H-1, H-3 and H-3) were tested to complete collapse. Each header was of 1219.20 mm clear length and 355.60 mm depth. Figures 4.1 to 4.15 summarize the experimental findings for this header group. Figure 4.1 shows view of header before loading, while Figure 4.2 shows view of the deformed header after failure for header H-1. Figure 4.3 shows close-up view of the permanent deformed shape of the Header after failure. It can be observed that the failure mode of the panel was due to flexural deformation of the top flange plates between the quarter points and the supports, associated with either nail bending or nail hole tear-out at the interface between the OSB facing and the top and bottom flange plates near the support and between the OSB facing and the vertical blocking at the end of the OSB web. The relative vertical movement of the header's OSB facing and the OSB facing of the wall was apparent in Figure 4.3. As such, one can

recommend revising the header design to extend the OSB facing to the end of the vertical wall stud or beyond to establish continuity in web shear. It should be noted that noise was heard when approaching failure load and the failure of the panel was abrupt causing a sudden drop in the applied jacking load as shown in the load-deflection relationship in Figure 4.4. Similar failure mode was observed in panels H-2 and H-3. Views of header H-2 before and after failure are shown in Figures 4.7 and 4.8. While Figure 4.9 shows view of the foam inside the panel H-2 at the location of the failure. Figure 4.10 shows the load-deflection relationship of header H-2. Figures 4.11 through 4.14 show similar trend for header H-3. While Figure 4.15 depicts the load-deflection relationship for header H-3.

Figures 4.4, 4.10, and 4.15 illustrate the jacking load-deflection history of panels H-1, H-2 and H-3, respectively. It can be observed that the ultimate jacking load was 63.54, 55.14 and 63.11 kN for panels H-1, H-2 and H-3, respectively. To determine the design factored ultimate load, a factor of safety of 3 was considered per AC-04. Thus, the design ultimate load for headers H-1, H-2 and H-3 were illustrated in these figures as 21.20, 18.38, and 21.04 kN, respectively. To establish design criteria for serviceability limit state, the jacking loads were determined at the deflection limit of $\text{span}/360$ for live loading and at the deflection limit of $\text{span}/180$ for combined dead and live loading. These values are recorded in these figures as 11.26, 8.07 and 10.74 kN for deflection limit of $\text{span}/360$ and 21.18, 14.64 and 19.02 kN for deflection limit of $\text{span}/180$ for headers, H-1, H-2, and H-3, respectively. These values will be further used to establish design tables for the headers in the form of maximum joist, roof or floor span served by the header. Figure 4.4 for the jacking load-deflection history of header H-1 shows that the header behavior is generally linear elastic for applied loads equal of less the

design factored ultimate load of 21.20 kN. Similar behavior was observed for headers H-2 and H-3. Figure 4.5 depicts the normal strain history at the mid-span section. While Figure 4.6 depicts the normal strain distribution at the mid-span location at one-third the experimental ultimate load. It can be observed that the strain distribution appears to be linear within the OSB facing, while it gave unreasonably distributed values at the extreme fibers of the top and bottom plates. It should be noted that strain readings were not used in this study to establish design criteria at the ultimate or serviceability limit states.

4.3 Panel Group B

In this group, three identical panels (H-4, H-5, and H-6) were tested to complete collapse. Each panel was of 1219.20 mm clear length and 660.40 mm depth. Figure 4.16 shows view of header after failure for Header H-1. Figures 4.17 to 4.19 show close-up view of the permanent deformed shape of the header after failure. It can be observed that the failure mode of the header was due to significant bending deformation of the top flange plates between the quarter points and the supports, associated with either nail bending or nail hole tear-out at the interface between the OSB facing and the top and bottom flange plates near the support and between the OSB facing and the vertical blocking at the end of the OSB web. The relative vertical movement of the header's OSB facing and the OSB facing of the wall was apparent in Figure 4.19. As such, one can recommend revising the header design to extend the OSB facing to the end of the vertical wall stud or beyond to establish continuity in web shear. It should be noted that noise was heard when approaching failure load and the failure of the panel was abrupt causing a sudden drop in the applied jacking load as shown in the load-deflection relationship in Figure 4.20.

Similar failure mode was observed in panels H-5 and H-6. View of header H-5 after failure is shown in Figure 4.21. While Figures 4.22 and 4.23 show views of the failure mode in header H-5. Figure 4.25 shows the load-deflection relationship of header H-5. Figures 4.25 through 4.28 show similar trend for header H-6. While Figure 4.29 depicts the load-deflection relationship for header H-6. Figures 4.20, 4.24, and 4.29 illustrate the jacking load-deflection history of panels H-4, H-5 and H-6, respectively. It can be observed that the ultimate jacking load was 78.04, 74.71, and 67.91 kN for headers H-4, H-5 and H-6, respectively. To determine the design factored ultimate load, a factor of safety of 3 was considered per AC-04. Thus, the design ultimate load for headers H-4, H-5 and H-6 were illustrated in these figures as 26.01, 24.90, and 22.64 kN, respectively. To establish design criteria for serviceability limit state, the jacking loads were determined at the deflection limit of span/360 for live loading and at the deflection limit of span/180 for combined dead and live loading. These values are recorded in these figures as 15.02, 17.46, and 15.46 kN for deflection limit of span/360 and 26.34, 36.43 and 25.12 kN for deflection limit of span/180 for headers, H-4, H-5, and H-6, respectively. These values will be further used to establish design tables for the headers in the form of maximum joist, roof or floor span served by the header.

Figure 4.20 for the jacking load-deflection history of header H-4 shows that the header behavior is generally linear elastic for applied loads equal of less the design factored ultimate load of 26.01 kN. Similar behavior was observed for headers H-5 and H-6. Figure 4.30 depicts the normal strain history at the mid-span section. While Figure 4.31 depicts the normal strain distribution at the mid-span location at one-third the experimental ultimate load. It can be observed that the strain distribution appears to be linear within the OSB facing, while it gave

unreasonably distributed values at the extreme fibers of the top and bottom plates. It should be noted that strain readings were not used in this study to establish design criteria at the ultimate or serviceability limit states.

4.4 Panel Group C

In this group, three identical panels (H-7, H-8 and H-9) were tested to complete collapse. Each panel was of 1828.80 mm clear length and 355.60 mm depth. Figures 4.32 to 4.47 summarize the experimental findings for this panel group. Figure 4.32 shows view of header H-7 after failure. While Figures 4.33 and 4.34 show close-up views of the failure shape at the header-wall junction. Figure 4.35 show this header-wall junction after removing the OSB facing. It is interesting to mention that in this header, tensile fracture occurred at bottom of OSB facing accompanied by OSB crushing in the top part of this facing as depicted in Figure 3.36. It should be noted that this type of failure occurred only on one OSB facing at the same location. However, the main cause of failure in header H-7 was due to flexural deformation of the top flange plates between the quarter points and the supports, associated with either nail bending or nail hole tear-out at the interface between the OSB facing and the top and bottom flange plates near the support and between the OSB facing and the vertical blocking at the end of the OSB web. The relative vertical movement of the header's OSB facing and the OSB facing of the wall was apparent in Figure 4.34. As such, one can recommend revising the header design to extend the OSB facing to the end of the vertical wall stud or beyond to establish continuity in web shear. It should be noted that noise was heard when approaching failure load and the failure of the panel was abrupt causing a sudden drop in the applied jacking load as shown in the load-deflection relationship in Figure 4.37. Similar

failure mode was observed in panels H-8 and H-9. Views of header H-8 after failure are shown in Figures 4.38 to 4.40. Figure 4.41 shows the load-deflection relationship of header H-8. Figure 4.42 depicts the normal strain history at the mid-span section. While Figure 4.43 depicts the normal strain distribution at the mid-span location at one-third the experimental ultimate load. It can be observed that the strain distribution appears to be linear within the OSB facing, while it gave unreasonably distributed values at the extreme fibers of the top and bottom plates. It should be noted that strain readings were not used in this study to establish design criteria at the ultimate or serviceability limit states.

Figure 4.44 the permanent deformed shape of the header H-9 after the failure. While Figures 4.45 and 4.46 show close-up views of the failure mode of this header at the header-wall junction. It should be noted the setup for this header included resting it over pure rollers per ASTM test method. However, this does not that case in practice since the point-load supports used in this test created very high flexible wall segment that in turn caused the wall stud and header bottom plates resting over the studs distort in the fashion shown in Figure 46 due to insufficient anchorage for the header bottom plates. However, the failure mode of this header also included the same failure features observed in Group A as noticed in Figures 45 and 46. Unlike header H-9, all other headers tested in this study has wall supports fully resting on the lab floor or steel pedestals over their length and width as in practice.

Figures 4.37, 4.41, and 4.47 illustrate the jacking load-deflection history of panels H-7, H-8 and H-9, respectively. It can be observed that the ultimate jacking load was 39.09, 49.19 and 34.14 kN for panels H-7, H-8 and H-9, respectively. To determine the design factored

ultimate load, a factor of safety of 3 was considered per AC-04. Thus, the design ultimate load for headers H-7, H-8 and H-9 were illustrated in these figures as 13.03, 16.40 and 11.38 kN, respectively. To establish design criteria for serviceability limit state, the jacking loads were determined at the deflection limit of span/360 for live loading and at the deflection limit of span/180 for combined dead and live loading. These values are recorded in these figures as 12.94, 10.12 and 9.11 kN for deflection limit of span/360 and 23.77, 19.91 and 15.75 kN for deflection limit of span/180 for headers, H-7, H-8, and H-9, respectively. These values will be further used to establish design tables for the headers in the form of maximum joist, roof or floor span served by the header. Figure 4.37 for the jacking load-deflection history of header H-7 shows that the header behavior is generally linear elastic for applied loads equal of less the design factored ultimate load of 13.03 kN. However, it is interesting to note the jacking load for the span/180 deflection limit of 23.77 is far greater than that for the established designed factored load of 13.03 kN. However, the header structural behavior is still maintained linear elastic up to this greater level as depicted in Figure 37. Similar behavior was observed for headers H-8 and H-9.

4.5 Panel Group D

In this group, three identical panels (H-10, H-11, and H-12) were tested to complete collapse. Each panel was of 1828.80 mm clear length and 660.40 mm depth. Figures 4.48 to 4.59 summarize the experimental findings for this header group. Figure 4.48 shows view of the deformed shape after failure for header H-1. Figures 4.49 and 4.50 show close-up views of the permanent deformed shape after failure at the header-wall area. It can be observed that the failure mode of the panel was due to significant flexural deformation of the

top flange plates between the quarter points and the supports, associated with either nail bending or nail hole tear-out at the interface between the OSB facing and the top and bottom flange plates near the support and between the OSB facing and the vertical blocking at the end of the OSB web. The relative vertical movement of the header's OSB facing and the OSB facing of the wall was apparent in Figure 4.50. As such, one can recommend revising the header design to extend the OSB facing to the end of the vertical wall stud or beyond to establish continuity in web shear. It should be noted that noise was heard when approaching failure load and the failure of the panel was abrupt causing a sudden drop in the applied jacking load as shown in the load-deflection relationship in Figure 4.51. Figure 4.52 depicts the normal strain history at the mid-span section. While Figure 4.53 depicts the normal strain distribution at the mid-span location at one-third the experimental ultimate load. It can be observed that the strain distribution appears to be linear within the OSB facing, while it gave unreasonably distributed values at the extreme fibers of the top and bottom plates. It should be noted that strain readings were not used in this study to establish design criteria at the ultimate or serviceability limit states.

Similar failure mode was observed in panels H-11 and H-12. Views of header H-11 after failure are shown in Figures 4.54 and 4.55. One may observe that local bearing failure occurred at the load support at the quarter point location as presented in Figures 55-c and 55-d. This may be attributed to the fabrication since the OSB facing was projecting few millimeters over the top flange plates as shown in Figures 55-c and 55-d. Figure 4.56 shows the load-deflection relationship of header H-11. Figures 4.57 and 4.58 show similar trends of

failure for header H-12 except that local bearing failure at load locations did not occur. Figure 4.59 depicts the load-deflection relationship for header H-12.

Figures 4.51, 4.56, and 4.59 illustrate the jacking load-deflection history of panels H-10, H-11 and H-12, respectively. It can be observed that the ultimate jacking load was 52.23, 52.97 and 53.41 kN for panels H-10, H-11 and H-12, respectively. To determine the design factored ultimate load, a factor of safety of 3 was considered per AC-04. Thus, the design ultimate load for headers H-10, H-11 and H-12 were illustrated in these figures as 17.41, 17.66 and 17.80 kN, respectively. To establish design criteria for serviceability limit state, the jacking loads were determined at the deflection limit of $\text{span}/360$ for live loading and at the deflection limit of $\text{span}/180$ for combined dead and live loading. These values are recorded in these figures as 19.50, 19.64, and 21.86 kN for deflection limit of $\text{span}/360$ and 41.28, 37.25 and 36.32 kN for deflection limit of $\text{span}/180$ for headers, H-10, H-11, and H-12, respectively. These values will be further used to establish design tables for the headers in the form of maximum joist, roof or floor span served by the header. Figure 4.51 for the jacking load-deflection history of header H-10 shows that the header behavior is generally linear elastic for applied loads equal of less the design factored ultimate load of 17.41 kN as well as for the jacking load of 19.50 kN for the $\text{span}/360$ deflection limit. However, the header entered the non-linear range at the jacking load of 41.28 kN for the $\text{span}/180$ deflection limit. Similar behavior was observed for headers H-11 and H-12.

4.6 Group E

In this group, three identical panels (H-13, H-14 and H-15) were tested to complete collapse. Each panel was of 2438.40 mm clear length and 355.60 mm depth. Figures 4.60 to 4.83 summarize the experimental findings for this panel group. Figures 4.60 and 4.61 show different overall views of panel H-15 after failure. While Figures 62 through 68 presents different close-up views of the mode of failure occurred in this header. It can be observed that the main cause of failure on combined shear and flexural failure at the quarter point zone. At this location, the failure line seemed diagonal to the longitudinal axis of the header with tensile fracture in the OSB facing at and near the bottom plates and OSB crushing and local buckling of the chips forming the OSB facing. A failure mode similar to that detected in Group A was observed at the header-wall junction of header H-13 as shown in Figure 4.62 but less severe. Similar failure behavior was observed for header H-13 as presented in Figures 4.70 to 4.74 and header H-14 as presented in Figures 4.77 to 4.82. It should be noted that noise was heard when approaching failure load and the failure was abrupt causing a sudden drop in the applied jacking load failure load as it can be seen in the load-deflection history of these headers.

Figures 4.69, 4.74, and 4.83 illustrate the jacking load-deflection history of panels H-13, H-14 and H-15, respectively. It can be observed that the ultimate jacking load was 35.99, 40.34 and 33.46 kN for panels H-13, H-14 and H-15, respectively. To determine the design factored ultimate load, a factor of safety of 3 was considered per AC-04. Thus, the design ultimate load for headers H-13, H-14 and H-15 were illustrated in these figures as 12.00, 13.45 and 11.15 kN, respectively. To establish design criteria for serviceability limit state, the

jacking loads were determined at the deflection limit of span/360 for live loading and at the deflection limit of span/180 for combined dead and live loading. These values are recorded in these figures as 12.81, 16.62 and 12.76 kN for deflection limit of span/360 and 23.38, 28.61 and 22.47 kN for deflection limit of span/180 for headers, H-13, H-14, and H-15, respectively. These values will be further used to establish design tables for the headers in the form of maximum joist, roof or floor span served by the header. Figure 4.69 for the jacking load-deflection history of header H-13 shows that the header behavior is generally linear elastic for applied loads equal of less the design factored ultimate load of 12.00 kN. However, for serviceability limit state check for deflection limits, the structural behavior was observed to be non-linear. Similar behavior was observed for headers H-14 and H-15. Figure 4.75 depicts the normal strain history at the mid-span section. While Figure 4.76 depicts the normal strain distribution at the mid-span location at one-third the experimental ultimate load. It was observed that no trend was found in the recorded strain data.

4.7 Group F

In this group, three identical panels (H-16, H-17 and H-18) were tested to complete collapse. Each panel was of 2438.40 mm clear length and 660.40 mm depth. Figure 4.84 shows view of header H- 16 after failure. While Figures 4.85 and 4.86 show close-up views of the permanent deformed shape of the header at location of the header-wall interface. It can be observed that the failure mode of the panel was due to flexural deformation of the top flange plates between the quarter points and the supports, associated with either nail bending or nail hole tear-out at the interface between the OSB facing and the top and bottom flange plates near the support and between the OSB facing and the vertical blocking at the end of the OSB

web. The relative vertical movement of the header's OSB facing and the OSB facing of the wall was apparent in Figure 4.85. As such, one can recommend revising the header design to extend the OSB facing to the end of the vertical wall stud or beyond to establish continuity in web shear. It should be noted that noise was heard when approaching failure load and the failure of the panel was abrupt causing a sudden drop in the applied jacking load as shown in the load-deflection relationship in Figure 4.87. Similar failure mode was observed in panels H-17 and H-18. Views of header H-17 after failure are shown in Figures 4.88 and 4.90. Figure 4.91 shows the load-deflection relationship of header H-17. Figures 4.92 through 4.94 show similar trend for header H-18. While Figure 4.95 depicts the load-deflection relationship for header H-18.

Figures 4.87, 4.91, and 4.95 illustrate the jacking load-deflection history of panels H-16, H-17 and H-18, respectively. It can be observed that the ultimate jacking load was 48.01, 50.75 and 48.90 kN for headers H-16, H-17 and H-18, respectively. To determine the design factored ultimate load, a factor of safety of 3 was considered per AC-04. Thus, the design ultimate load for headers H-16, H-17 and H-18 were illustrated in these figures as 16.00, 16.92 and 16.30 kN, respectively. To establish design criteria for serviceability limit state, the jacking loads were determined at the deflection limit of span/360 for live loading and at the deflection limit of span/180 for combined dead and live loading. These values are recorded in these figures as 18.94, 26.48 and 21.53 kN for deflection limit of span/360 and 35.51, 45.46 and 41.54 kN for deflection limit of span/180 for headers, H-16, H-17, and H-18, respectively. These values will be further used to establish design tables for the headers in the form of maximum joist, roof or floor span served by the header. Figure 4.87 for the jacking load-

deflection history of header H-1 shows that the header behavior is generally linear elastic for applied loads equal or less than the design factored ultimate load of 16.00 kN which is the lowest design load for both ULS and SLS design requirements. Similar behavior was observed for headers H-17 and H-18. Figure 4.96 depicts the normal strain history at the mid-span section. While Figure 4.97 depicts the normal strain distribution at the mid-span location at one-third the experimental ultimate load. It can be observed that the strain distribution appears to be linear within the OSB facing, while it gave unreasonably distributed values at the extreme fibers of the top and bottom plates. It should be noted that strain readings were not used in this study to establish design criteria at the ultimate or serviceability limit states.

Chapter V

ANALYSIS and DISCUSSION

5.1 General

Eighteen SIP header panels in full-scale size were experimentally tested, following the ASTM standard testing procedures in order to determine their structural behavior at ultimate load and service load levels. This chapter provides discussion of the experimental results with respect to the failure modes of the tested header panels for possible use in residential construction with emphasis on code requirements for ultimate and serviceability limit states design of such panels. The CSA Wood Design Code procedure for calculating flexure resistance of OSB web beam based on box-beam design procedure, by neglecting the effect of foam, along with a sample calculation of one header panel is presented. Design tables based both on the experimental results and the requirements of Canadian standards are presented at the end of this chapter.

5.2 Experimental Findings

5.2.1 General

For evaluation of experimental results, the Acceptance criteria for Sandwich Panels ICC-ES AC04 (2005) were followed. According to this evaluation report, three tests of each type of header panel group are required. To pass the test qualification criteria, the results can not vary more than 15 percent from the average of the three, unless the lowest test value is

used. The average value of two tests may be used when the higher value does not exceed the lower by more than 5%. Factors of safety are dependent on consistency of materials and the range of test results. Generally, a minimum factor of safety of 3 is applied to the ultimate load based on the average of three tests. Lower factors of safety can be assigned to panels or systems employing consistent physical properties. A factor of safety of 3 is further assumed to obtain header flexural capacity from the recorded experimental failure load.

In Chapter IV, the experimental results are presented in the form of graphs and photos, while in this chapter the experimental findings are summarized in Tables 5.1, 5.2, and 5.3. Table 5.1 presents a summary of experimental results for applied ultimate jacking load while Table 5.2 and Table 5.3 summarizes experimental results for applied jacking load at deflection limit $L/360$ and deflection limit $L/180$, respectively. For each panel group, all tables state if a panel group passed or did not pass the test qualification criteria which happens if the difference between an average value and a corresponding value of any of the three headers is more than 15%. In the case that the qualification criteria were not met, the lowest test value is considered for further evaluation.

5.2.2 Header Group A

In this group, three identical headers (H-1, H-3 and H-3) were tested to complete collapse. Each panel was of 1219.20 mm clear length and of 355.60 mm depth. According to the summary of the results in Table 5.1, the header group passed the test qualification criteria of difference less than 15% for average ultimate jacking load. However, as it is shown in Tables 5.2 and 5.3, the test qualification criteria of difference less than 15% for average

jacking load at deflection limit of $L/360$ and $L/180$ have not been met. As such, the smallest load value of the three was considered for further evaluations.

5.2.3 Header Group B

In this group, three identical headers (H-4, H-5, and H-6) were tested to complete collapse. Each panel was 1219.20 mm long and 660.40 mm deep. According to experimental findings in the Table 5.1, the header group B passed the test qualification criteria of difference less than 15% for average ultimate jacking load. As shown in Table 5.2, this header group also passed the test qualification criteria for average jacking load at deflection limit of $L/360$. However, Table 5.3 shows that the difference between the average value and the jacking loads at deflection limit of $L/180$ is more than 15%. As such, the smallest load value of the three was considered for further evaluations.

5.2.4 Header Group C

In this group, three identical panels (H-7, H-8 and H-9) were tested to complete collapse. Each panel was of 1828.80 mm clear length and of 355.60 mm depth. According the summary in the Tables 5.1, 5.2, and 5.3, the panel group did not pass the test qualification criteria of difference less than 15% for none of the recorded stages of jacking load. Moreover, the experimental test of the panel H-9 was not counted on since the header H-9 was not supported on flat surface as were the other panels. To use the results of this group, the test of the panel H-9 would have to be repeated. According to "*The Acceptance Criteria for SIPs*", the average test value from two tests may be used when the higher value does not exceed the

lower value by more than 5%. This condition was not met. As such, the lowest value for this header group was taken for the further evaluation group.

5.2.5 Header Group D

In this group, three identical panels (H-10, H-11, and H-12) were tested to complete collapse. Each panel was 1828.80 mm long and 660.40 mm deep. The experimental results summarized in Tables 5.1, 5.2, and 5.3 show that this panel group passed qualification criteria of difference less than 15% for all recorded stages of jacking load.

5.2.6 Header Group E

In this group, three identical panels (H-13, H-14 and H-15) were tested to complete collapse. Each panel was of 2438.40 mm clear length and 355.60 mm depth. According the summary in the Table 5.1, the panel group passed the test qualification criteria of difference less than 15% for average ultimate jacking load. However, as it is shown in Tables 5.2, and 5.3, the test qualification criteria of difference less than 15% were not met for both average jacking load at deflection limit of $L/360$ and average jacking load at deflection limit of $L/180$. As such, the smallest load value of the three was considered for further evaluations.

5.2.7 Header Group F

In this group, three identical panels (H-16, H-17 and H-18) were tested to complete collapse. Each panel was of 2438.40 mm clear length and 660.40 mm depth. Table 5.1, this panel group passed the test qualification criteria of difference less than 15% for average ultimate jacking load. Table 5.3 shows that the test qualification criteria were also met for

average jacking load at deflection limit of $L/180$. However, as it is shown in Table 5.2, the test qualification criteria of difference less than 15% for average Jacking load at deflection limit of $L/360$ were not met. As such, the smallest load value of the three was considered for further evaluations.

5.3 Proposed Design Tables

5.3.1 General

The function of headers in a building is to transfer vertical loads from above wall openings to the foundations through a network of structural elements. As it is shown in cross section of few residential houses in Figure 5.1, headers can be situated in different locations and thus – depending on a structural system of a house and the location of the header – the amount of load they need to transfer varies. The width of the opening above which a header is placed is another important factor in determining the structural capacity of headers. Figure 5.2 shows how the length of headers can vary, depending on the size of the wall opening. In general, the load that needs to be transferred is dead load that includes weight of roof, ceilings, floors and walls and live load that is snow load on a roof or live load on the floors. The individual load combinations of the load mentioned above depends on the structural type of a building, location of the header, size of an existing opening and the number of storeys. In a single-storey residential house, the load will be represented by weight of a roof as dead load and snow load as live load. Figure 5.3 illustrates snow load acting on a sloped roof of a residential house.

5.3.2 Code Requirements for the Structural Qualification of SIP Header Panels

The code requirements provided in the National Building Code of Canada (NBCC, 2005) and the general design principles provided in CSA Standard CAN/CSA-O86.1, Engineering Design of Wood, are used to assess the structural adequacy of the tested header panels. Based on provisions in Part 4 and Part 9 of NBCC, the following load and load factors are used to examine the structural adequacy of the headers as serviceability and ultimate limit states design:

Dead load for roofs (DL) = 0.5 kPa

Live load = specified snow load flat roofs (LL) of 1.0, 1.5, 2.0, 2.5 and 3.0 kPa

Dead load factor = 1.25

Live load factor = 1.50

Load Combination = 1.25 DL + 1.5 LL

According to Part 9 of NBCC (2005), deflection limit for serviceability for all beams is span / 360. This condition can be waived in case of roof beams with when replaced with span / 180 if no ceiling is provided. If ceilings other than plaster or gypsum are provided, span / 240 deflection limit is acceptable.

5.3.3 Design Tables

For proprietary structural products that are available on a construction market, the manufactures provide design tables that determine maximum allowable span length or maximum design load that must not be exceeded. In this thesis, an attempt was made to establish design tables (Tables 5.4, 5.5, 5.6 and 5.9) for SIP header panels of different sizes

that were tested in this experimental program. It should be mentioned that the load case that was considered in creating the design tables included dead load and snow load on roofs assuming single-storey building or a header carrying a roof in a multi-storey construction as shown in Figures 5.1.a and 5.1.c. Similar procedure and design tables can be established for headers carrying two or three storeys in residential construction as shown in Figures 5.1.b and 5.1.d.

Based on design ultimate jacking load capacity of each header panel that was determined as $F_{ULT}/3L$ and is summarized in Table 5.1, Table 5.4 provides a summary of the maximum length of roof structural members that can be supported by headers considered in this study. The maximum supported length of the roof joists in the Table 5.4 is calculated as:

$$L_s = \frac{w_d}{1.25 \times DL + 1.5 \times LL}$$

(5.1)

where

L_s is the maximum supported length of roof members (m),

w_d is the design ultimate jacking load capacity in (kN.m) as specified in Table 5.1,

DL is the dead load taken as 0.5 kPa,

LL is the specified snow load on flat roof and taken as 1.0, 1.5, 2.0, 2.5, and 3.0 kPa,

1.25 is the dead load factor, and

1.5 is the live load factor.

It should be noted that “supported length” means half the sum of the joist spans on both sides of the internal header or the joist span of the exterior header in a residential building.

Tables 5.5 and 5.6 present a summary of maximum length of a roof member that can be supported by header panels, based on jacking loads at deflection limit $L/360$ and $L/180$, respectively, that were summarized in Tables 5.2 and 5.3. The maximum supported length in the Tables 5.5 and 5.6 is calculated as:

$$L_s = \frac{W_s}{L_H \times LL}$$

(5.2)

where

L_s is the maximum supported length of a roof member in (m),

W_s is the jacking load capacity in (kN) at deflection limit $L/360$ or $L/180$ as specified in Tables 5.2 and 5.3, respectively,

L_H is the length of a header panel in (mm), and

LL is the specified snow load on flat roof and taken as 1.0, 1.5, 2.0, 2.5, and 3.0 kPa.

As an example for Header Group A, the headers of this group are 1219 mm long and 356 mm deep. Table 5.4 shows that the maximum supported length of the roof or roof joist based on design ultimate jacking load capacity, a roof dead load of 0.5 kPa and specified minimal snow load of values ranging from 1.0 to 3.0 kPa. The served roof joist span is then ranged from 7.80 m to 3.23 m based on the amount of the snow load. Tables 5.5 and 5.6 present the maximum supported length based on jacking load at deflection limits of $L/360$ and $L/180$, respectively. It can be observed that the maximum served roof joist span ranges from 6.62 to 2.21 and from 12.0 m to 4.00 m to limit the live load deflection and the combined dead and live load deflection to span/360 and span/180, respectively. A design table can then be created from Tables 5.4, 5.5 and 5.6 by considering the smallest served joist spans that satisfy

the three design requirements considered herein for ULS and SLS design. Finally, Table 5.9 summarizes the findings in those 3 tables (Tables 5.4, 5.5 and 5.6) and gives the minimum values of the maximum allowable span.

5.4 General Design Procedure for Calculating Web Beam Resistance according to CAN/CSA-O86-01

5.4.1 General

Clause 8.5 of *Canadian Standard for Engineering Design of Wood, CAN/CSA-O86-01 (2001)* specifies the effective stiffness, bending resistance and shear resistance of plywood and OSB Web Beams. This design method is presented in this chapter and then used further for calculating flexural resistance, shear resistance and flexural stiffness of the studies header but with ignoring the presence of core foam. Figure 5.3 shows a panel web beam cross section as illustrated in the Clause 8.5 of the CAN/CSA-O86-01 which is used in the design calculation of header panels.

5.4.2 Effective Stiffness

The effective stiffness, $(EI)_{ef}$ of a web beam shall be taken as

$$(EI)_e = (\sum B_a)K_S \frac{(c_t^3 + c_c^3)}{3} + (EI)_f K_{SE}$$

(5.3)

Where:

$(\sum B_a)$ = sum of axial stiffness of panel webs, N/mm

K_S = service condition factor for web material

$(EI)_f$ = stiffness of flanges with respect to neutral axis of composite section, N/mm^2

K_{SE} = service condition factor for modulus of elasticity of flange

5.4.3 Bending Resistance

The factor bending moment resistance of a web beam shall be the lesser of the factored resistance of the tension or the compression flanges determined as follows:

(a) compression flange

$$M_r = \phi F_c K_{Zc} \frac{(EI)_e}{EK_{SE} C_c}$$

(5.4)

Where:

$\phi = 0.8$ for sawn lumber,

$F_c = f_c (K_D K_{Sc} K_T K_H)$,

f_c = specified strength of flange in compression, MPa,

K_H = system factor,

K_{Zc} = size factor for compression for sawn lumber,

E = modulus of elasticity of flange, MPa,

K_{SE} = service condition factor for modulus of elasticity of flange, and

C_c = distance from neutral axis to compression face.

(b) tension flange

$$M_r = \phi F_t K_{zt} \frac{(EI)_e}{EK_{SE} c_t}$$

(5.5)

Where:

$$\phi = 0.9,$$

$$F_t = f_t (K_D K_{Sc} K_T K_H),$$

f_t = specified strength of flange in tension, MPa,

K_{zt} = size factor for tension for sawn lumber,

E = modulus of elasticity of flange, MPa,

c_t = distance from neutral axis to tension face,

5.4.5 Web Shear-through Thickness

The factored shear resistance of the web of a panel web beam at its neutral axis shall be taken as

$$V_r = \phi V_p X_J \frac{(EI)_e}{EK_{SE} Q_f + 0.5(\sum B_a) K_S c_w^2}$$

(5.6)

where

$$\phi = 0.95,$$

$$V_p = (\sum V_p) (K_D K_S K_T),$$

$(\sum V_p)$ = sum of specified strength of all panel webs in shear-through-thickness, N/mm,

X_J = stress joint factor,

E = modulus of elasticity of flange, MPa,

Q_f = moment of area of flange about neutral axis, mm^3 ,

$(\sum B_a)$ = sum of specified axial stiffness of all panel webs, N/mm, and

C_w = greatest distance from neutral axis to outer edge of web, mm,

5.4.6 Flange -Web Shear

The factored resistance of the glued area between the flange and web of a panel web beam shall be the lesser of the shear capacities of the web or flange components determined as follows:

$$V_{rp} = \phi V_g (\sum b_g X_v) \frac{(EI)_e}{EK_{SE} Q_f}$$

(5.7)

Where:

$(\sum b_g)$ = sum of contact widths between flange and web,

E = modulus of elasticity of flange, MPa,

Q_f = moment of area of flange about neutral axis, mm^3 ,

a) for web:

$\phi = 0.95$,

$V_g = v_{pf}(K_D K_S K_T)$,

v_{pf} = specified strength in planar shear, MPa,

X_v = shear modification factor,

b) for flange:

$\phi = 0.9$,

$$V_g = f_v(K_D K_{Sv} K_T),$$

V_{pf} = specified strength in shear, MPa, and

$$X_v = 2.0.$$

5.4.7 Deflection

Deflection shall be calculated as the sum of the deflections due to moment, using the effective stiffness, $(EI)_e$, and due to shear as determined by the following formula:

$$\Delta_s = \frac{B_a M h^2 X_s}{B_v (EI)_e}$$

(5.8)

Where:

B_a = specified axial stiffness, N/mm,

M = maximum bending moment due to specified loads, N/mm,

h = height of web beam, mm,

X_s = section shear coefficient, and

B_v = specified shear rigidity, N/mm.

5.5 Calculations of Flexural Resistance of Header Panels

5.5.1 General

In this part of the Chapter V, the flexural resistance, shear resistance, and flexural stiffness of the header panels are calculated. The calculations follow the design procedure as specified in Clause 8.5 of CAN/CSA-O86-01 that was summarized in section 5.4 of this chapter. Two sets of calculations of the flexural resistance of the headers are presented in the

sections 5.6 and 5.7, taking into account two different cross sections of the headers. The first set of calculations applies to 356-mm deep header panels that belong to header groups A, C, and E. The second set of calculations applies to 660 mm deep headers that belong to header groups B, D, and F. It should be noted that the resisting moment, shear and flexural stiffness depend only on the cross section geometry of the headers and do not depend on the length of the headers. The exception is the coefficient factor for compression for sawn lumber, K_{Zc} which in general, is dependent on the length of the beam. However, when substituting the different length of each header to the equation to calculate this coefficient, the value K_{Zc} becomes the same for all headers. The flexural resistance, shear resistance and flexural stiffness for all header panels are summarized in Table 5.7, while Appendix I includes the CAN/CSA-O86-01 tables that are used in the calculations of the flexural resistance of the header panels.

5.5.2 Geometrical Characteristics and Other Specifications of the Headers

Figure 5.4 shows cross section of box web beam as is illustrated in CAN/CSA-O86-01. Figure 5.5 shows geometrical characteristic of the cross section of 356 mm deep header panels, while Figure 5.6 illustrate the headers that are 660 mm deep. According to these figures, the cross-section characteristics that are further used in the calculations are summarized as:

1) For the 356-mm deep header:

$$h = 356 \text{ mm}, c_c = c_t = 178 \text{ mm}, y_c = y_t = 140 \text{ mm}, h_c = h_t = 76 \text{ mm}$$

2) For the 360-mm deep header:

$$h = 660 \text{ mm}, c_c = c_t = 330 \text{ mm}, y_c = y_t = 292 \text{ mm}, h_c = h_t = 76 \text{ mm}$$

Regarding the material characteristics of the headers, Thermapan Industries Inc. specifies that the webs of the SIP header are made of two equal layers of APA rated sheathing, 11 mm (7/16") OSB and sawn lumber compression and tension flanges are of No.1 Grade S-P-F. For the calculations, dry service conditions are assumed. The headers are assumed to be simply-supported at its header-posts connections. Thus, the length of a box beam considered in the calculations is the clear length of the header.

5.5.3 Coefficients

In the calculations of bending and shear resistance and deflections of the headers, the following coefficients determined according to CAN/CSA-O86-01 are used:

$K_D = 1.0$ (Table 4.3.2.2 "Load duration factor" – determined for "standard load duration")

$K_{Sc} = 1.0$ (Table 5.4.2 "Service condition factor for compression parallel to grain" – determined for "dry service condition")

$K_{St} = 1.0$ (Table 5.4.2 "Service condition factor for tension parallel to grain" – determined for "dry service condition")

$K_T = 1.0$ (Table 5.4.3 "Treatment factor" – determined for "dry service condition, untreated lumber")

$K_H = 1.1$ (Table 5.4.4 "System factor" – determined for "built-up beam in bending")

$K_{SE} = 1.0$ (Table 5.4.2 "Service condition factor for modulus of elasticity of flange", determined for "dry service condition")

$K_{Zt} = 1.3$ (Table 5.4.5 "Size factor" – determined for "sawn lumber in tension")

K_{Zc} (Table 5.4.5 and Clause 5.5.6.2.2 "Size factor" – determined for "sawn lumber in compression")

$K_{Zc} = 6.3(dL)^{-0.13}$ but not more than 1.3 $K_{Zc} = 6.3(76 \times L)^{-0.13} = 6.3(46 \times 1219)^{-0.13} = 1.42$, taken as $K_{Zc} = 1.3$

For the three different clear lengths of headers, coefficient K_{Zc} was determined as follows:

- 1) For header Group "A" and "B", clear length $L = 1219$ mm, thus $K_{Zc} = 1.42$, take $K_{Zc} = 1.3$
- 2) For header Group "C" and "D", clear length $L = 1829$ mm, thus $K_{Zc} = 1.35$, take $K_{Zc} = 1.3$
- 3) For header Group "E" and "F", clear length $L = 2438$ mm, thus $K_{Zc} = 1.30$

It should be noted that the coefficients determined above are the same for all headers - as they depend on the wood properties not on the geometrical characteristics of the headers. The coefficient K_{Zc} depends on the length of a beam but as it is shown in the text above, the value of K_{Zc} remains the same for all header panels.

5.6 Calculations of the Flexural Resistance of the 356-mm deep Headers (Groups A, C, and E)

5.6.1 Calculation of the Moment Resistance of the Headers

The bending resistance of a panel is the lesser of

$$(a) \quad M_r = \phi F_c K_{Zc} \frac{(EI)_e}{EK_{SE} C_c} \quad (\text{compression flange}),$$

where

$\phi = 0.8$ for sawn lumber in compression

$F_c = f_c(K_D K_{Sc} K_T K_H)$, where

$f_c = 7.9$ MPa (Table 5.3.1C “Specified strength of flange in compression” determined for S-P-F No.1, “parallel to grain”), thus

$$F_c = f_c(K_D K_{Sc} K_T K_H) = 7.9(1 \times 1 \times 1 \times 1.1) = 8.69 \text{ MPa}$$

$$(b) \quad M_r = \phi F_t K_z \frac{(EI)_e}{EK_{SE} c_t} \quad (\text{tension flange}),$$

where

$\phi = 0.9$ for sawn lumber in tension

$F_t = f_t(K_D K_{Sc} K_T K_H)$, where

$f_t = 4.9$ MPa (Table 5.3.1C “Specified strength of flange in tension” determined for S-P-F No.1, “parallel to grain”), thus

$$F_t = f_t(K_D K_{Sc} K_T K_H) = 4.9(1 \times 1 \times 1 \times 1.1) = 5.39 \text{ MPa}$$

and

$E_f = 8500$ MPa (Table 5.3.1C “Modulus of elasticity of flange”, MPa - determined for S-P-F No.1)

$I_f =$ moment of inertia of the flanges about the neutral axis.

Thus I_f is determined as follows:

$$I_f = 2 \left[\frac{140 \times 76^3}{12} + 140 \times 76 \times 140^2 \right] = 427.33 \times 10^6 \text{ mm}^4$$

$(EI)_f$ is the stiffness of flanges with respect to neutral axis of composite section, N/mm^2 is determined as follows:

$$(EI)_e = \left(\sum B_a \right) K_s \frac{(c_t^3 + c_c^3)}{3} + EI_f K_{SE},$$

where

$(\sum B_a) = 2 \times 22000 \text{ N/mm} = \text{sum of axial stiffness of panel webs, (Table 7.3C - "Axial stiffness" determined for "Type I (Standard) Design-Rated OSB")}$

Thus

$$(EI)_e = 2 \times 22000 \times 1 \left(\frac{178^3 + 178^3}{3} \right) + 8500 \times 427.33 \times 10^6 \times 1 = 0.3798 \times 10^{13} \text{ MPa/mm}^4$$

The bending moment resistance is the lesser of

$$(a) M_{rc} = 0.8 \times 8.69 \times 1.3 \times \frac{0.3798 \times 10^{13}}{8500 \times 178 \times 1} = 22.68 \text{ kN.m}$$

$$(b) M_{rt} = 0.9 \times 5.39 \times 1.3 \times \frac{0.3798 \times 10^{13}}{8500 \times 178 \times 1} = 15.83 \text{ kN.m}$$

Thus the bending resistance for header of Group A is $M_r = 15.83 \text{ kN.m}$ as presented in Table 5.7.

5.6.2 Calculation of the Shear Resistance of the Headers

The factored shear resistance of the header at its neutral axis is taken as

$$V_r = \phi V_p X_J \frac{(EI)_e}{EK_{SE} Q_f + 0.5(\sum B_a) K_S c_w^2}$$

where

$$\phi = 0.95$$

$V_p = (\sum V_p) (K_D K_S K_T) (\sum V_p) = 35 \text{ N/mm} = \text{sum of specified strength of all panel webs in shear-through-thickness, (Table 7.3C - "Shear-through-thickness" determined for "Type I (Standard) Design-Rated OSB")}$

$$\text{Thus } V_p = 2 \times 35 (1 \times 1 \times 1) = 70 \text{ N/mm}$$

$X_J = 0.6$ = stress joint factor (Table 7.4.4.1 – determined for slope 1:4, which is the limit for OSB scarf joints (Clause 8.4.3.1))

$(\sum B_a)$ = sum of specified axial stiffness of all panel webs, N/mm

C_w = greatest distance from neutral axis to outer edge of web, mm

Q_f = moment of area of flange about neutral axis, mm^3

Q_f is determined as follows:

$$Q_f = (140 \times 76) \times 292 = 3106.9 \times 10^3 \text{ mm}^3$$

Thus,

$$V_r = 0.95 \times 70 \times 0.6 \times \frac{0.3798 \times 10^{13}}{8500 \times 1 \times 1489.6 \times 10^3 + 0.5 \times 2 \times 22000 \times 1 \times 178^2} = 11\,344 \text{ N}$$

The shear resistance for header panel of Group A is $V_r = 11.34 \text{ kN}$ as shown in Table 5.7.

5.6.3 Calculation of the Deflection of the Headers

The shear deflection of the headers due to live load is determined as:

$$\Delta_s = \frac{B_a M h^2 X_s}{B_v (EI)_e}$$

where

$B_a = 22000 \text{ N/mm}$ = specified axial stiffness, N/mm

$B_v = 11000 \text{ N/mm}$ = specified shear rigidity, (Table 7.3C)

X_s = section shear coefficient – to be calculated from Figure 8.5.6 of the Standard, based on

$$\frac{h_f}{h} \text{ and } \sum \frac{t}{b_i}$$

For header of panel Group A, X_s is determined as follows:

$$\frac{h_f}{h} = \frac{76}{356} = 0.213 \text{ and } \sum \frac{t}{b_i} = \frac{2 \times 11}{356 - 2 \times 76} + \frac{2 \times 76}{140} = 1.19, \text{ thus } X_s = 0.10$$

Based on live load deflection limit $L/180$, the total deflection is calculated as:

$$\Delta_T = \frac{5 \times wL^4}{384 \times (EI)_s} + \frac{B_a M h^2 X_s}{B_v (EI)_e} \quad (5.9)$$

where

$(EI)_{ef} = 0.3798 \times 10^{13} \text{ MPa/mm}^4$ is effective stiffness of a web beam and equals, and

L is length of the header for each header group.

Based on this equation, the maximum uniform load of the header can be obtained at the serviceability limit state.

5.7 Calculation of the Flexural Resistance of 660-mm deep Headers (Groups B, D, and F)

5.7.1 Calculation of the Moment Resistance of the Headers

The bending resistance of a header is the lesser of

$$(a) \quad M_r = \phi F_c K_{Zc} \frac{(EI)_e}{EK_{SE} C_c} \text{ (compression flange),}$$

Where:

$$K_{Zc} = 6.3(76 \times L)^{-0.13} = 6.3(46 \times 1219)^{-0.13} = 1.42, \text{ take } K_{Zc} = 1.3$$

$\phi = 0.8$ for sawn lumber in compression

$F_c = f_c(K_D K_{Sc} K_T K_H)$, where

$f_c = 7.9$ MPa (Table 5.3.1C “Specified strength of flange in compression” determined for S-P-F No.1, “parallel to grain”), thus

$$F_c = f_c(K_D K_{S_c} K_T K_H) = 7.9(1 \times 1 \times 1 \times 1.1) = 8.69 \text{ MPa}$$

$$(b) \quad M_r = \phi F_t K_z \frac{(EI)_e}{EK_{SE} c_t} \quad (\text{tension flange}),$$

Where:

$\phi = 0.9$ for sawn lumber in tension

$F_t = f_t(K_D K_{S_c} K_T K_H)$, where

$f_t = 4.9$ MPa (Table 5.3.1C “Specified strength of flange in tension” determined for S-P-F No.1, “parallel to grain”), thus

$$F_t = f_t(K_D K_{S_c} K_T K_H) = 4.9(1 \times 1 \times 1 \times 1.1) = 5.39 \text{ MPa}$$

and

$E_f = 8500$ MPa (Table 5.3.1C “Modulus of elasticity of flange”, MPa - determined for S-P-F No.1)

$I_f =$ moment of inertia of the flanges about the neutral axis.

Thus I_f is determined as follows:

$$I_f = 2 \left[\frac{140 \times 76^3}{12} + 140 \times 76 \times 292^2 \right] = 1824.66 \times 10^6 \text{ mm}^4$$

$(EI)_f$ is the stiffness of flanges with respect to neutral axis of composite section, N/mm^2 is determined as follows:

$$(EI)_e = \left(\sum B_a \right) K_S \frac{(c_t^3 + c_c^3)}{3} + EI_f K_{SE},$$

Where:

$(\sum B_a) = 2 \times 22000 \text{ N/mm} = \text{sum of axial stiffness of panel webs, (Table 7.3C - "Axial stiffness" determined for "Type I (Standard) Design-Rated OSB")}$

Thus

$$(EI)_e = 2 \times 22000 \times 1 \left(\frac{330^3 + 330^3}{3} \right) + 8500 \times 1824.66 \times 10^6 \times 1 = 1.656 \times 10^{13} \text{ MPa/mm}^4$$

The bending moment resistance is the lesser of

$$(a) M_{rc} = 0.8 \times 8.69 \times 1.3 \times \frac{1.656 \times 10^{13}}{8500 \times 330 \times 1} = 53.35 \text{ kN.m}$$

$$(b) M_r = 0.9 \times 5.39 \times 1.3 \times \frac{1.656 \times 10^{13}}{8500 \times 330 \times 1} = 37.23 \text{ kN.m}$$

Thus the bending resistance for header of panel group B is $M_r = 37.23 \text{ kN.m}$ as shown in Table 5.7.

5.7.2 Calculation of the Shear Resistance of the Headers

The factored shear resistance of the header at its neutral axis is taken as

$$V_r = \phi V_p X_J \frac{(EI)_e}{EK_{SE} Q_f + 0.5(\sum B_a) K_S c_w^2}$$

where

$$\phi = 0.95$$

$V_p = (\sum V_p) (K_D K_S K_T) (\sum V_p) = 35 \text{ N/mm} = \text{sum of specified strength of all panel webs in shear-through-thickness, (Table 7.3C - "Shear-through-thickness" determined for "Type I (Standard) Design-Rated OSB")}$

Thus $V_p = 2 \times 35(1 \times 1 \times 1) = 70 \text{ N/mm}$

$X_j = 0.6 =$ stress joint factor (Table 7.4.4.1 – determined for slope 1:4, which is the limit for OSB scarf joints (Clause 8.4.3.1))

$(\sum B_a) =$ sum of specified axial stiffness of all panel webs, N/mm

$C_w =$ greatest distance from neutral axis to outer edge of web, mm

$Q_f =$ moment of area of flange about neutral axis, mm^3

where Q_f is determined as follows:

$$Q_f = (140 \times 76) \times 140 = 1489.6 \times 10^3 \text{ mm}^3$$

Thus,

$$V_r = 0.95 \times 70 \times 0.6 \times \frac{1.656 \times 10^{13}}{8500 \times 1 \times 3106.9 \times 10^3 + 0.5 \times 2 \times 22000 \times 1 \times 330^2} = 22\,939 \text{ N}$$

The shear resistance for Section “2” is $V_r = 22.94 \text{ kN}$ as shown in Table 5.7.

5.7.3 Calculation of the Deflection of the Headers

Deflection of the header panels is determined as:

$$\Delta_s = \frac{B_a M h^2 X_s}{B_v (EI)_e}$$

where

$B_a = 22000 \text{ N/mm} =$ specified axial stiffness, N/mm

$B_v = 11000 \text{ N/mm} =$ specified shear rigidity, (Table 7.3C)

$X_s =$ section shear coefficient – to be calculated from Figure 8.5.6 of the Standard, based on

$$\frac{h_f}{h} \text{ and } \sum \frac{t}{b_t}$$

X_s is determined as follows:

$$\frac{h_f}{h} = \frac{76}{660} = 0.115 \text{ and}$$

$$\sum \frac{t}{b_t} = \frac{2 \times 11}{660 - 2 \times 76} + \frac{2 \times 76}{140} = 1.13, \text{ thus } X_s = 0.10$$

Based on live load deflection limit $L/180$, the total deflection is calculated as:

$$\Delta_T = \frac{5 \times wL^4}{384 \times (EI)_s} + \frac{B_a M h^2 X_s}{B_v (EI)_e}$$

where

$(EI)_{ef} = 1.656 \times 10^{13} \text{ MPa/mm}^4$ is effective stiffness of a web beam and equals, and

L is length of the header for each header group.

Based on this equation, this maximum uniform load over the header can be obtained at the serviceability limit state.

5.8 Comparison between CAN/CSA-O86-01 Calculations and Experimental Findings

In this part of the Chapter V, the uniformly distributed loads on the headers as obtained based on the box beam calculations as well as the experimental findings are summarized in Table 5.8. Based on the simple-beam formulas, the maximum uniform load that can be carried by an individual header is calculated and compared with the uniform load capacity of a header obtained from the tests results. For each header group, the theoretical uniform load based on calculated resistance moment, resisting shear and deflection limit of span/360 of simulated box beam were determined as follows.

The uniform load based on resisting moment is determined as

$$w_M = \frac{8M_r}{L^2}$$

(5.10)

The uniform load based on shear resistance is determined as

$$w_V = \frac{2V_r}{L}$$

(5.11)

The uniform load based on flexural stiffness is determined as

$$w_\Delta = \frac{8M}{L^2} \tag{5.11}$$

(5.12)

It can be observed from Table 5.8 that the uniform load based on shear resistance of the header panels is critical in evaluating the structural capacity of the headers considering that foam core is not accounted for. When comparing the theoretical shear capacity of the box beams and the experimental findings, it can be observed that:

- 1) For header Group A, the uniform load based on shear resistance is 11 % higher than the design ultimate uniform load capacity determined based on the experimental results.
- 2) For header Group B, the uniform load based on shear resistance is 46.5 % higher than the design ultimate uniform load capacity determined based on the experimental results.
- 3) For header Group C, the uniform load based on shear resistance is 52 % higher than the design ultimate uniform load capacity determined based on the experimental results.

- 4) For header Group D, the uniform load based on shear resistance is 61.5 % higher than the design ultimate uniform load capacity determined based on the experimental results.
- 5) For header Group E, the uniform load based on shear resistance is 46 % higher than the design ultimate uniform load capacity determined based on the experimental results.
- 6) For header Group F, the uniform load based on shear resistance is 64 % higher than the design ultimate uniform load capacity determined based on the experimental results.

Overall, the uniform load based on the shear resistance calculations is considerably higher (i.e. 46.8 % in average) than the design capacity based on the results of the experimental testing. The design uniform load based on the calculated moment resistance of headers – if compared to design capacity based on experimental results – exceeds this percentage value even more. For header groups A, B, C, D, E and F, the uniform design load based on calculated moment resistance is observed to be 80 %, 90 %, 84 %, 89 %, 76.5 % and 86 % higher than the design ultimate uniform load capacity determined from the experimental results, respectively. One may conclude that the discontinuity of the OSB facing in header at the header-wall interface contributed to lowering the design capacity as depicted in Table 5.8.

Chapter VI

SUMMARY, CONCLUSION AND RECOMMENDATION

6.1 Summary

An extensive experimental program was conducted to investigate the static behavior of structural insulated foam-timber headers under flexural loading. A literature review was conducted in order to establish the foundation of the study. The experimental program included testing to-collapse 18 actual-size timber headers according to ASTM standards. Discussion of the experimental results with respect to the structural adequacy of tested headers for possible use in residential construction with emphasis on code requirements for ultimate and serviceability limit states design of such panels was presented.

6.2 Conclusion

Based on the experimental finding theoretical calculations, the following conclusions can be drawn:

- 1) The dominant failure mode in the headers considered in this study is due to large flexural deformation of the top flange plates between the quarter points and the supports, associated with either nail bending or nail hole tear-out at the interface between the OSB facing and the top and bottom flange plates near the support and between the OSB facing and the vertical blocking at the end of the OSB web. In addition, the relative vertical movement of the header's OSB facing and the OSB facing of the wall was apparent, all due to the discontinuity of the OSB facing with the wall.

- 2) Based on the failure mode stated above and the header configuration as supplied by the manufacturer, it is recommended to revise the header design to extend the OSB facing to the end of the vertical wall stud or beyond to establish continuity in web shear.
- 3) Other failure criterion was observed in some headers as flexural-shear failure in the OSB facing at the quarter point load location. This failure occurred in association with the failure mode mentioned above as a result of the discontinuous OSB facing at the supports.
- 4) Based on the experimental finding, design table for the maximum roof joist served by selected header sizes is developed for use in practice. This design table is limited to headers carrying a single roof. However, this design table can be extended for headers carrying floors and a roof by following the same concept in producing this design table. Also, this design table is limited to selected header sizes and their material characteristics, the adhesive type, and nail size and spacing used to fabricate these headers.
- 5) The uniform load determined from the calculated flexural resistance, shear resistance and flexural stiffness of a box-beam section based on design procedure specified in CAN/CSA-O86-01 exceed the design ultimate uniform load capacity determined from the experimental results. This may be attributed to the discontinuity of the OSB facing of the header at the interface with the supporting wall.

6.3 Recommendations for Future Research

- 1) Observing that the primary failure mode occurs in vertical shear at the interface of the OSB facing and the supporting wall gives the suggestion that the SIP header-posts connection is adequate to transfer the shear forces at the supports. However, this does not imply the size of the post (i.e. timber stud) connected to the end of the wall is enough to carry the header load

since the length of this stud was limited to about 300 mm length. As such, it is recommended that a wall panel with end stud it to be tested to-collapse by applying a concentrated load over the stud while stabilizing the wall during the test. This would assist in determining the stud load carrying capacity as influenced by column buckling as well as the nail size and spacing used to connect the stud to the wall panel to carry the header reaction forces.

- 2) Conduct the finite-element analysis of the tested headers to develop empirical expressions for the ultimate and serviceability capacity for various sizes of SIP header panels.
- 3) Develop an enhanced header-wall connection to provide continuity in shear and hence increase the header's load carrying capacity.
- 4) Study the long-term creep behavior of the headers under sustained loading since it is expected to affect the deflection limit of $\text{span}/180$ for combined dead and live loading.

REFERENCES

- APA, "Design and Fabrication of Plywood Sandwich Panels", APA – The Engineering Wood Association, Tacoma, WA, USA (1993).
- APA, "Load-Bearing Plywood Sandwich Panels", APA – The Engineering Wood Association, Tacoma, WA, USA, (1993).
- ASTM, "Standard Test Methods of Conducting Strength Tests of Panels for Building Construction, ASTM E72-02". American Society for Testing Materials, Philadelphia, PA, USA, (2002).
- ASTM, "Standard Test Methods for Determining Structural Capacities of insulated Panels. ASTM E 1803-96", American Society for Testing Materials, Philadelphia, PA, USA, (1988).
- Butt, A.S, "Experimental Study on the Flexural Behavior of Structural Insulated Sandwich Timber Panels", M.A.Sc. Thesis, Ryerson University, Toronto, Canada, (2008).
- Canadian Standard Association, "Construction of Preserved Wood Foundation, CAN/CSA-S406-92", Etobicoke, Ontario, Canada, (1992).
- Canadian Standard Association, "Engineering Design of Wood", Etobicoke, Ontario, Canada, (2001).
- Canadian Wood Council, "Wood Design Manual, 2005", Ottawa, Canada, (2005).
- Fisette, P., "Calculating Loads on Headers and Beams", Building Materials and Wood Technology, University of Massachusetts, Amherst, USA, Journal of Light Construction, www.umass.edu/bmawt/publications/articles , (2005).

- Fisette, P., "Sizing Engineered Beams and Headers", Building Materials and Wood Technology, University of Massachusetts, Amherst, USA, Journal of Light Construction, www.umass.edu/bmawt/publications/articles, (2003).
- Gagnon, M.A., Adams, R.D., "A Marketing Profile of the U.S. Structural Insulated Panel Industry", Forest Products Journal, Jul/Aug (1999); 49, 7/8.
- Hunt, M.O., "Structural Particleboard for Webs of Composite Beams?", Forest Products Journal, (1974).
- Hunt, M.O. et al., "Pilot test of Four 16-Foot, Wood-Based Composite Garage Headers", Forest Products Journal, (1977).
- ICC AC04, "Acceptance Criteria for Sandwich Panels", International Code Council (ICC) Evaluation Service Inc., USA, (2007).
- ICC AC130, "Acceptance Criteria for Prefabricated Wood Shear Panels", International Code Council (ICC) Evaluation Service Inc., USA, (2007).
- Institute for Research in Construction, "National Building Code of Canada, NBCC-2005", National Research Council, Ottawa, Ontario, Canada, (2005).
- Institute for Research in Construction, "Technical Guide for Stressed Skin Panels (with lumber 1200 mm o.c. and EPS Core) for Walls and Roofs", National Research Council, Ottawa, Ontario, Canada, (2007).
- Kermani, A. et al., "Influence of Cross-Section on the Strength of Timber Beams", Proceedings of the Institution of Civil Engineers, Structures and Buildings, April (2006).
- Kermani, A., "Investigating the Structural Performance of Multi-Webs I-Beams", Journal of the Institute of Wood Science, (2006).

- Kermani, A., Hairstans, R., "Racking Performance of Structural Insulated Panels", *Journal of Structural Engineering*, Nov. (2006).
- Kermani A., "Performance of Structural Insulated Panels", *Proceedings of the Institution of Civil Engineers, Structures and Buildings*, Feb. (2006).
- Kosny, J., Desjarlais, A., Christian, J., "Whole Wall Rating/Label for Structural Insulated Panels: Steady-State Thermal Analysis", *Oak Ridge National Laboratory Buildings Technology Center*, June (1999).
- Lewicke, E.T., "Web behavior in Wood Composite Box Beams", *MASc. Thesis, University of Alberta, Canada* (1992).
- Li, X., "Composite Beams of Cold Form Steel Sections and Wood Members", *MASc., Thesis, The University of New Brunswick, Canada* (2005).
- Malko, P., "Engineering for SIPs", *SIPA presentation, Build Boston Presentation* (2008).
- Menun, C.A., "Reliability-based Optimization of Plywood-Web Beams", *M.A.Sc. Thesis, The University of British Columbia, Canada* (1988).
- Milner, H.R., Tan, H.H., "Modelling deformation in Nailed, Thin-webbed timber Box Beams", *Computers and Structures* (2001).
- Mullens, M.A., Arif, M., "Structural Insulated Panels: Impact on the Residential Construction Process", *Journal of Construction Engineering and Management*, July (2006).
- Murus, *Structural Insulated panels*, (2008), www.murus.com.
- Payne, R.J., "Plywood Construction Manual", 2nd edition, *Council of the Forest Industries of British Columbia, Vancouver, Canada* (1971).
- Racher, P., "Effect of Web Stiffness on the Bending Behavior of Timber Composite I-Beams", *Materials & Design* (2005).

Structural Board Association, (2004), "OSB Performance by Design Manual: Construction Sheathing and Design Rated Oriented Strand Board", Markham, Ontario, Canada, (2004).

Structural Insulated Panel Association (SIPA), 2007, www.sips.org.

Thermapan Structural Insulated Panels Inc. 2007. www.thermapan.com.

Wang, S.M.T., "Shear Behavior of OSB wood Composite I-beams with Web Openings", M.A.Sc., Thesis, University of Alberta, Canada (1994).

1	1970-1971	1970-1971	1970-1971
2	1972-1973	1972-1973	1972-1973
3	1974-1975	1974-1975	1974-1975
4	1976-1977	1976-1977	1976-1977
5	1978-1979	1978-1979	1978-1979
6	1980-1981	1980-1981	1980-1981
7	1982-1983	1982-1983	1982-1983
8	1984-1985	1984-1985	1984-1985
9	1986-1987	1986-1987	1986-1987
10	1988-1989	1988-1989	1988-1989
11	1990-1991	1990-1991	1990-1991
12	1992-1993	1992-1993	1992-1993
13	1994-1995	1994-1995	1994-1995
14	1996-1997	1996-1997	1996-1997
15	1998-1999	1998-1999	1998-1999
16	2000-2001	2000-2001	2000-2001
17	2002-2003	2002-2003	2002-2003
18	2004-2005	2004-2005	2004-2005
19	2006-2007	2006-2007	2006-2007
20	2008-2009	2008-2009	2008-2009
21	2010-2011	2010-2011	2010-2011
22	2012-2013	2012-2013	2012-2013
23	2014-2015	2014-2015	2014-2015
24	2016-2017	2016-2017	2016-2017
25	2018-2019	2018-2019	2018-2019
26	2020-2021	2020-2021	2020-2021
27	2022-2023	2022-2023	2022-2023
28	2024-2025	2024-2025	2024-2025

TABLES

No.	Description	Unit	Quantity	Rate	Amount
1
2
3
4
5
6
7
8
9
10
11
12
13
14
15
16
17
18
19
20
21
22
23
24
25
26
27
28
29
30
31
32
33
34
35
36
37
38
39
40
41
42
43
44
45
46
47
48
49
50
51
52
53
54
55
56
57
58
59
60
61
62
63
64
65
66
67
68
69
70
71
72
73
74
75
76
77
78
79
80
81
82
83
84
85
86
87
88
89
90
91
92
93
94
95
96
97
98
99
100

Table 3.1 Main characteristic of standard SIPs as specified by Thermapan

SIP Thickness	4.5"	6.5"	8.25"	10.25"	12.25"
EPS Core Thickness	3-5/8"	5-5/8"	7-3/8"	9-3/8"	11-3/8"
Dimensional Lumber	2x4	2x6	2x8	2x10	2x12
Weight (lbs/sq.ft.)	3.13	3.32	3.48	3.66	3.84
R-Value	19.147	29.147	37.897	47.897	57.897

Table 3.2 Allowable axial loads for header panels as specified by Thermapan

	Panel Dimension				
Skin Thickness	7/16"	7/16"	7/16"	7/16"	7/16"
Core Thickness	5-5/8"	5-5/8"	5-5/8"	5-5/8"	5-5/8"
Panel Depth	6-1/2"	6-1/2"	6-1/2"	6-1/2"	6-1/2"
Flanges	2x6	2x6	2x6	2x6	2x6
Header Height (inches)	13.5	16	20	24	48
Length of opening (feet)	Allowable Axial Loads (Pounds per Linear Foot)				
4	1825	2170	2500	2500	2500
6	1215	1445	1666	1666	1666
8	910	1085	1250	1250	1250
10	710	860	1000	1000	1000
12	545	695	833	833	833
16	305	390	625	625	625

Table 3.3 Geometric characteristics of tested header panels

Group	Test No.	Panel size - clear length × depth, inches (mm)	Panel size - total length × depth, inches (mm)	Thickness of sheathing, inches (mm)	Panel size - width, inches (mm)
A	H-1	14 × 48 (355 × 1219)	24 × 72 (610 × 1829)	7/16" (11.1)	6 ½" (165.1)
	H-2	14 × 48 (355 × 1219)	24 × 72 (610 × 1829)	7/16" (11.1)	6 ½" (165.1)
	H-3	14 × 48 (355 × 1219)	24 × 72 (610 × 1829)	7/16" (11.1)	6 ½" (165.1)
B	H-4	26 × 48 (660 × 1219)	36 × 72 (914 × 1829)	7/16" (11.1)	6 ½" (165.1)
	H-5	26 × 48 (660 × 1219)	36 × 72 (914 × 1829)	7/16" (11.1)	6 ½" (165.1)
	H-6	26 × 48 (660 × 1219)	36 × 72 (914 × 1829)	7/16" (11.1)	6 ½" (165.1)
C	H-7	14 × 72 (355 × 1829)	24 × 96 (610 × 2438)	7/16" (11.1)	6 ½" (165.1)
	H-8	14 × 72 (355 × 1829)	24 × 96 (610 × 2438)	7/16" (11.1)	6 ½" (165.1)
	H-9	14 × 72 (355 × 1829)	24 × 96 (610 × 2438)	7/16" (11.1)	6 ½" (165.1)
D	H-10	26 × 72 (660 × 1829)	36 × 96 (914 × 2438)	7/16" (11.1)	6 ½" (165.1)
	H-11	26 × 72 (660 × 1829)	36 × 96 (914 × 2438)	7/16" (11.1)	6 ½" (165.1)
	H-12	26 × 72 (660 × 1829)	36 × 96 (914 × 2438)	7/16" (11.1)	6 ½" (165.1)
E	H-13	14 × 96 (355 × 2438)	24 × 120 (610 × 3048)	7/16" (11.1)	6 ½" (165.1)
	H-14	14 × 96 (355 × 2438)	24 × 120 (610 × 3048)	7/16" (11.1)	6 ½" (165.1)
	H-15	14 × 96 (355 × 2438)	24 × 120 (610 × 3048)	7/16" (11.1)	6 ½" (165.1)
F	H-16	26 × 96 (660 × 2438)	36 × 120 (914 × 3048)	7/16" (11.1)	6 ½" (165.1)
	H-17	26 × 96 (660 × 2438)	36 × 120 (914 × 3048)	7/16" (11.1)	6 ½" (165.1)
	H-18	26 × 96 (660 × 2438)	36 × 120 (914 × 3048)	7/16" (11.1)	6 ½" (165.1)

Table 3.4 Header configuration – dimensions as specified by Thermapan Inc. and as measured before testing

Panel Group	Panel #	D	L	l	a1	d2	d1	a2
A	Specified by Thermapan	24"	48"	72"	14"	10"	12"	12"
	H-1	24"	48"	72"	14"	10"	12"	12"
	H-2	22"	48"	72 ¼"	14"	8"	12 ¼"	12"
	H-3	24"	48 ½"	72"	14"	10"	12 ¼"	12 ¼"
B	Specified by Thermapan	35"	48"	72"	26"	10"	12"	12"
	H-4	35"	48"	72"	26"	9 ¼"	12"	12"
	H-5	35 ½"	48"	72"	26"	9 ½"	12 ¼"	11 ¾"
	H-6	36"	48"	72"	26"	10"	12"	12"
C	Specified by Thermapan	24"	72"	95"	14"	10"	12"	12"
	H-7	24"	71 ¾"	95 ¾"	14 ¼"	9 ¾"	12"	12"
	H-8	24"	72"	95"	14"	10"	11 ½"	11 ½"
	H-9	24"	71 ¾"	96"	14"	10"	12"	12 ¼"
D	Specified by Thermapan	36"	72"	96"	26"	10"	12"	12"
	H-10	36"	72"	96"	26 ¼"	9 ¾"	9 ¾"	12"
	H-11	36"	71 ½"	96"	26"	10"	11 ½"	10"
	H-12	36"	72 ¾"	96"	26"	10"	11 ¾"	11 ½"
E	Specified by Thermapan	24"	96"	120"	14"	10"	12"	12"
	H-13	24"	96 ¾"	120 ¼"	14"	10"	11 ½"	12"
	H-14	22"	96"	120"	14"	8"	11 ¾"	12 ¼"
	H-15	24"	96"	120"	14"	10"	12"	12"
F	Specified by Thermapan	36"	96"	120"	26"	10"	12"	12"
	H-16	36"	96"	120"	26"	10"	11 ¾"	12 ¼"
	H-17	36 ¼"	96 ½"	116"	26"	10 ¼"	10"	10"
	H-18	36"	96"	119"	26"	10"	12"	11 ¼"

Table 5.1 Summary of experimental results for Applied Ultimate Jacking Load

Panel Group	Head. Panel	Clear Length (mm)	Header Depth (mm)	Exper. Failure Load (kN)	Aver. Exper. Failure Load (kN)	Test Qualific. Criteria	Value of Jack. Load used for further calculations	Design Ultim. Uniform Load Capacity ⁽¹⁾ = Average Exp. Failure Load/3L (kN/m)
A	H-1	1219	356	63.54	60.60	Passed	60.60	16.57
	H-2	1219	356	55.14				
	H-3	1219	356	63.11				
B	H-4	1219	660	78.04	73.55	Passed	73.55	20.11
	H-5	1219	660	74.71				
	H-6	1219	660	67.91				
C	H-7	1829	356	39.09	40.81*	Difference more than 15%	34.14**	6.22**
	H-8	1829	356	49.19				
	H-9	1829	356	34.14*				
D	H-10	1829	660	52.23	52.87	Passed	20.33	9.64
	H-11	1829	660	52.97				
	H-12	1829	660	53.41				
E	H-13	2438	356	35.99	36.60	Passed	12.76	5.00
	H-14	2438	356	40.34				
	H-15	2438	356	33.46				
F	H-16	2438	660	48.01	49.22	Passed	18.94	6.73
	H-17	2438	660	50.75				
	H-18	2438	660	48.90				

⁽¹⁾ Factor of safety of 3 is assumed to obtain header flexural capacity from the recorded experimental failure load.

* This test should be repeated since the header was supported over rollers rather than flat surface.

** The difference between experimental ultimate load and the average is more than 15%. Thus, consider the smallest experimental ultimate load as the value to be used for header qualification.

Table 5.2 Summary of experimental results for Applied Jacking Load
at Deflection Limit L/360

Panel Group	Header Panel	Clear Length L (mm)	Header Depth (mm)	Applied jacking Load at deflection Limit of L/360, kN	Average exp. Jacking load at deflection limit of L/360, kN	Test Qualification Criteria	Value of Jacking Load used for further calculations
A	H-1	1219	356	11.26	10.02	Difference more than 15%	8.07**
	H-2	1219	356	8.07			
	H-3	1219	356	10.74			
B	H-4	1219	660	15.02	15.98	Passed	15.98
	H-5	1219	660	17.46			
	H-6	1219	660	15.46			
C	H-7	1829	356	12.94	10.72	Difference more than 15%	9.11**
	H-8	1829	356	10.12			
	H-9	1829	356	9.11*			
D	H-10	1829	660	19.50	20.33	Passed	20.33
	H-11	1829	660	19.64			
	H-12	1829	660	21.86			
E	H-13	2438	356	12.81	14.06	Difference more than 15%	12.76**
	H-14	2438	356	16.62			
	H-15	2438	356	12.76			
F	H-16	2438	660	18.94	22.32	Difference more than 15%	18.94**
	H-17	2438	660	26.48			
	H-18	2438	660	21.53			

* This test should be repeated since the header was supported over rollers rather than flat surface.

** The difference between experimental ultimate load and the average is more than 15%. Thus, consider the smallest experimental ultimate load as the value to be used for header qualification.

Table 5.3 Summary of experimental results for Applied Jacking Load
at Deflection Limit L/180

Panel Group	Header Panel	Clear Length L (mm)	Header Depth (mm)	Applied jacking Load at deflection Limit of L/360, kN	Average exp. Jacking load at deflection limit of L/360, kN	Test Qualification Criteria	Value of Jacking Load used for further calculations
A	H-1	1219	356	21.20	18.29	Difference more than 15%	14.64**
	H-2	1219	356	14.64			
	H-3	1219	356	19.02			
B	H-4	1219	660	26.34	29.30	Difference more than 15%	25.12**
	H-5	1219	660	36.43			
	H-6	1219	660	25.12			
C	H-7	1829	356	23.77	19.81	Difference more than 15%	15.75**
	H-8	1829	356	19.91			
	H-9	1829	356	15.75*			
D	H-10	1829	660	41.28	38.28	Passed	38.28
	H-11	1829	660	37.25			
	H-12	1829	660	36.32			
E	H-13	2438	356	23.38	24.82	Passed	24.82
	H-14	2438	356	28.61			
	H-15	2438	356	22.47			
F	H-16	2438	660	35.51	40.84	Passed	40.84
	H-17	2438	660	45.46			
	H-18	2438	660	41.54			

* This test should be repeated since the header was supported over rollers rather than flat surface.

** The difference between experimental ultimate load and the average is more than 15%. Thus, consider the smallest experimental ultimate load as the value to be used for header qualification.

Table 5.4 Design Table for Ultimate Limit State

Panel Group	Header Panel	Clear Length L (mm)	Header Depth (mm)	Design Ult. Uniform Load Capacity (kNm)	Maximum supported length ^{(1),(2)} (m)				
					Specified snow load (kPa)				
					1.00	1.50	2.00	2.50	3.00
A	H-1	1219	356	16.57	7.80	5.76	4.57	3.79	3.23
	H-2	1219	356						
	H-3	1219	356						
B	H-4	1219	660	20.11	9.46	6.99	5.55	4.60	3.92
	H-5	1219	660						
	H-6	1219	660						
C	H-7	1829	356	6.22**	2.92	2.16	1.71	1.42	1.21
	H-8	1829	356						
	H-9	1829	356						
D	H-10	1829	660	9.64	4.54	3.35	2.66	2.20	1.88
	H-11	1829	660						
	H-12	1829	660						
E	H-13	2438	356	5.00	2.35	1.74	1.38	1.14	0.98
	H-14	2438	356						
	H-15	2438	356						
F	H-16	2438	660	6.73	3.17	2.34	1.86	1.54	1.31
	H-17	2438	660						
	H-18	2438	660						

⁽¹⁾ Supported length means half the sum of the joist spans on both sides of the internal header or the joist span of the exterior header.

⁽²⁾ Maximum supported length of roof is based on 0.5 kPa dead load and a specified snow load as shown on flat roofs.

Table 5.5 Design Table for Serviceability Limit State
at Deflection Limit L/360

Panel Group	Header Panel	Clear Length L (mm)	Header Depth (mm)	Jacking Load at L/360 (kN)	Maximum supported length ^{(1), (2)} based on deflection limit of L/360 (m)				
					Specified snow load (kPa)				
					1.00	1.50	2.00	2.50	3.00
A	H-1	1219	356	8.07**	6.62	4.41	3.31	2.64	2.21
	H-2	1219	356						
	H-3	1219	356						
B	H-4	1219	660	15.98	13.10	8.73	6.55	5.24	4.37
	H-5	1219	660						
	H-6	1219	660						
C	H-7	1829	356	9.11**	4.98	3.32	2.49	1.99	1.66
	H-8	1829	356						
	H-9	1829	356						
D	H-10	1829	660	20.33	11.12	7.41	5.56	4.45	3.71
	H-11	1829	660						
	H-12	1829	660						
E	H-13	2438	356	12.76**	5.23	3.49	2.62	2.09	1.74
	H-14	2438	356						
	H-15	2438	356						
F	H-16	2438	660	18.94**	7.77	5.18	3.88	3.11	2.59
	H-17	2438	660						
	H-18	2438	660						

⁽¹⁾ Supported length means half the sum of the joist spans on both sides of the internal header or the joist span of the exterior header.

⁽²⁾ Maximum supported length of roof is based on 0.5 kPa dead load and a specified snow load as shown on flat roofs.

Table 5.6 Design Table for Serviceability Limit State
at Deflection Limit L/180

Panel Group	Header Panel	Clear Length L (mm)	Header Depth (mm)	Jacking Load at L/180 (kN)	Maximum supported length ^{(1), (2)} based on deflection limit of L/180 (m)				
					Specified snow load (kPa)				
					1.00	1.50	2.00	2.50	3.00
A	H-1	1219	356	14.64**	12.00	8.00	6.00	4.80	4.00
	H-2	1219	356						
	H-3	1219	356						
B	H-4	1219	660	25.12**	20.60	13.73	10.30	8.24	6.87
	H-5	1219	660						
	H-6	1219	660						
C	H-7	1829	356	15.75**	8.61	5.74	4.31	3.44	2.87
	H-8	1829	356						
	H-9	1829	356						
D	H-10	1829	660	38.28	20.93	13.95	10.46	8.37	6.98
	H-11	1829	660						
	H-12	1829	660						
E	H-13	2438	356	24.82	9.21	6.14	4.61	3.69	3.07
	H-14	2438	356						
	H-15	2438	356						
F	H-16	2438	660	40.83	16.74	11.16	8.37	6.70	5.58
	H-17	2438	660						
	H-18	2438	660						

⁽¹⁾ Supported length means half the sum of the joist spans on both sides of the internal header or the joist span of the exterior header.

⁽²⁾ Maximum supported length of roof is based on 0.5 kPa dead load and a specified snow load as shown on flat roofs.

Table 5.7 Summary of header panels flexural resistance, shear resistance and deflection

Panel Group	Panel No.	Clear Length, [mm]	Depth, [mm]	Bending Resistance, M_r [kN.m]	Shear Resistance, V_r [kN]
A	H-1	1219	356	15.83	11.34
	H-2				
	H-3				
B	H-4	1219	660	37.23	22.94
	H-5				
	H-6				
C	H-7	1829	356	15.83	11.34
	H-8				
	H-9				
D	H-10	1829	660	37.23	22.94
	H-11				
	H-12				
E	H-13	2438	356	15.83	11.34
	H-14				
	H-15				
F	H-16	2438	660	37.23	22.94
	H-17				
	H-18				

Table 5.8 Comparison summary of uniform load as per CAN/CSA-O86-01 calculations and uniform load determined from the experimental findings

Panel Group	Panel No.	Clear Length, [mm]	Depth [mm]	Based on the calculations		Based on Experimental Findings
				Uniform Load, w_M [kN.m]	Uniform Load w_V [kN.m]	Design ultimate uniform load capacity, [kN.m]
A	H-1	1219	356	85.22	18.60	16.57
	H-2					
	H-3					
B	H-4	1219	660	200.43	37.64	20.11
	H-5					
	H-6					
C	H-7	1829	356	37.86	13.06	6.22
	H-8					
	H-9					
D	H-10	1829	660	89.03	25.08	9.64
	H-11					
	H-12					
E	H-13	2438	356	21.31	9.30	5.00
	H-14					
	H-15					
F	H-16	2438	660	50.11	18.82	6.73
	H-17					
	H-18					

Table 5.9 Design Table of maximum supported length of roof members

Panel Group	Header Panel	Clear Length L (mm)	Header Depth (mm)	Criteria	Minimum value of "Maximum supported length"(m)				
					Specified snow load (kPa)				
					1.00	1.50	2.00	2.50	3.00
A	H-1	1219	356	Deflection limit L/360	6.62	4.41	3.31	2.64	2.21
	H-2	1219	356						
	H-3	1219	356						
B	H-4	1219	660	Ultimate strength	9.46	6.99	5.55	4.60	3.92
	H-5	1219	660						
	H-6	1219	660						
C	H-7	1829	356	Ultimate strength	2.92	2.16	1.71	1.42	1.21
	H-8	1829	356						
	H-9	1829	356						
D	H-10	1829	660	Ultimate strength	4.54	3.35	2.66	2.20	1.88
	H-11	1829	660						
	H-12	1829	660						
E	H-13	2438	356	Ultimate strength	2.35	1.74	1.38	1.14	0.98
	H-14	2438	356						
	H-15	2438	356						
F	H-16	2438	660	Ultimate strength	3.17	2.34	1.86	1.54	1.31
	H-17	2438	660						
	H-18	2438	660						

FIGURES



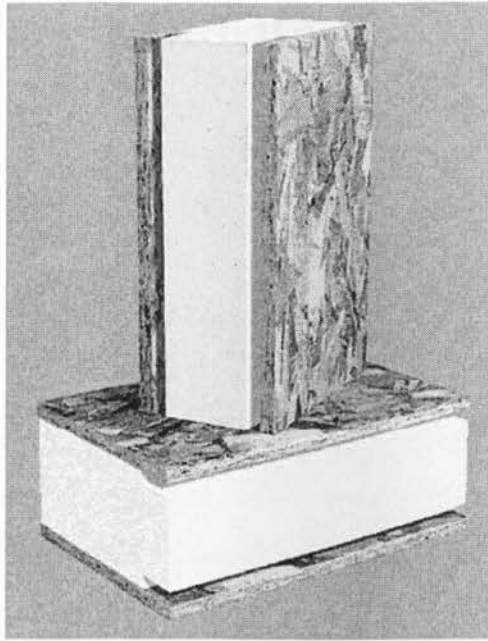


Figure 1.1 Sample of Structural Insulated Panels
(SIPA, 2007, www.sips.org)

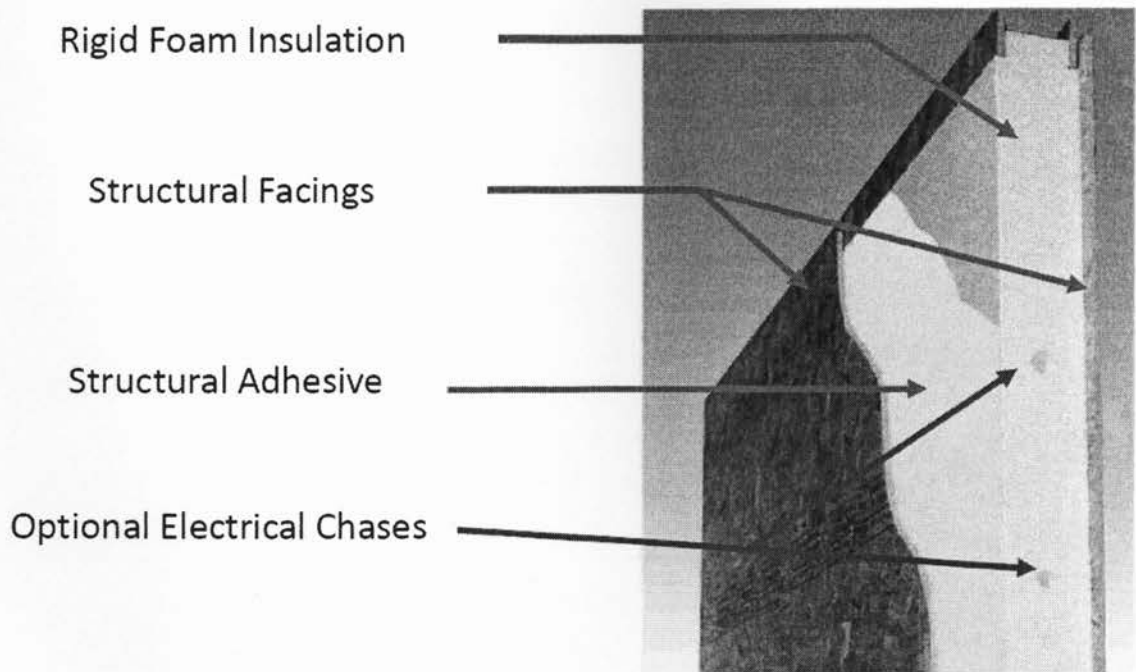


Figure 1.2 Layers in a Structural Insulated Panel
(SIPA, 2007, www.sips.org)

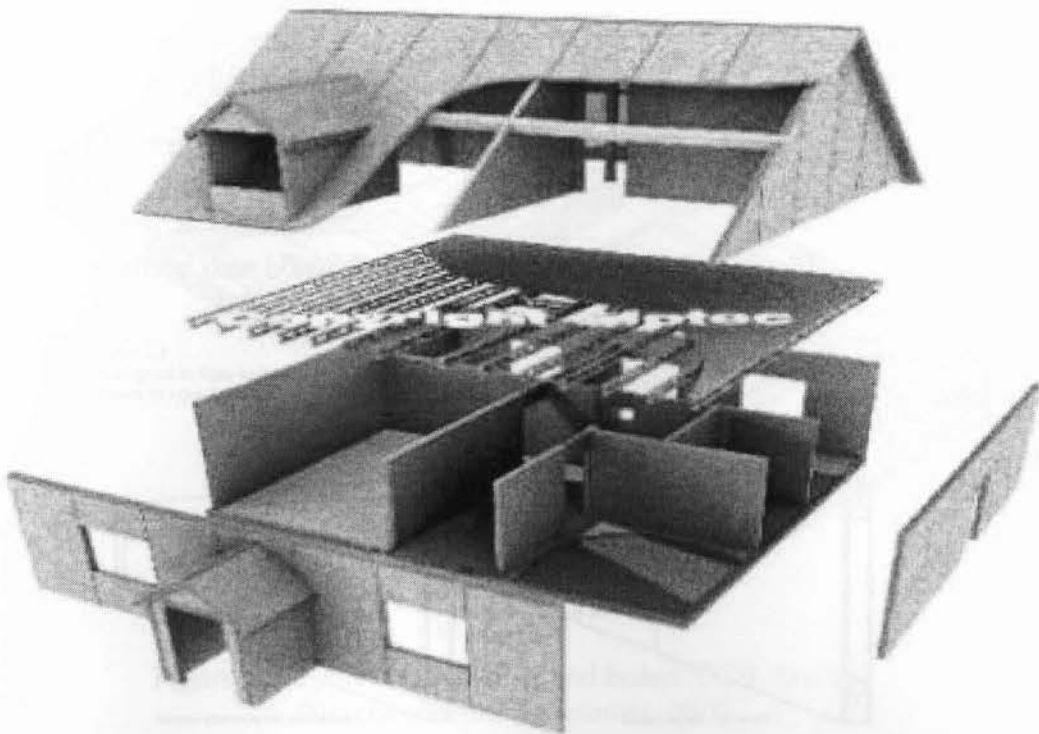


Figure 1.3 View of residential building construction using SIPs
(Butt, 2008)

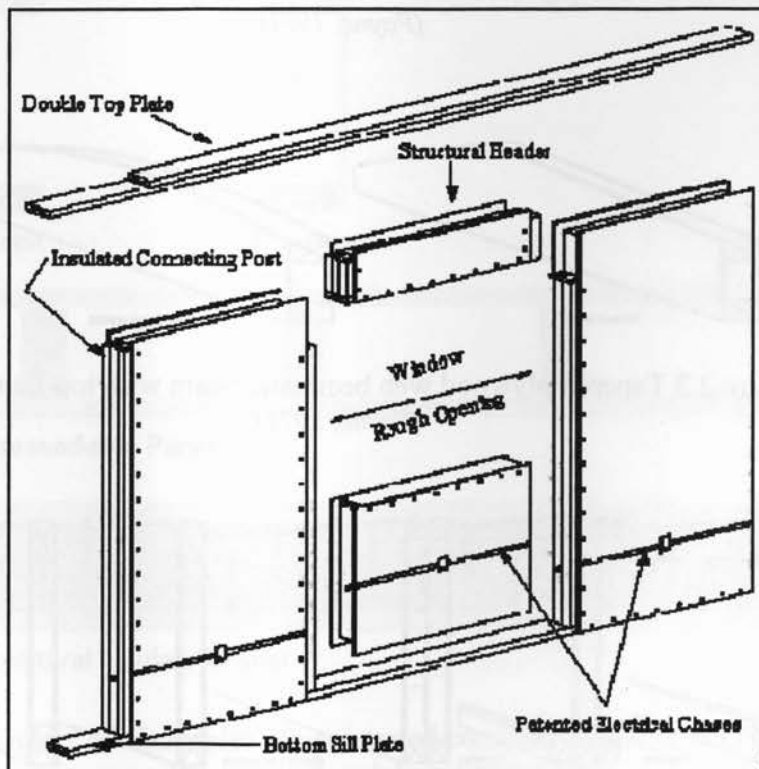


Figure 1.4. Typical SIP wall assemblage with a SIP header above the opening
(SIPA, 2007, www.sips.org)

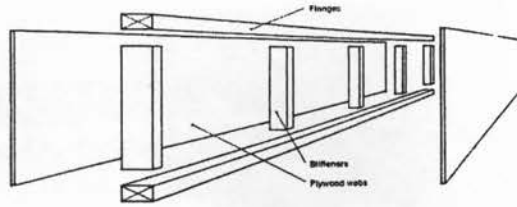


Figure 2.1 Components of typical plywood web beam
(Payne, 1971)

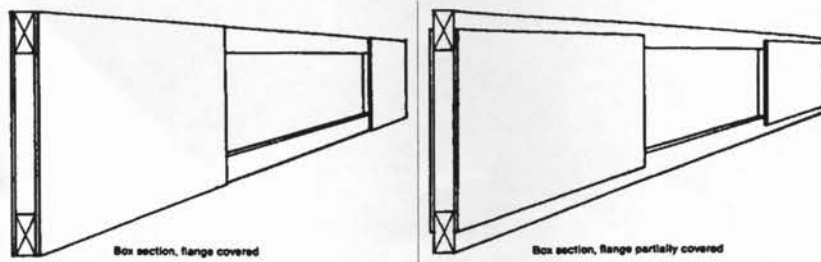


Figure 2.2 Box section plywood web beam with flange covered or partially covered
(Payne, 1971)

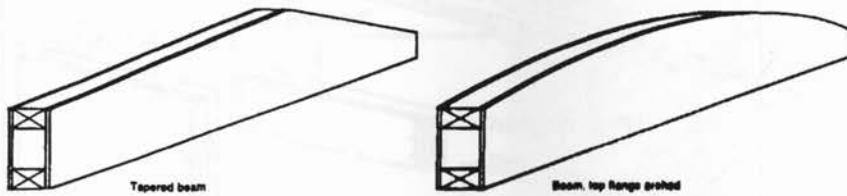


Figure 2.3 Tapered plywood web beam and beam with top flange arched
(Payne, 1971)

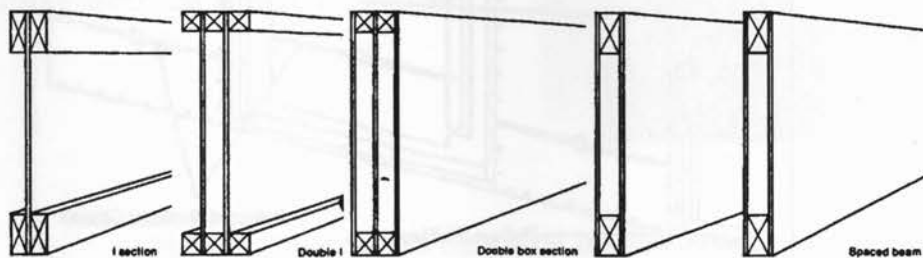


Figure 2.4 I-section, double I and double box and spaced plywood web beams
(Payne, 1971)

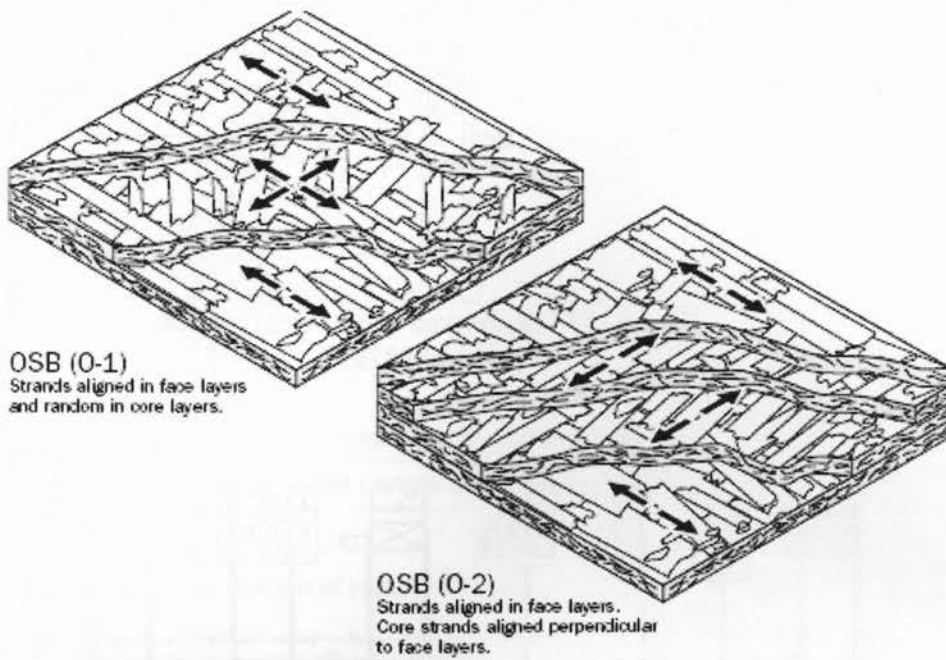


Figure 2.5 Typical Oriented strand board (OSB) lay-ups
(Structural Board Association, 2004)

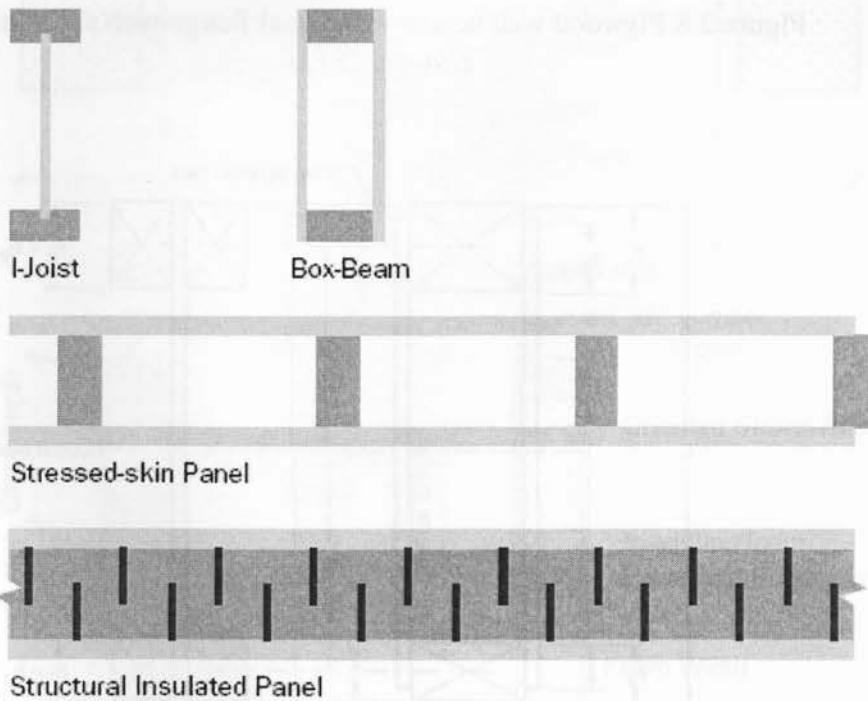


Figure 2.6 Examples of engineered components made of OSB
(Structural Board Association, 2004)

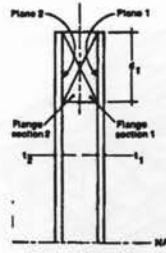


Figure 2.7 Flange-web shear stress planes
(Payne, 1971)

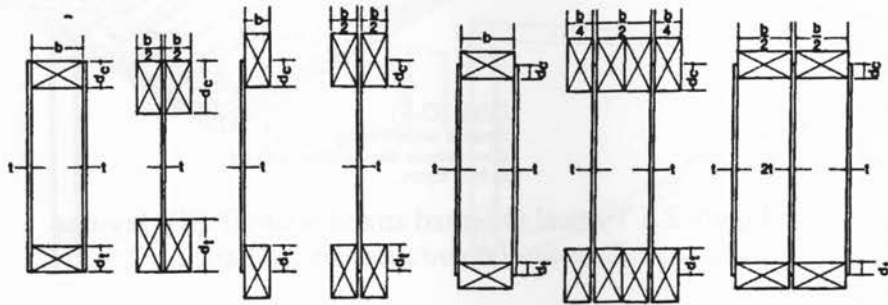


Figure 2.8 Plywood web beams with equal flange-web shear stress
(Payne, 1971)

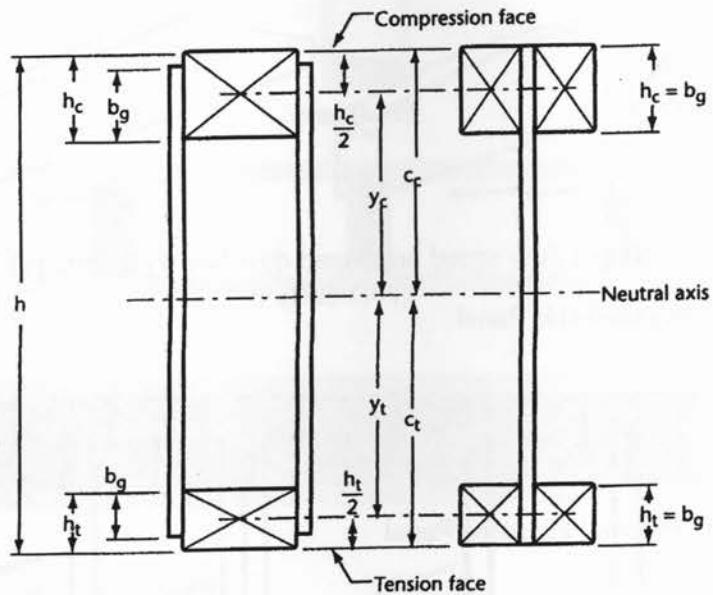


Figure 2.9 Panel web beam section
(CWC, 2005))

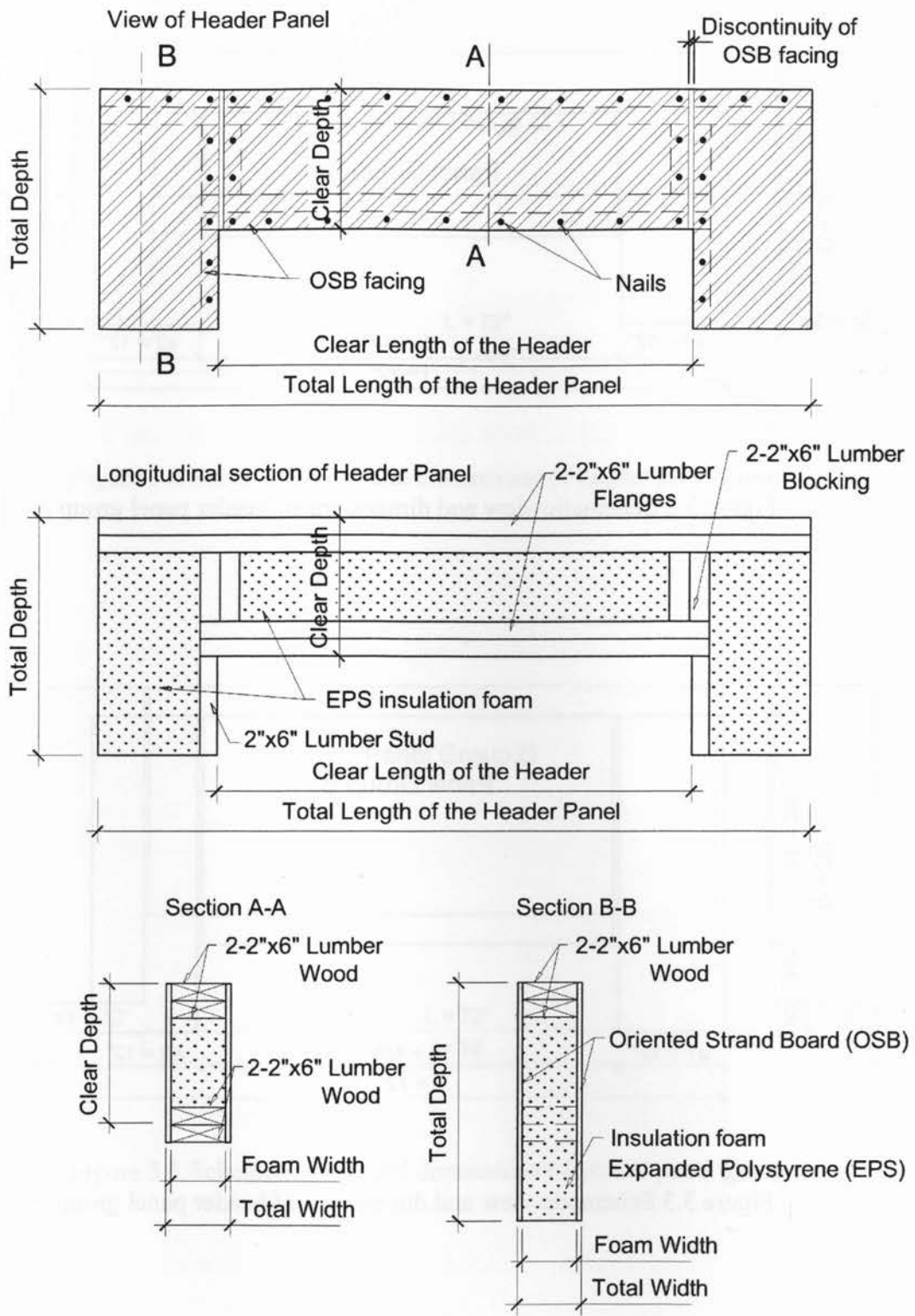


Figure 3.1 Schematic view of a tested header panel

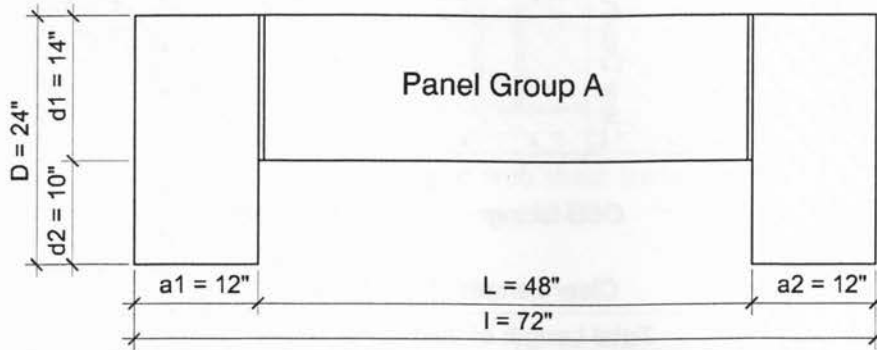


Figure 3.2 Schematic view and dimensions of header panel group A

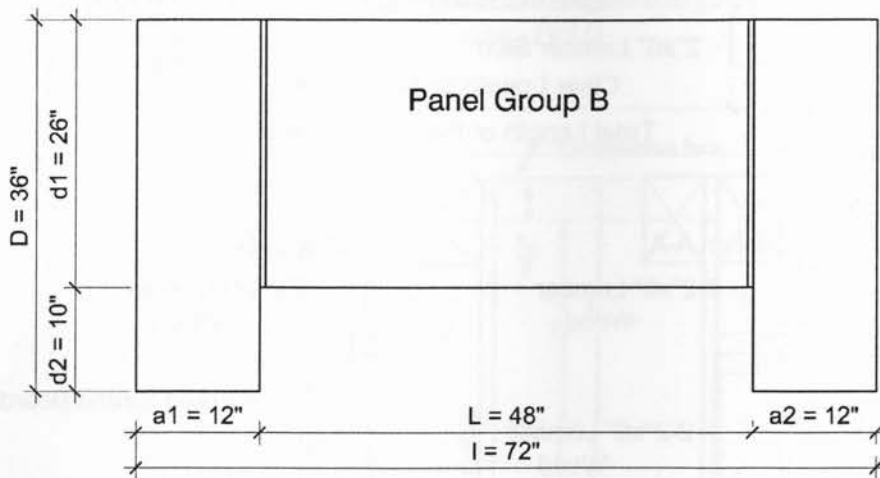


Figure 3.3 Schematic view and dimensions of header panel group B

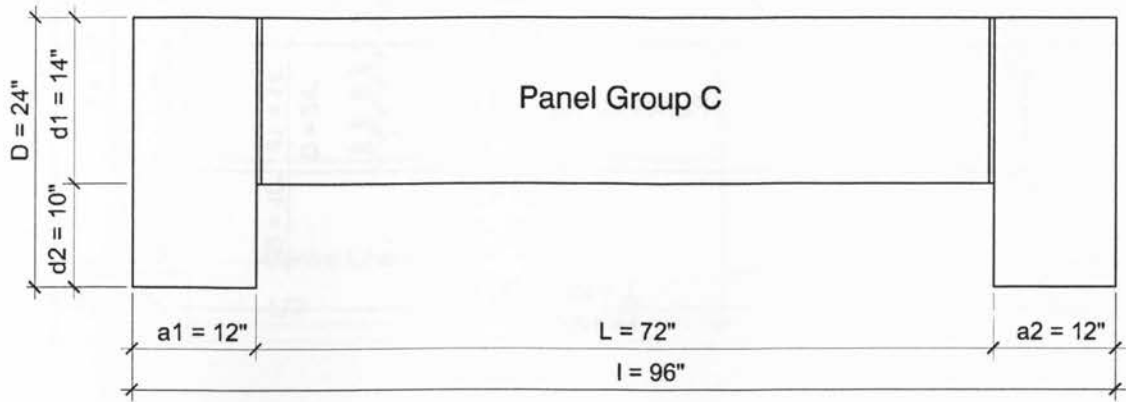


Figure 3.4 Schematic view and dimensions of header panel group C

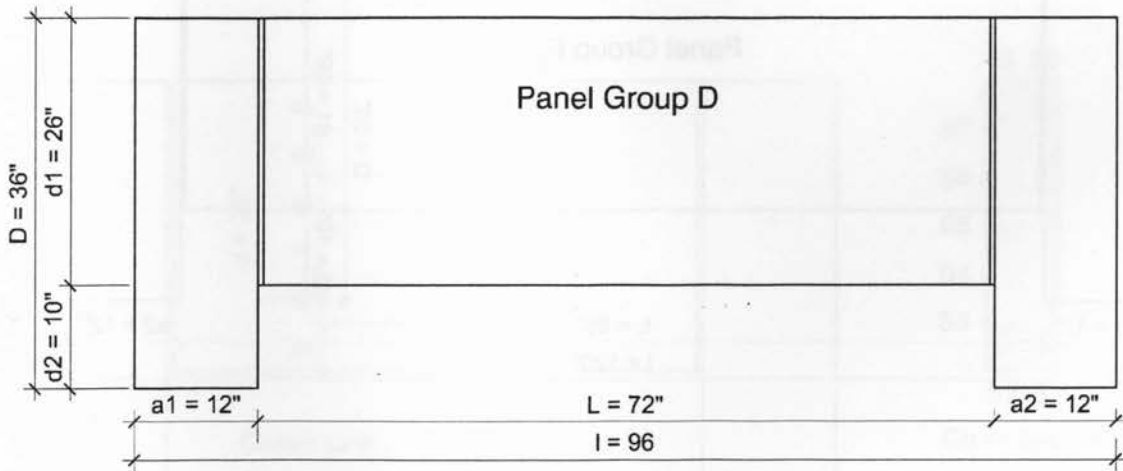


Figure 3.5 Schematic view and dimensions of header panel group D

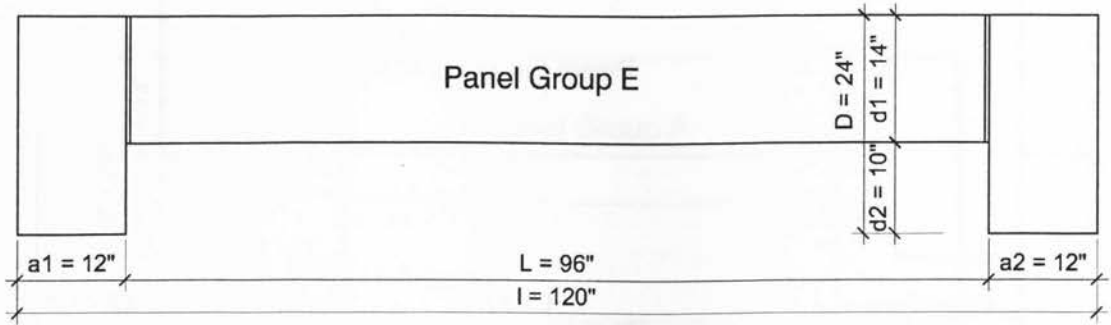


Figure 3.6 Schematic view and dimensions of header panel group E

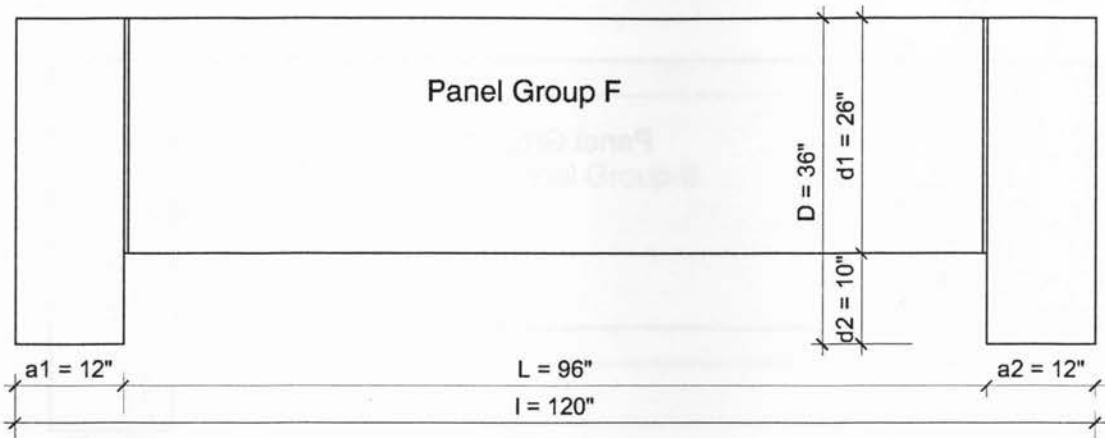


Figure 3.7 Schematic view and dimensions of header panel group F

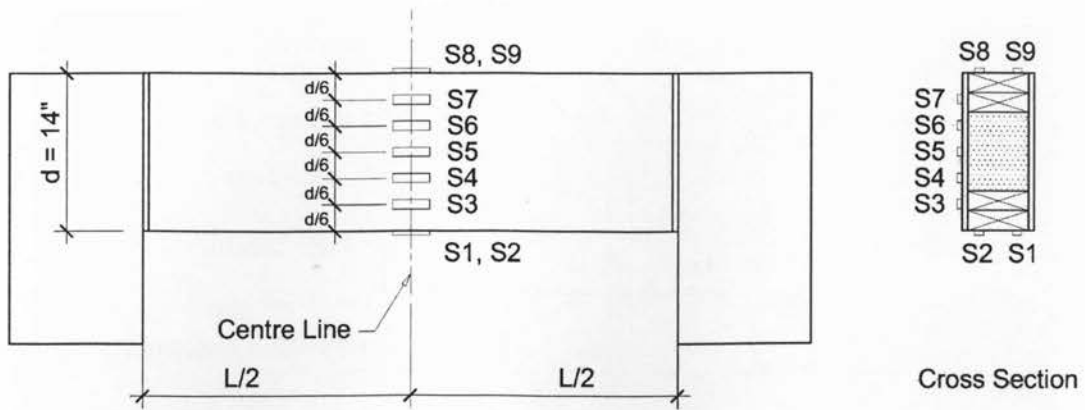


Figure 3.8 Schematic diagram of arrangement of strain gauges for 14" deep header panels
(Group A, C, and E)

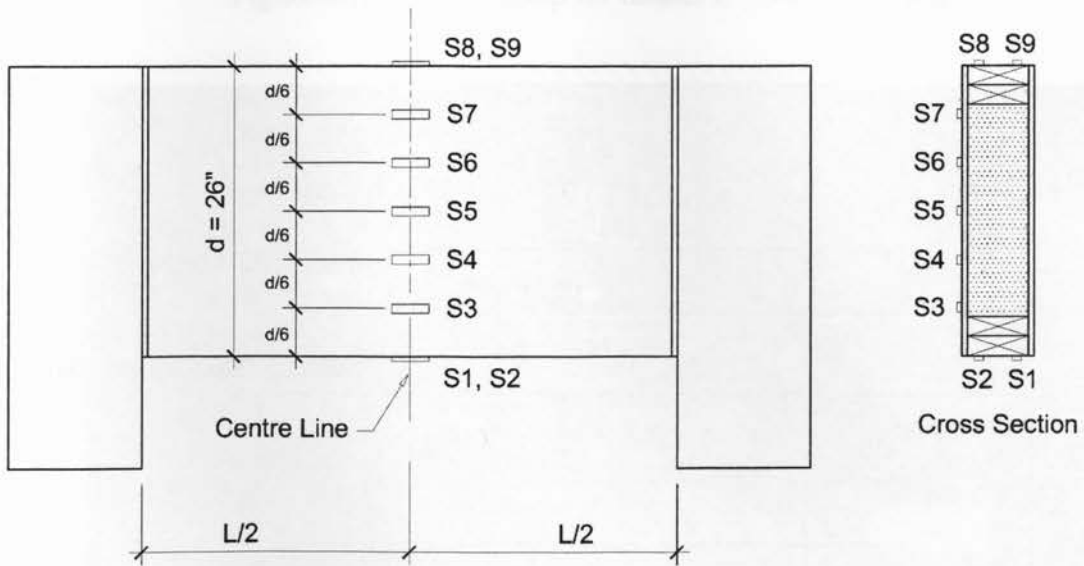


Figure 3.9 Schematic diagram of arrangement of strain gauges for 26" deep header panels
(Group B, D, and F)

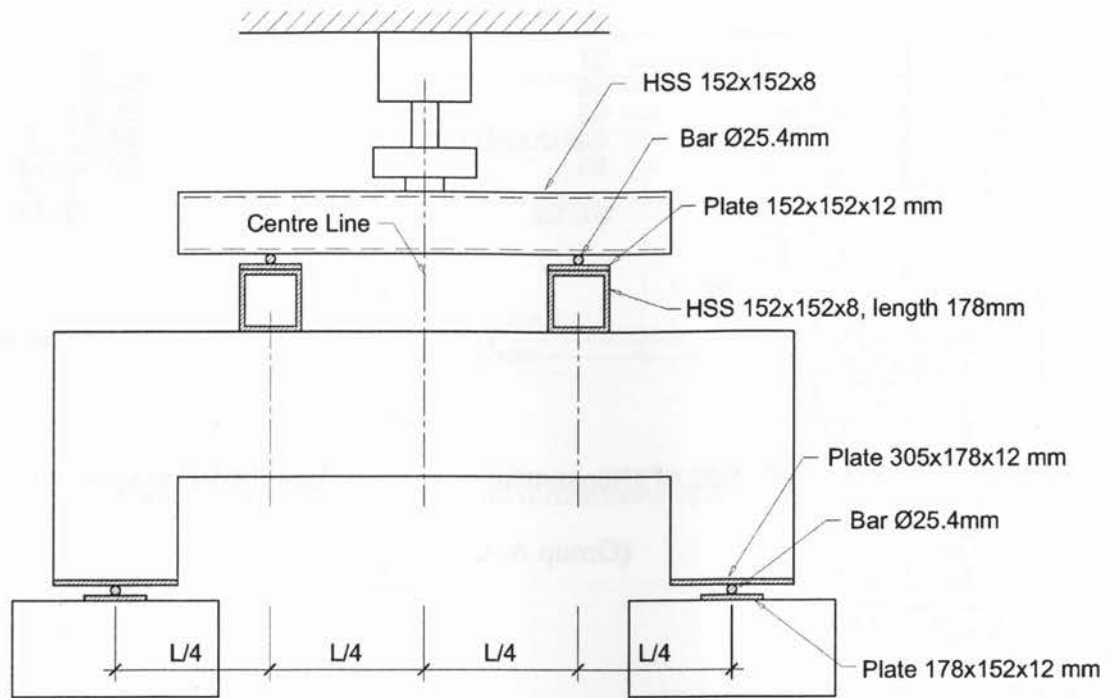


Figure 3.10 Schematic diagram of test setup with steel rollers used for testing H-9 only

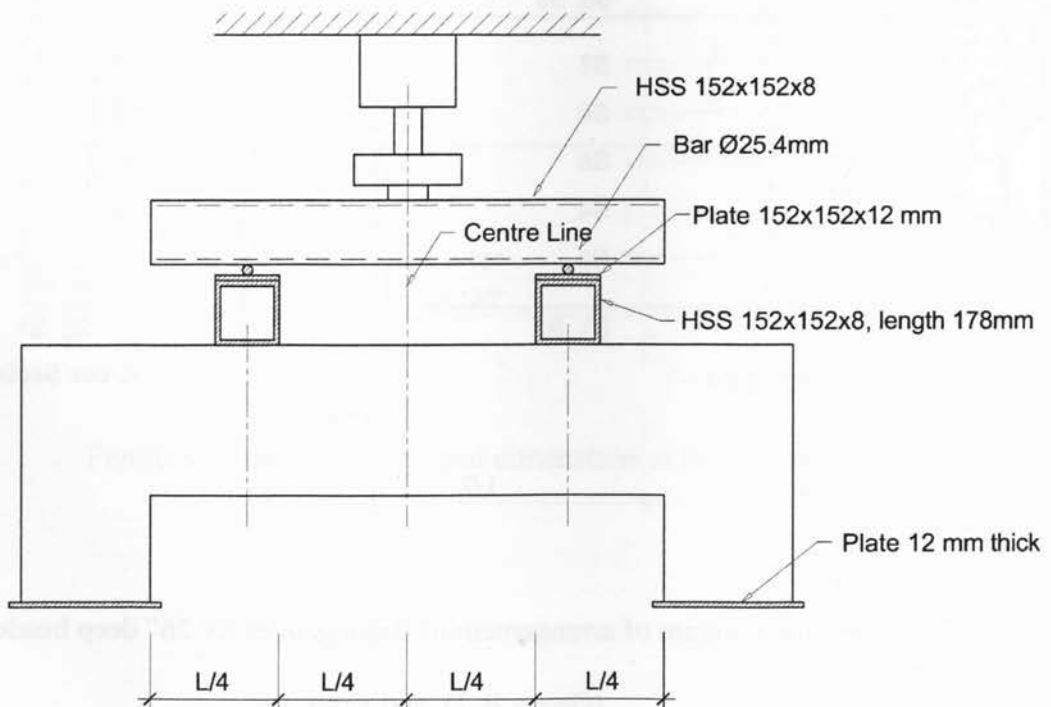


Figure 3.11 Schematic diagram of test setup with flat surface used for testing all headers except the header H-9



Figure 3.12 View of setup for header H-1 before testing

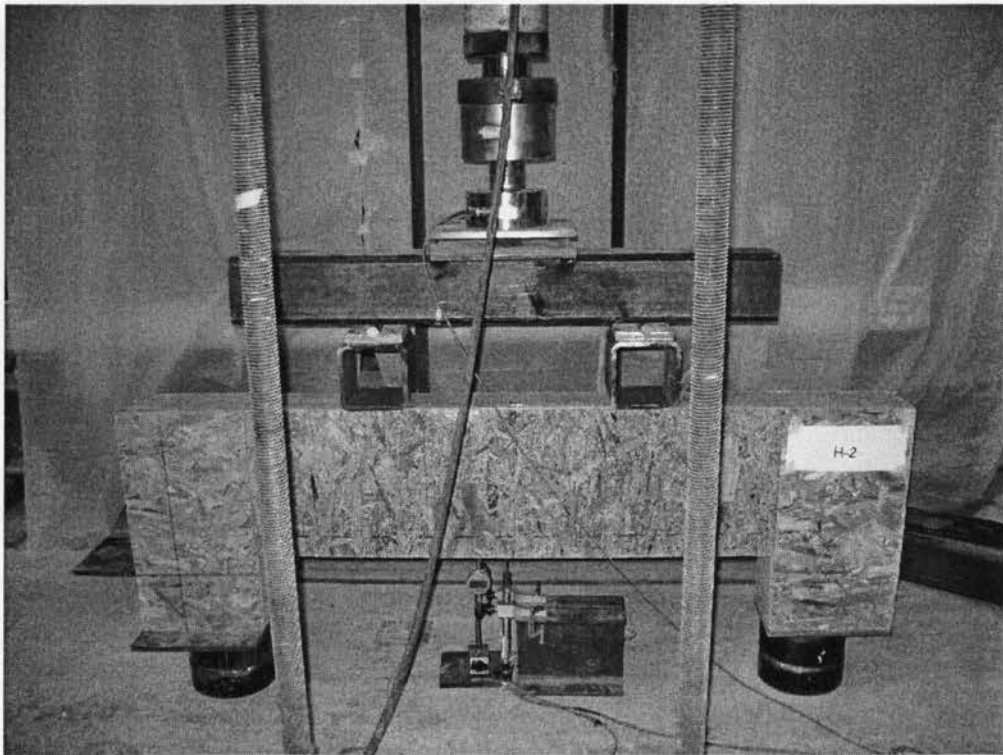


Figure 3.13 View of setup for header H-2 before testing

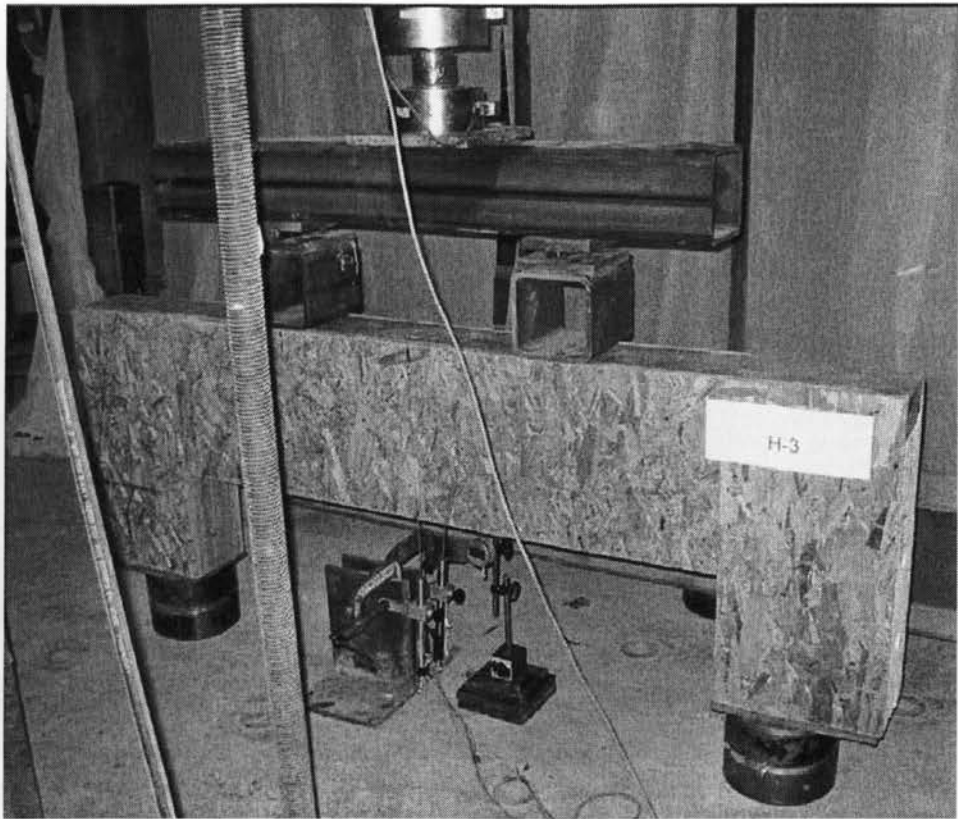


Figure 3.14 View of setup for header H-3 before testing

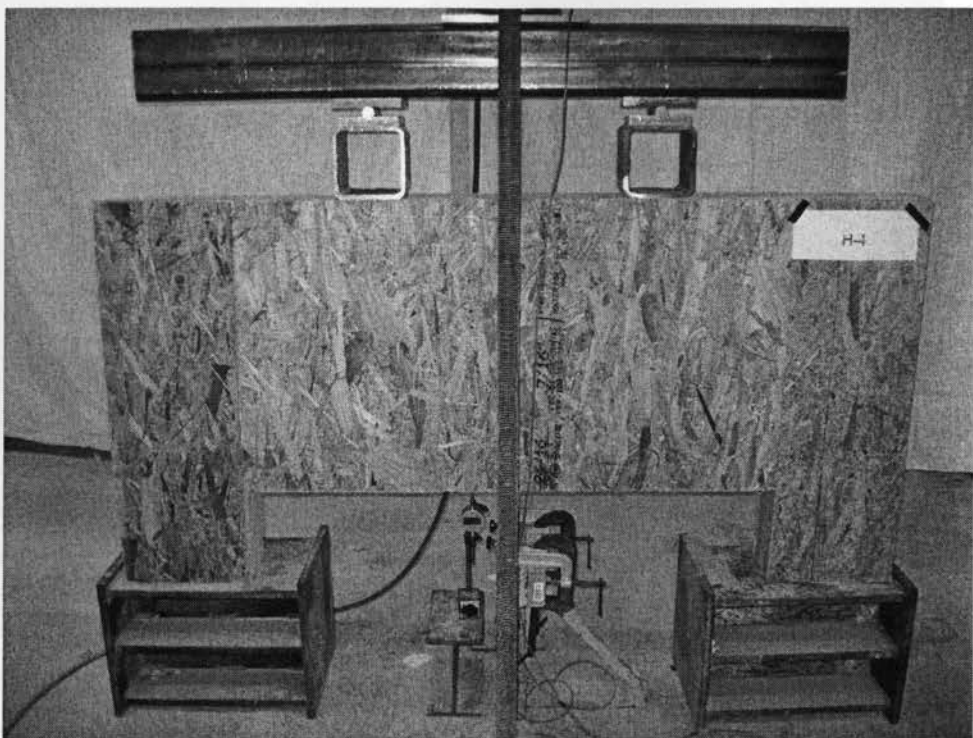


Figure 3.15 View of setup for header H-4 before testing

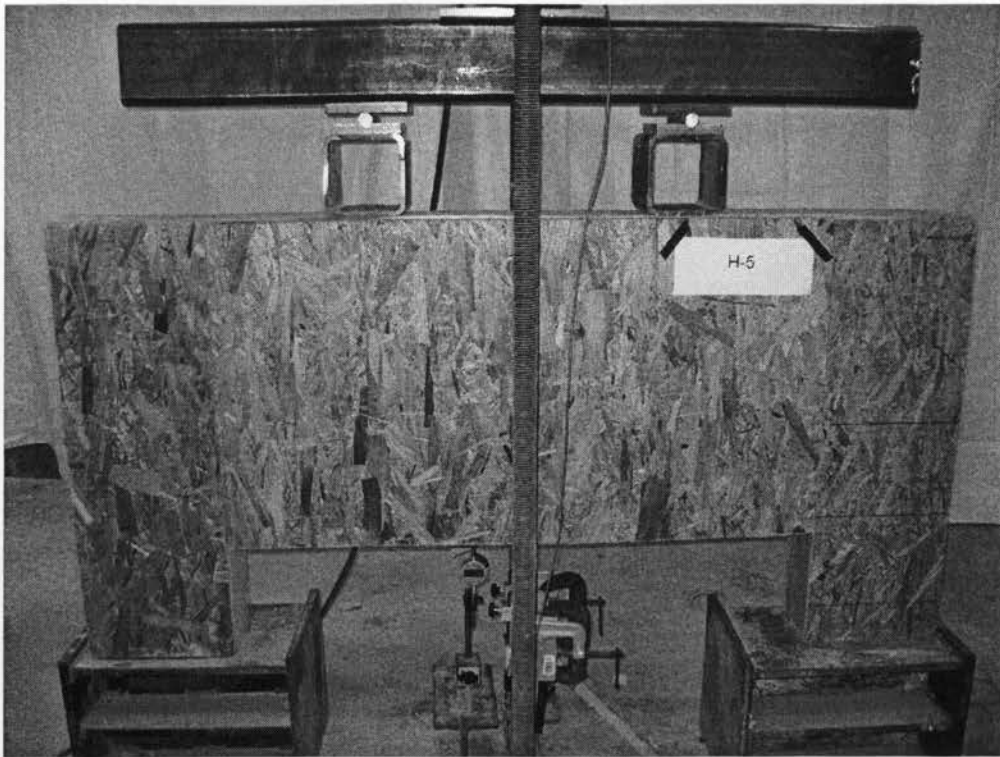


Figure 3.16 View of setup for header H-5 before testing



Figure 3.17 View of setup for header H-6 before testing

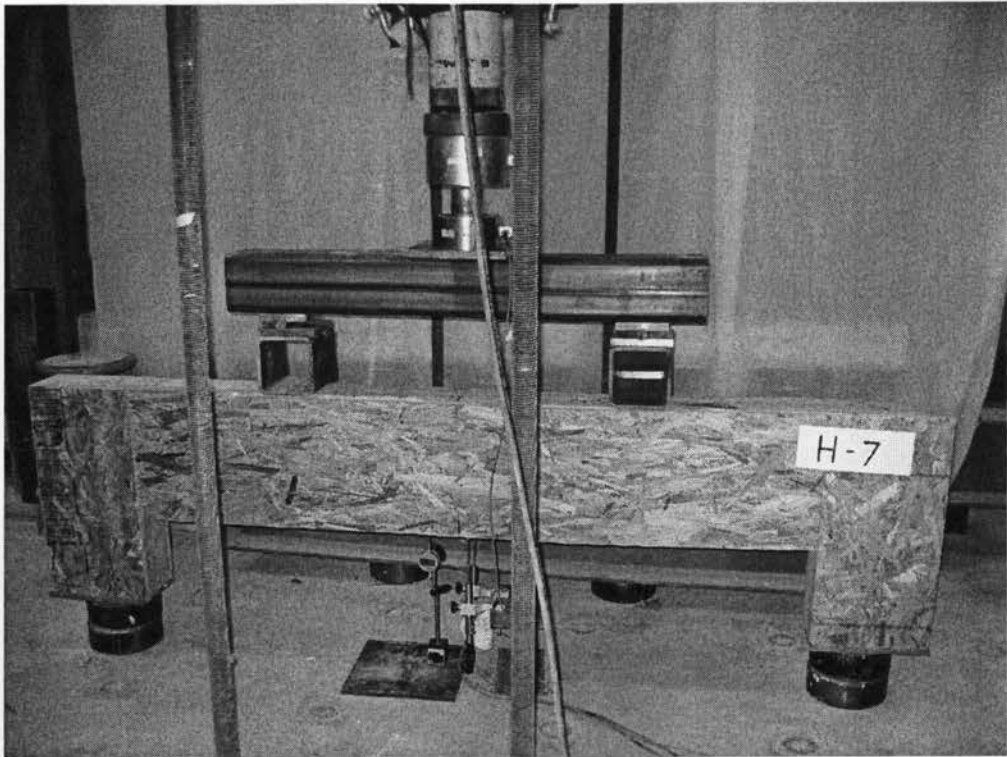


Figure 3.18 View of setup for header H-7 before testing

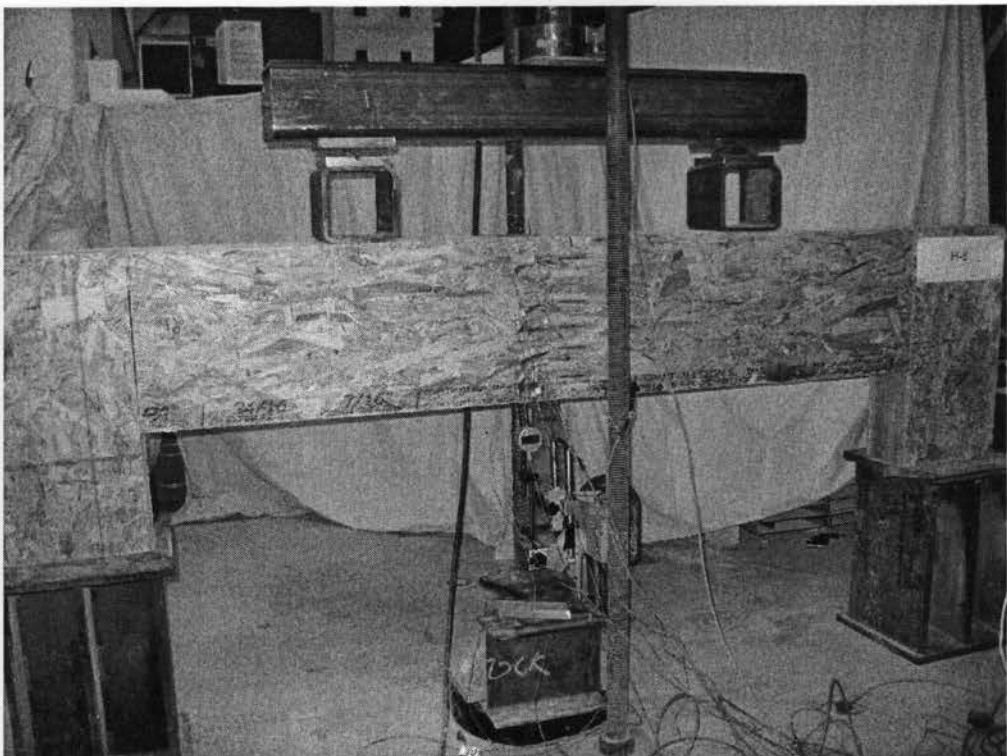


Figure 3.19 View of setup for header H-8 before testing



Figure 3.20 View of setup on steel rollers for header H-9 before testing

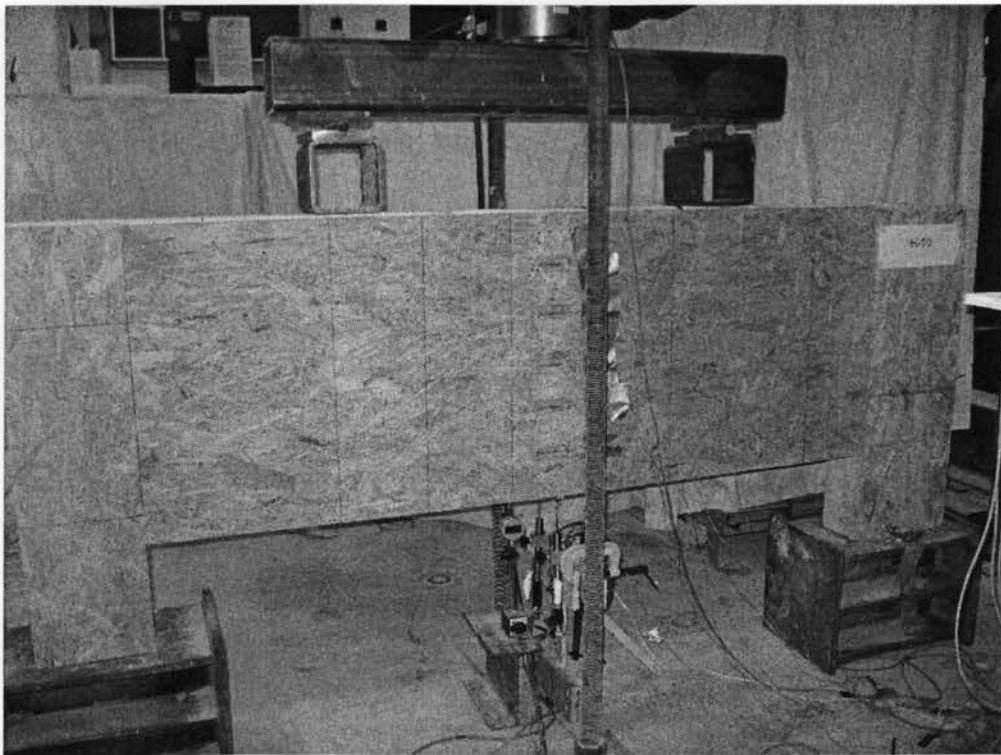


Figure 3.21 View of setup for header H-10 before testing

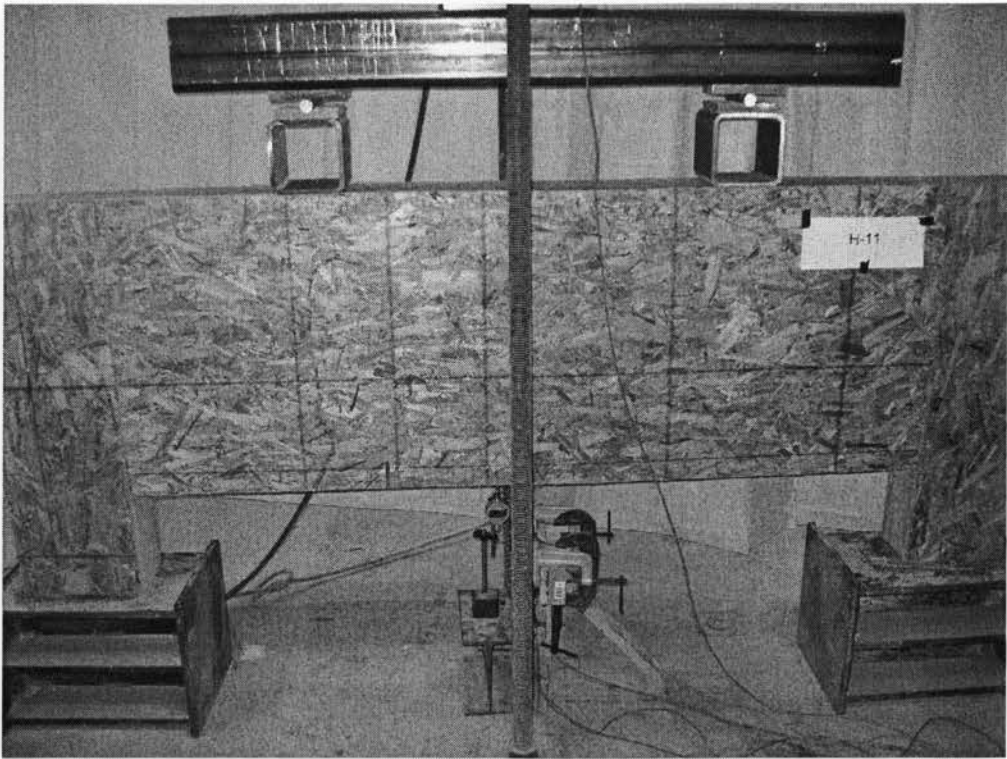


Figure 3.22 View of setup for header H-11 before testing

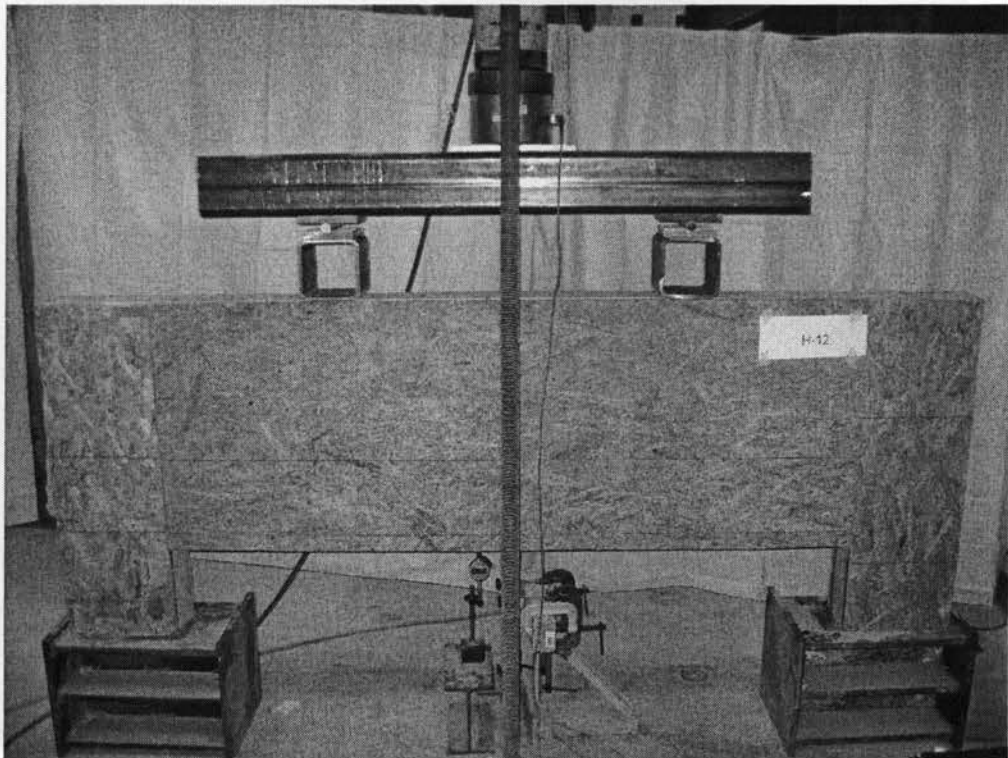


Figure 3.23 View of setup for header H-12 before testing

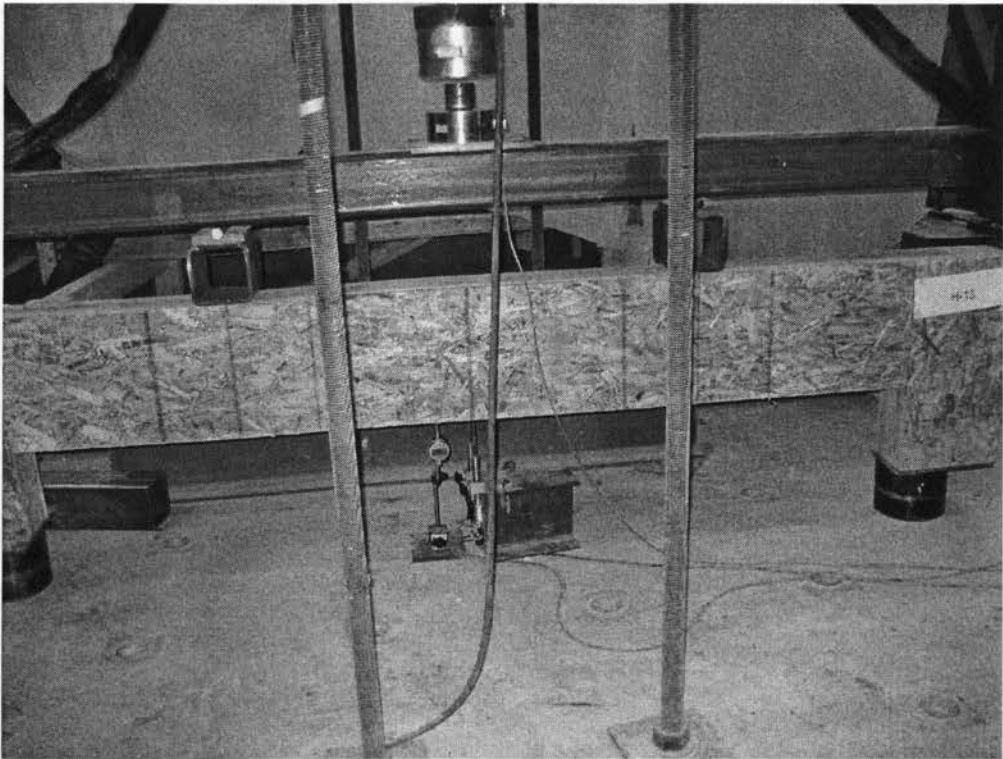


Figure 3.24 View of setup for header H-13 before testing

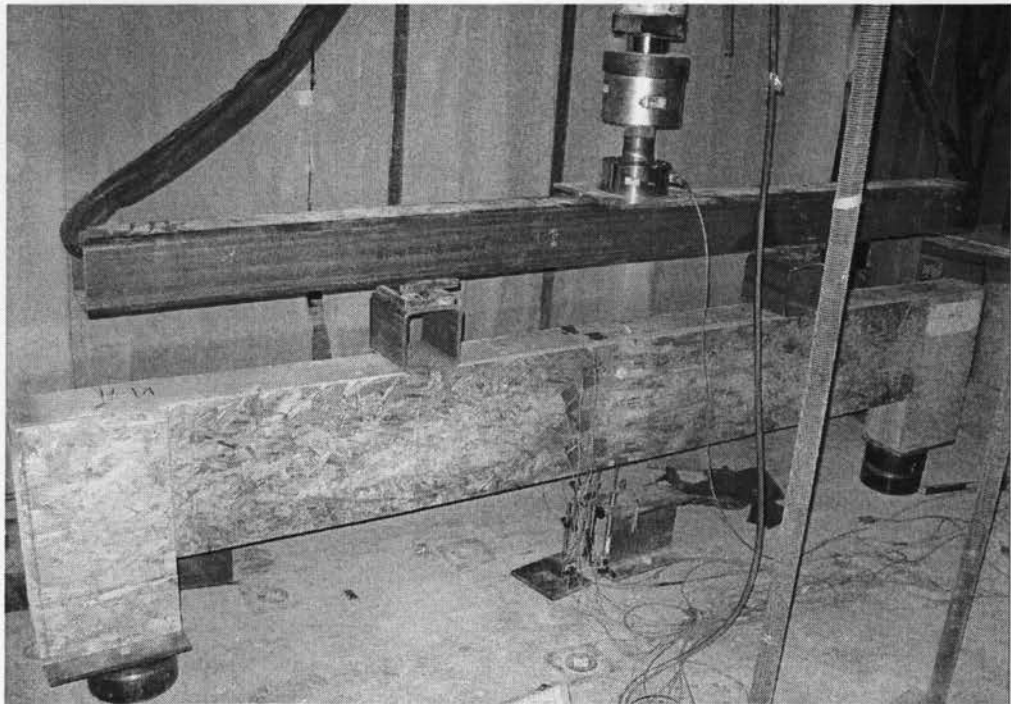


Figure 3.25 View of setup for header H-14 before testing

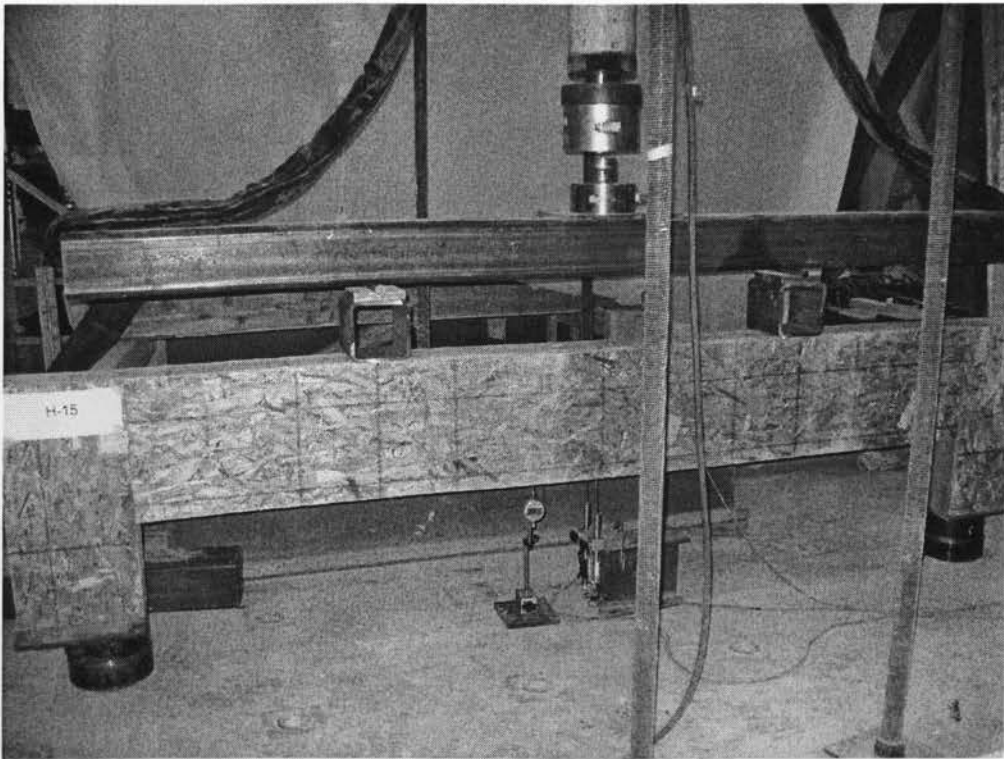


Figure 3.26 View of setup for header H-15 before testing

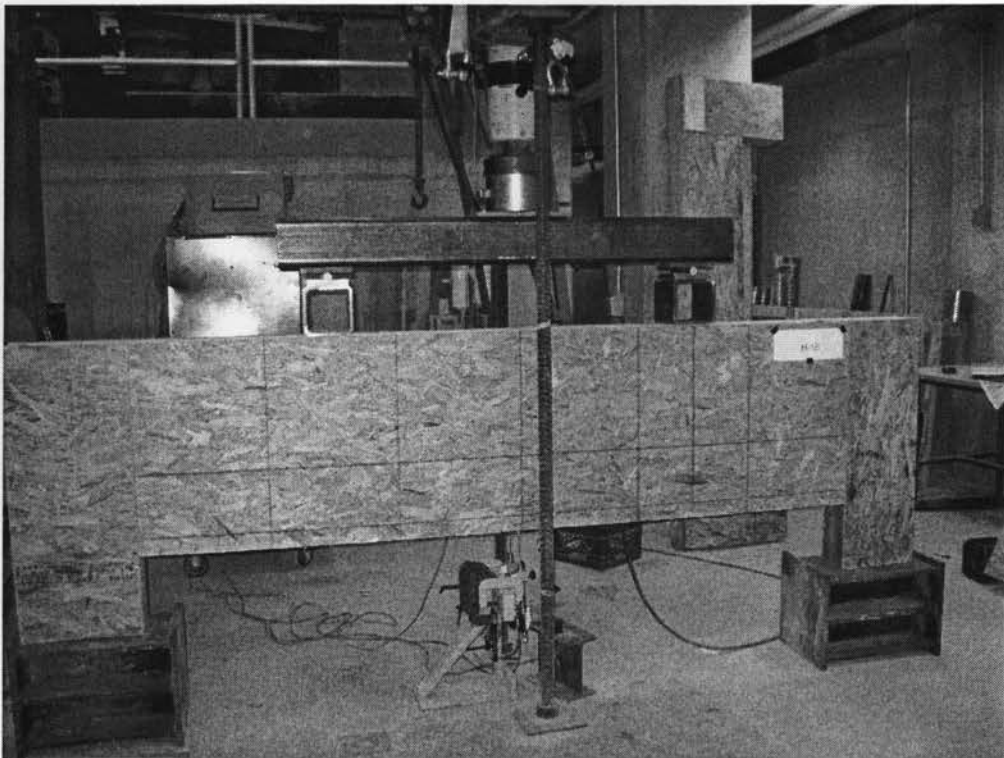


Figure 3.27 View of setup for header H-16 before testing

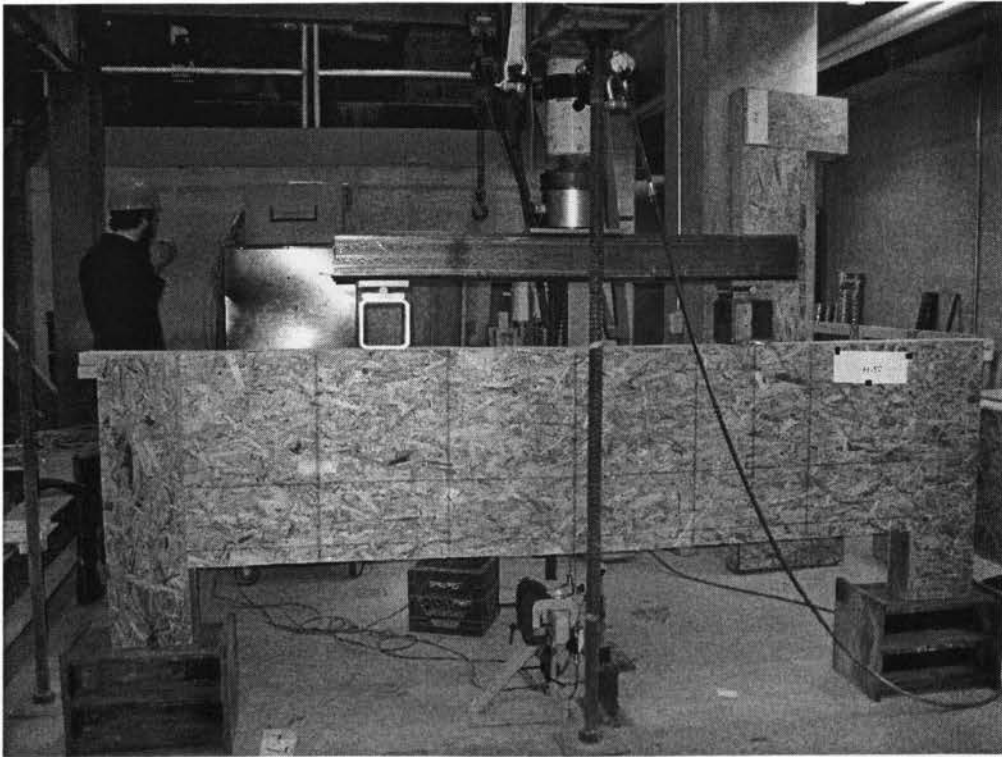


Figure 3.28 View of setup for header H-17 before testing

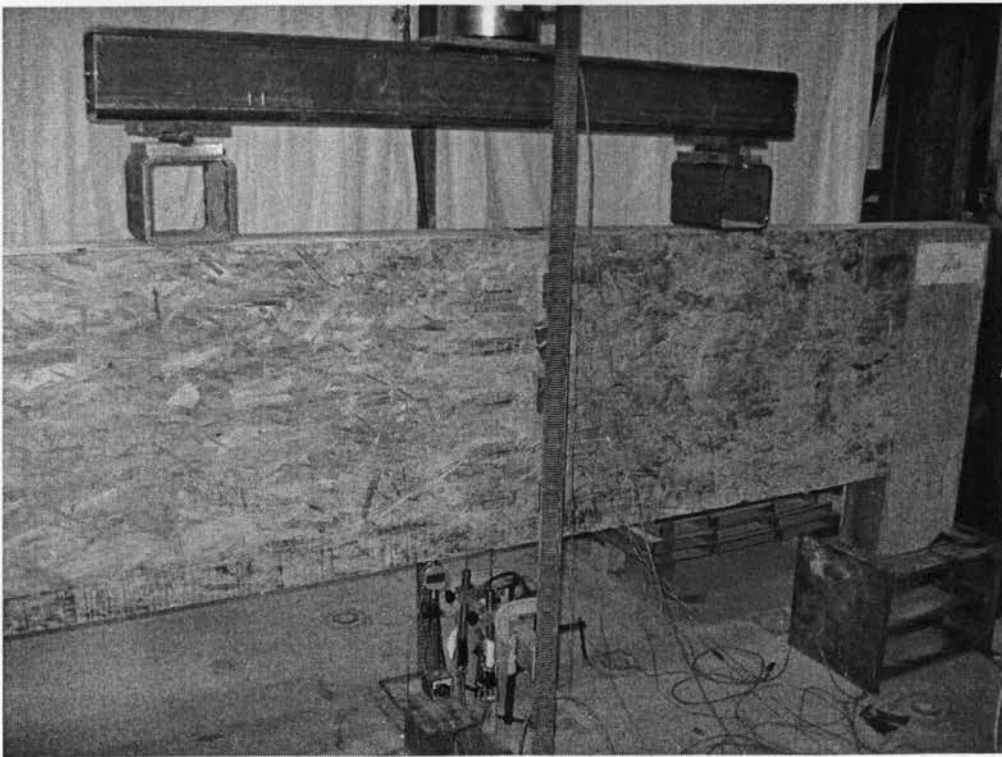


Figure 3.29 View of setup for header H-18 before testing

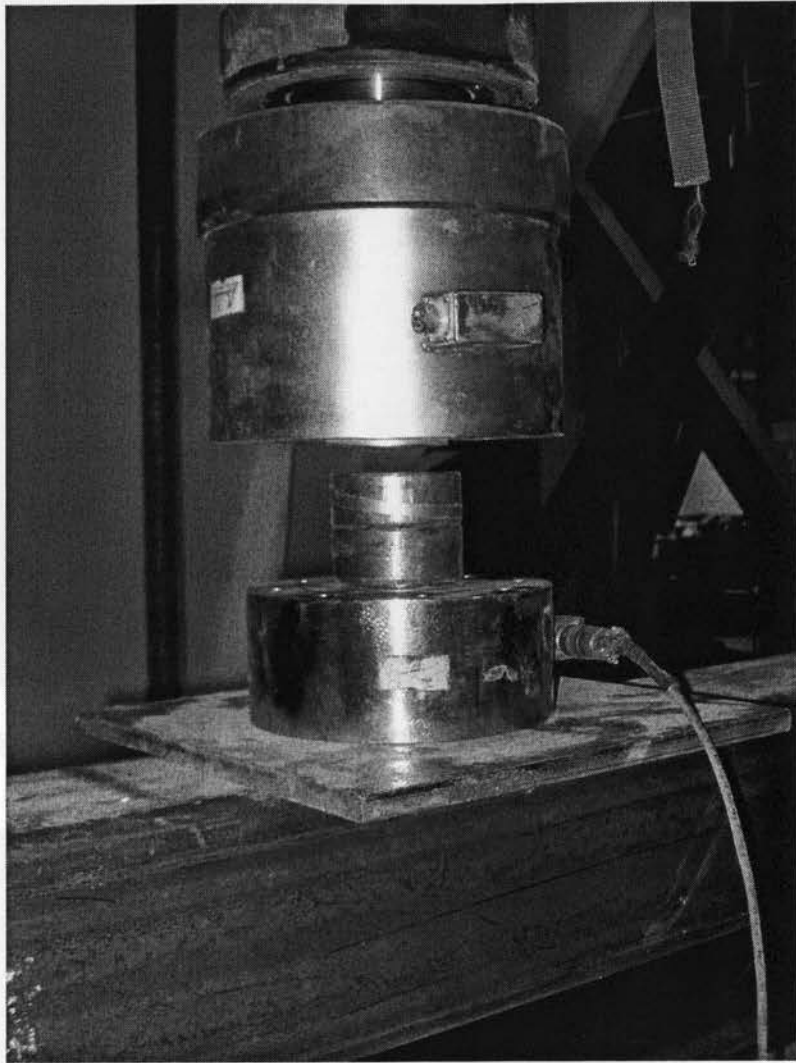


Figure 3.30 View of load cell assembly used in testing

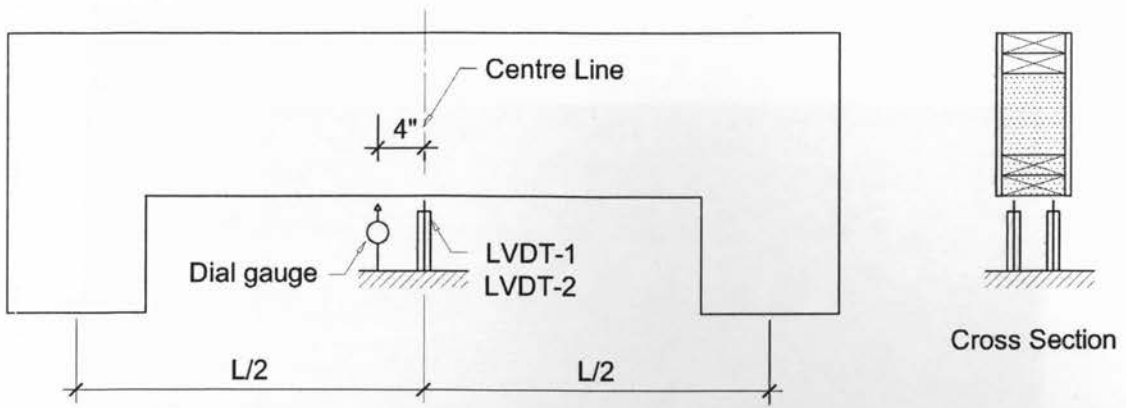


Figure 3.31 Schematic diagram of dial gauge and LVDT's

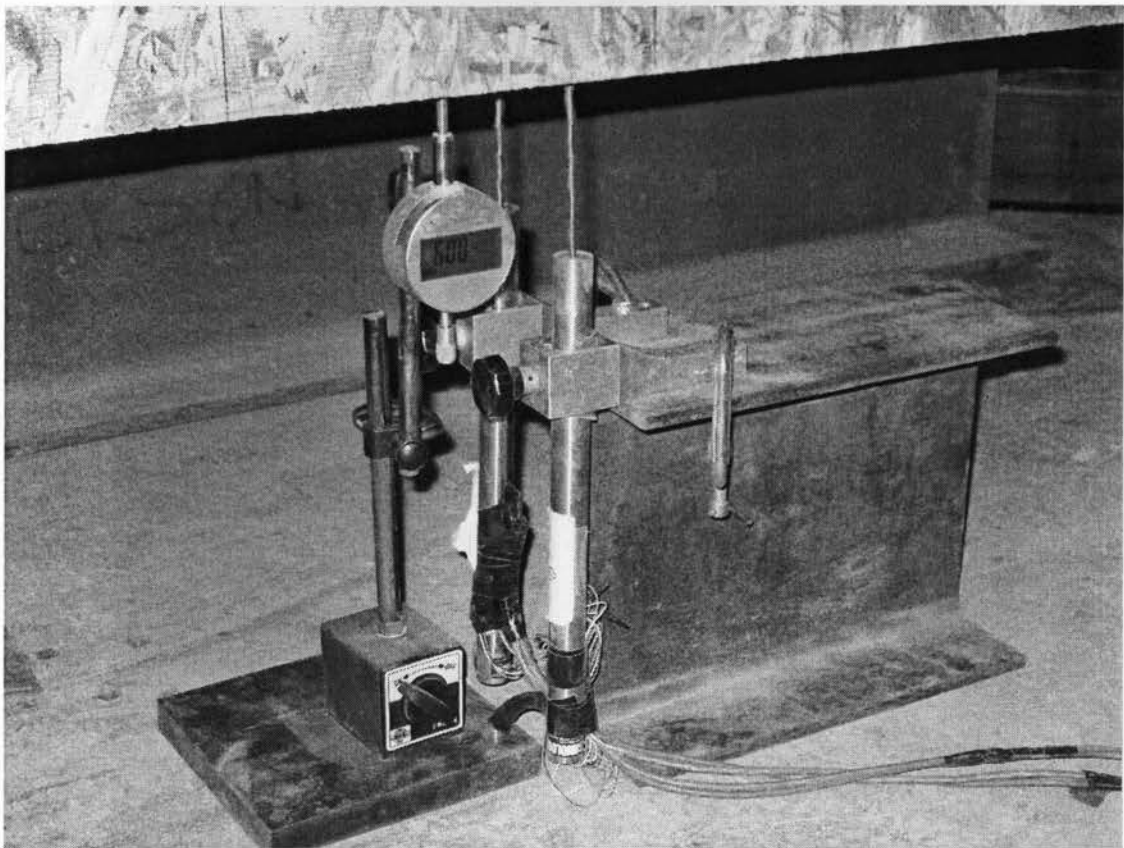


Figure 3.32 view of deflection sensors used in testing

4.2 Panel Group A

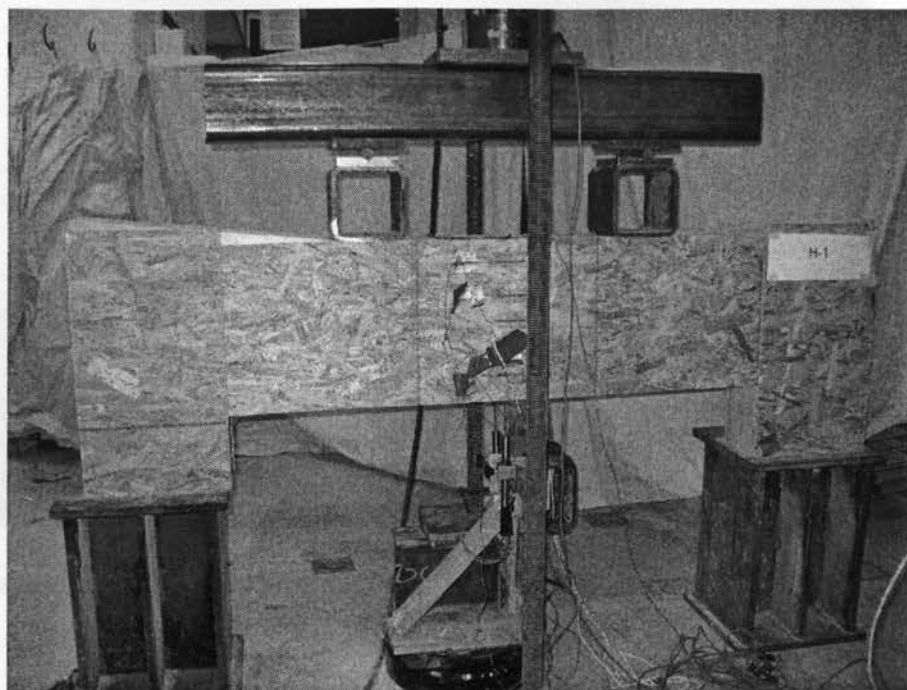


Figure 4.1 View of header H-1 after failure

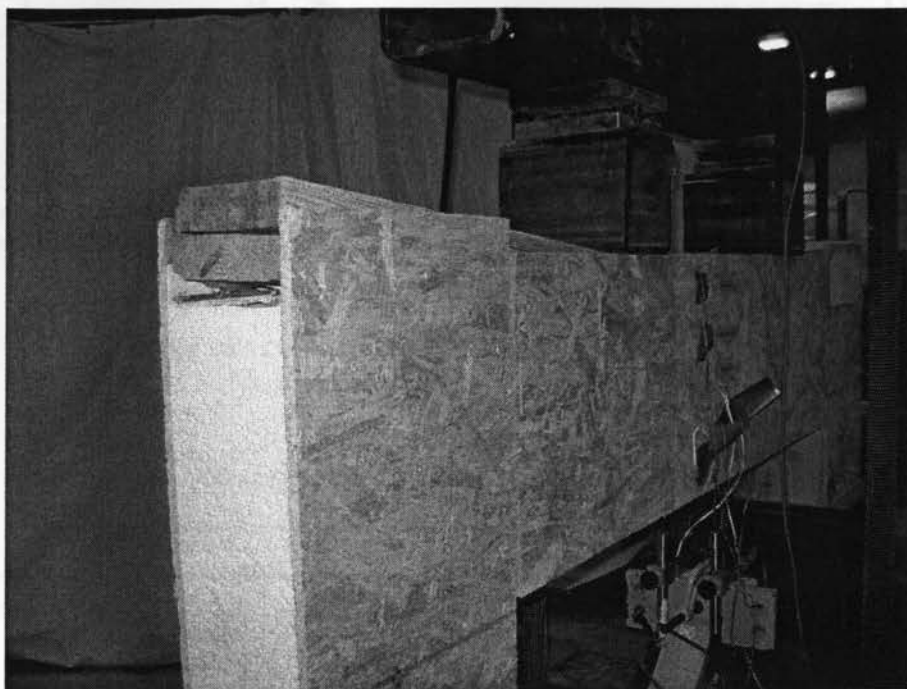


Figure 4.2 Close-up view of the failure mode in the left side of header H-1



Figure 4.3 Close-up view of the failure mode of the right side of header H-1

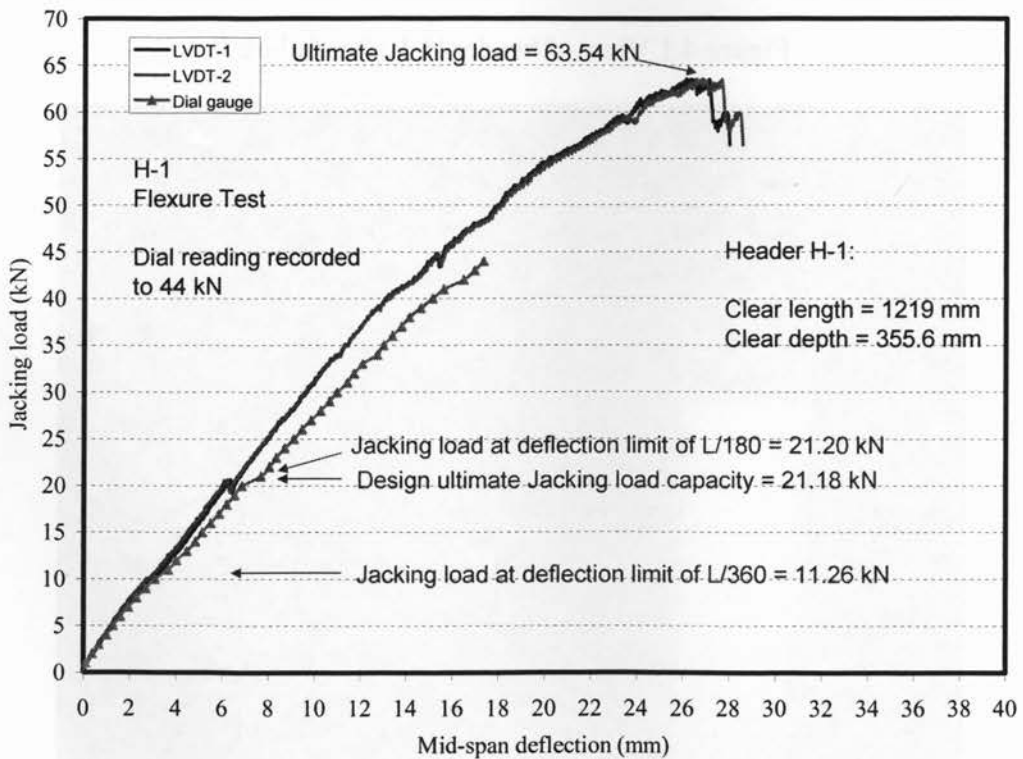


Figure 4.4 Jacking load-deflection relationship for header H-1

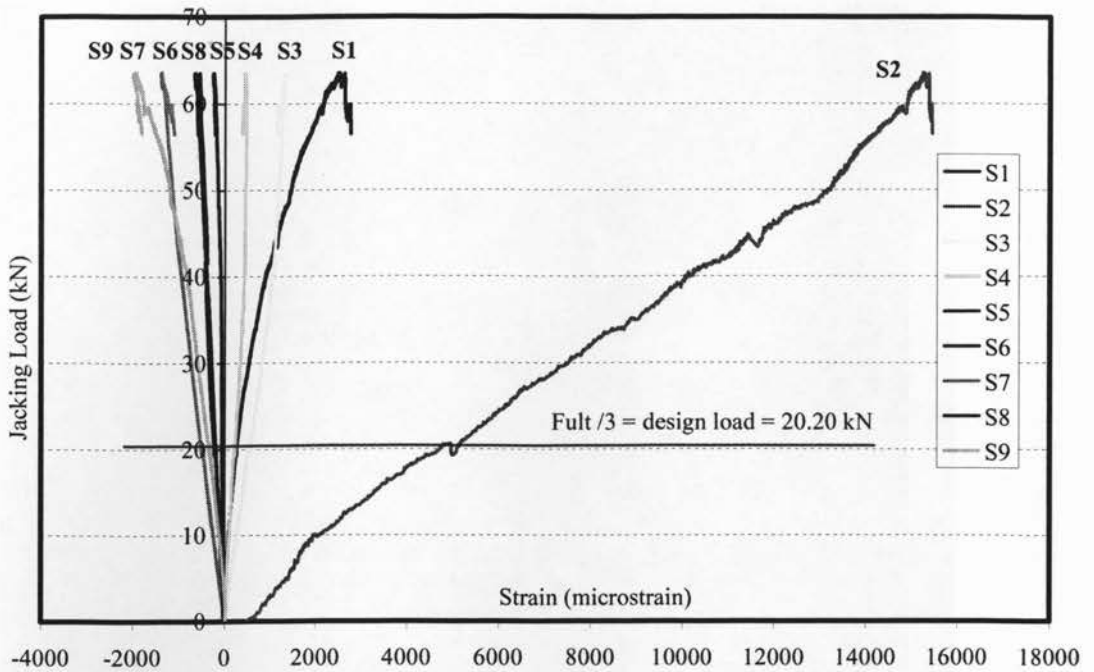


Figure 4.5 History of Jacking Load-Strain relationship for Header H-1

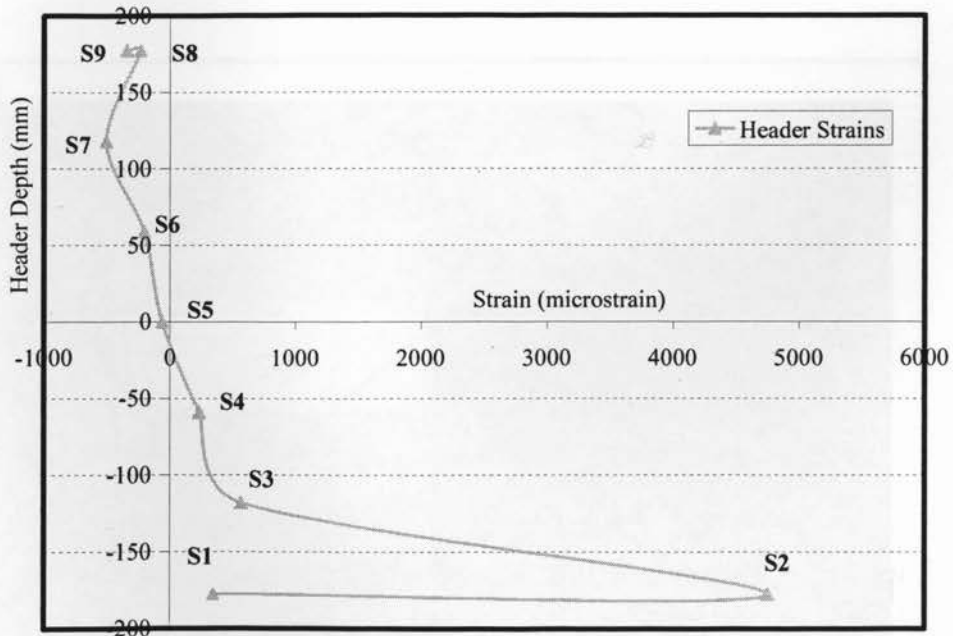


Figure 4.6 Strains across the header section for Header H-1 at $F_{ULT}/3$

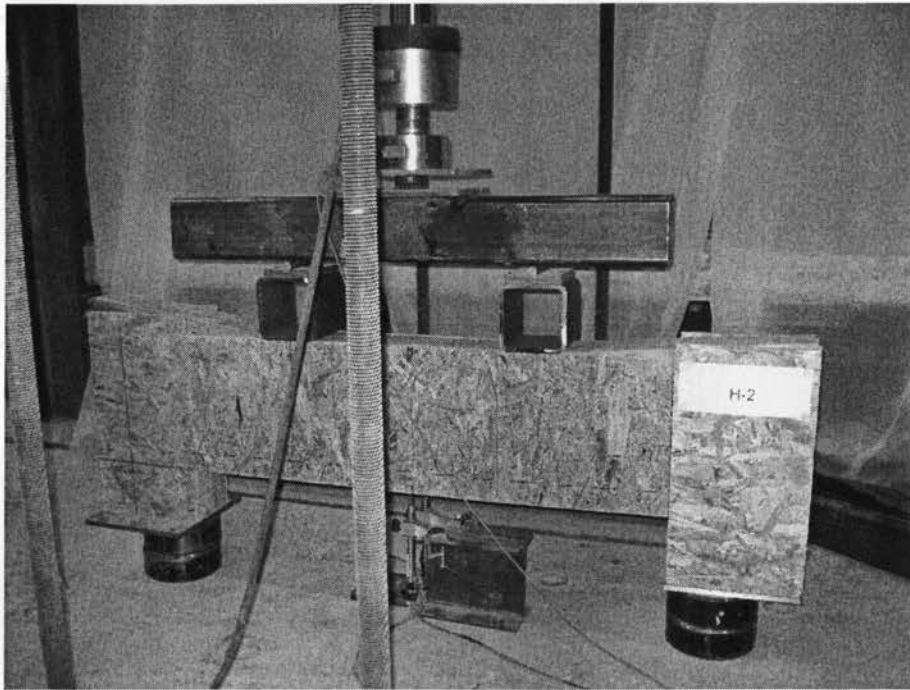


Figure 4.7 View of header H-2 after failure



Figure 4.8 Close-up view of the failure mode of header H-2



Figure 4.9 Close-up view of the foam and header end after removing the deformed OSB web of header H-2

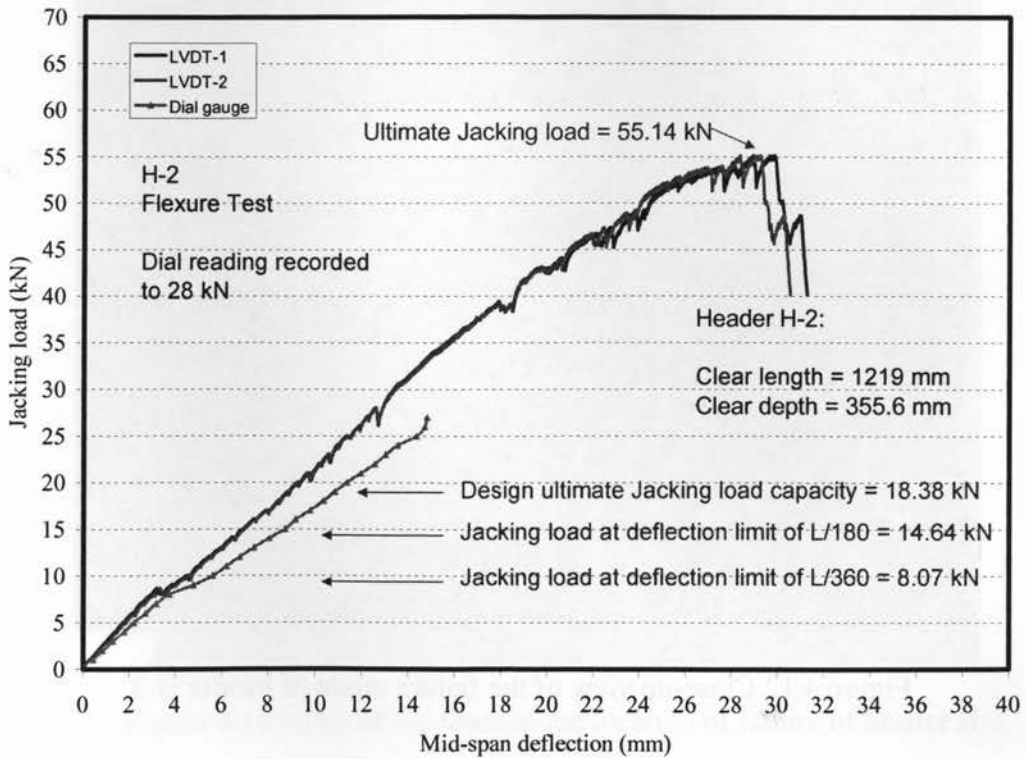


Figure 4.10 Jacking load-deflection relationship for header H-2

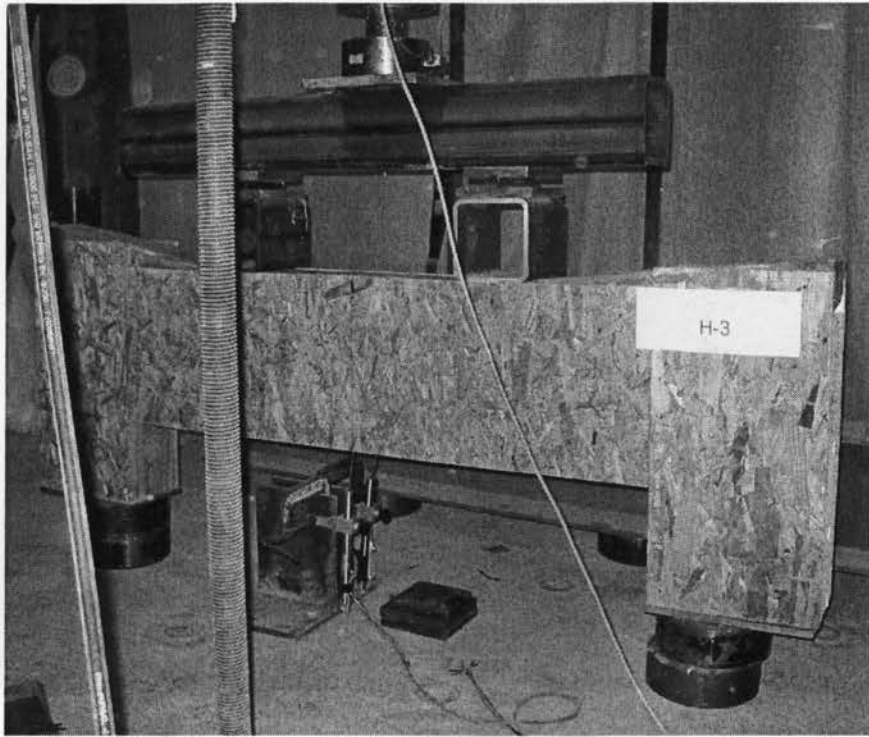


Figure 4.11 View of header H-3 after failure



Figure 4.12 Close-up view of the failure mode of header H-3

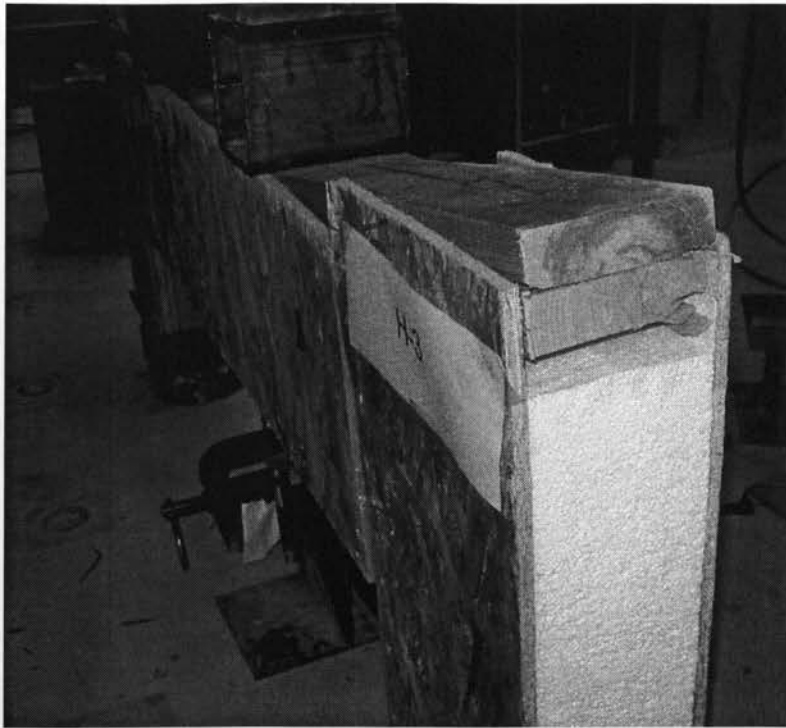


Figure 4.13 Close-up view of the failure mode of header H-3

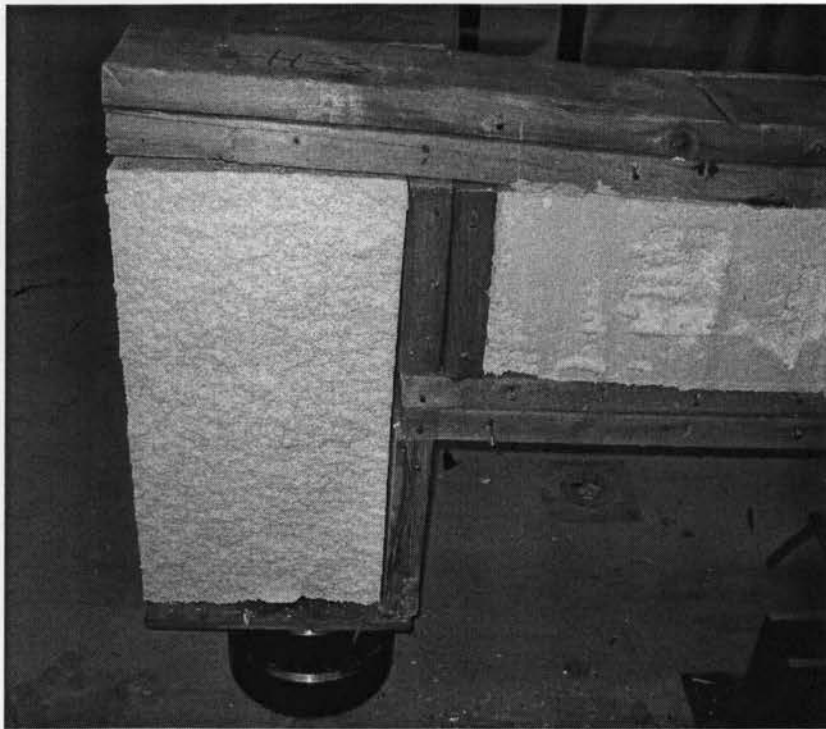


Figure 4.14 View of the foam at the location of failure of header H-3

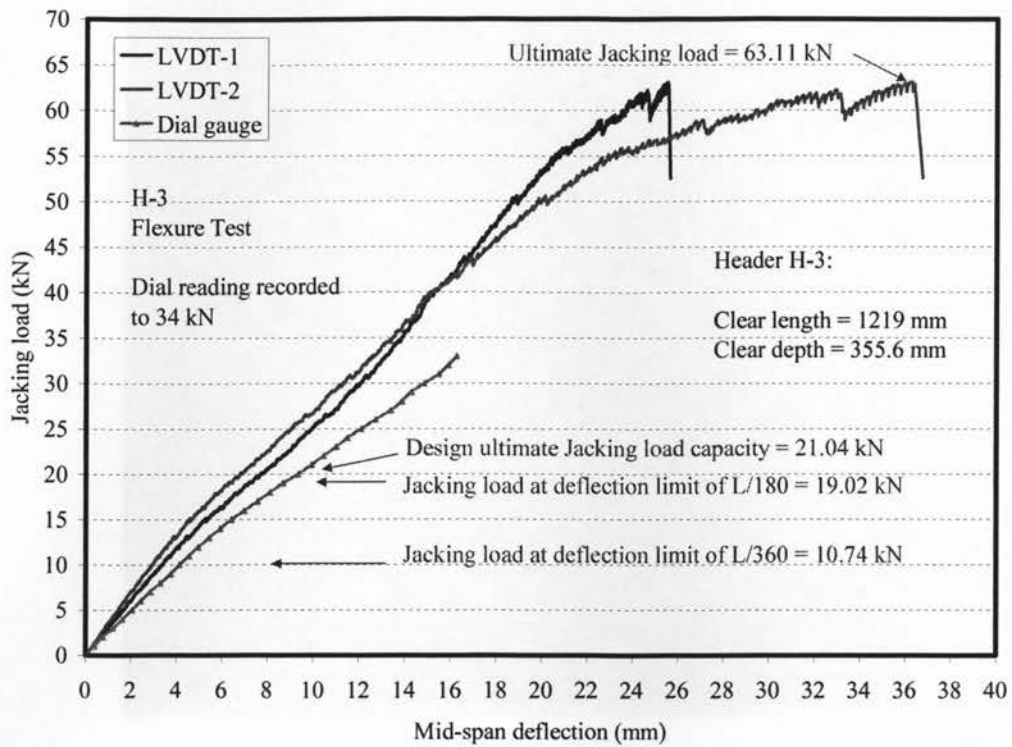


Figure 4.15 Jacking load-deflection relationship for header H-3

4.3 Panel Group B

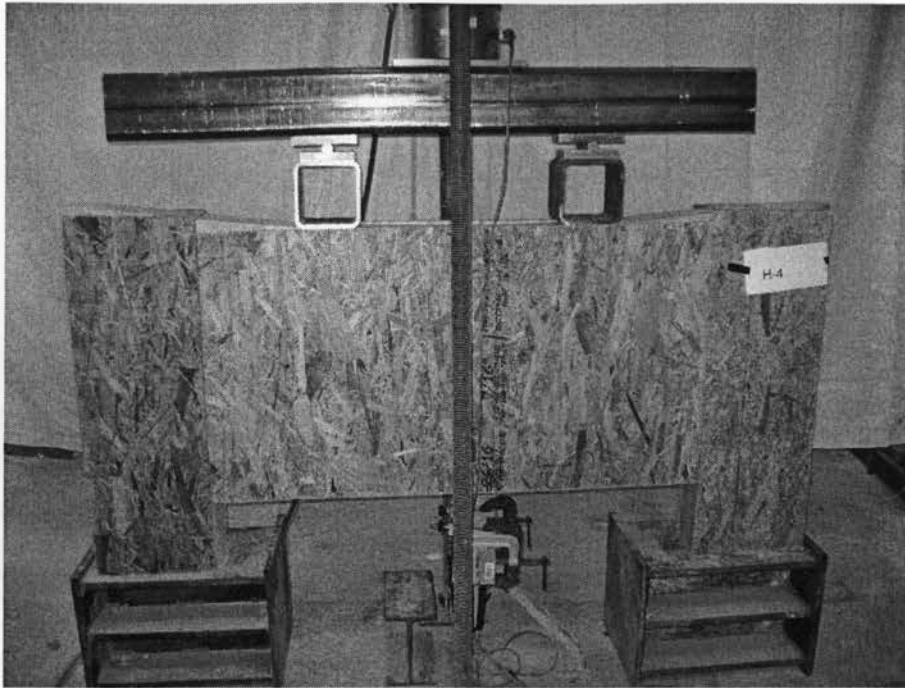


Figure 4.16 View of header H-4 after failure



Figure 4.17 Close-up view of the failure mode of the right side of header H-4

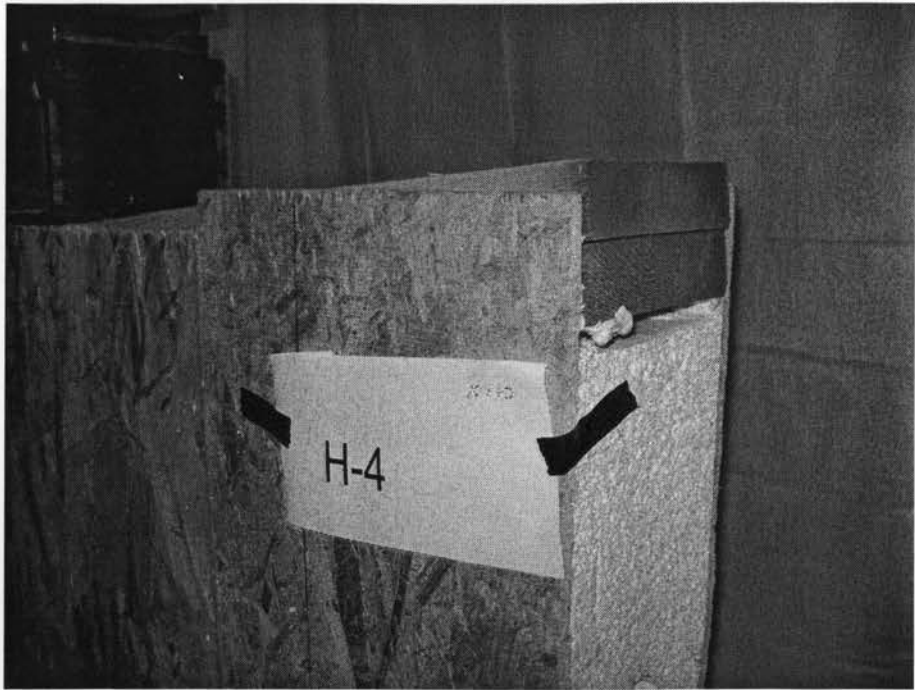


Figure 4.18 Close-up view of the failure mode of the right side of header H-4



Figure 4.19 Close-up view of the failure mode of the left side of header H-4

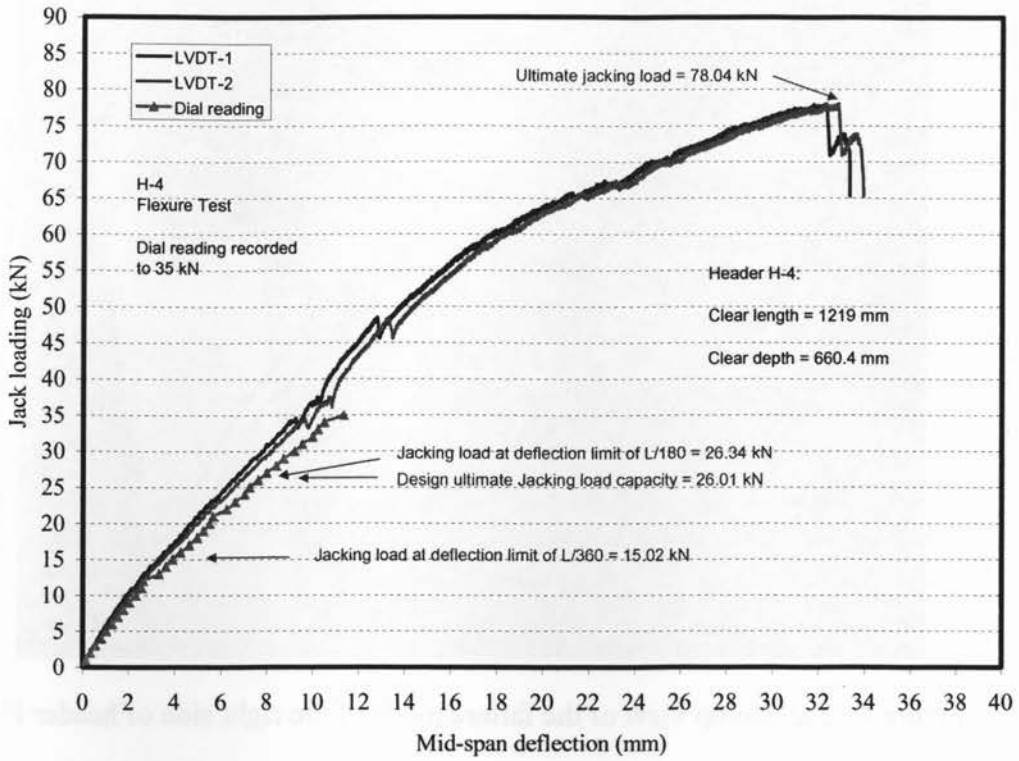


Figure 4.20 Jacking load-deflection relationship for header H-4

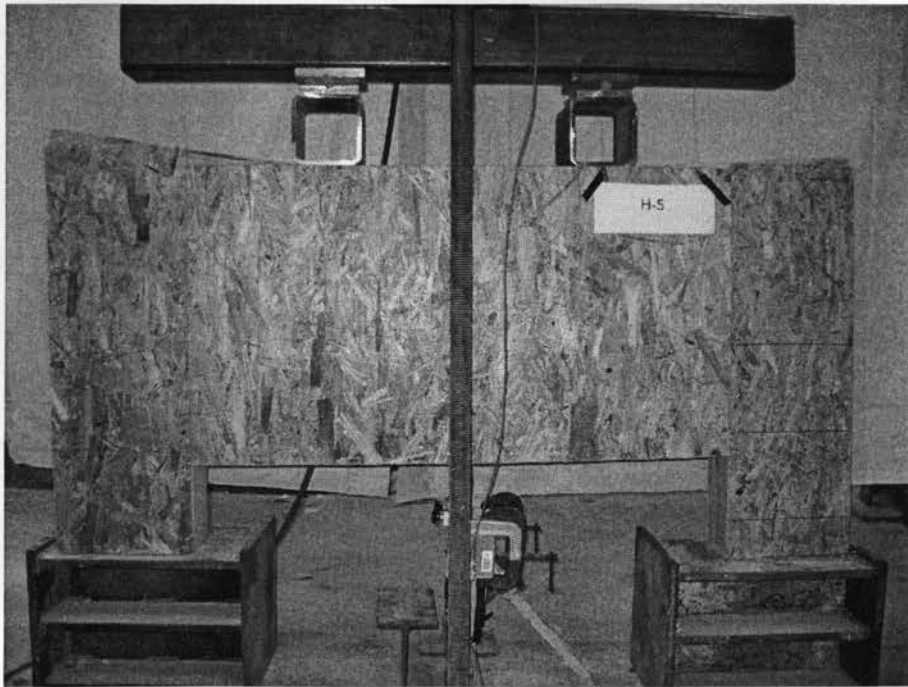


Figure 4.21 View of header H-5 after failure



Figure 4.22 Close-up view of the failure mode of the right side of header H-5

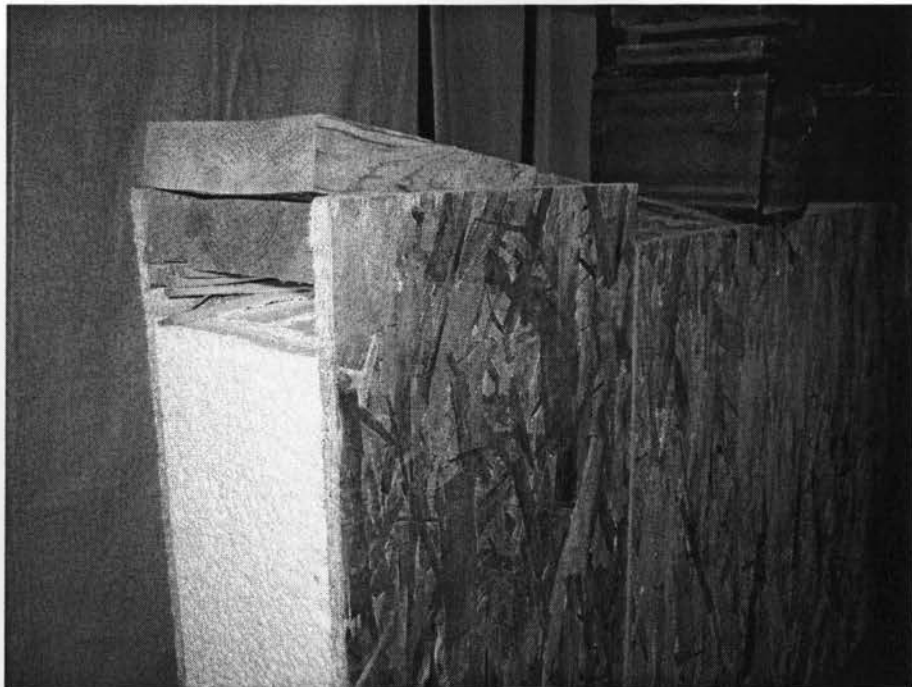


Figure 4.23 Close-up view of the failure mode of the left side of header H-5

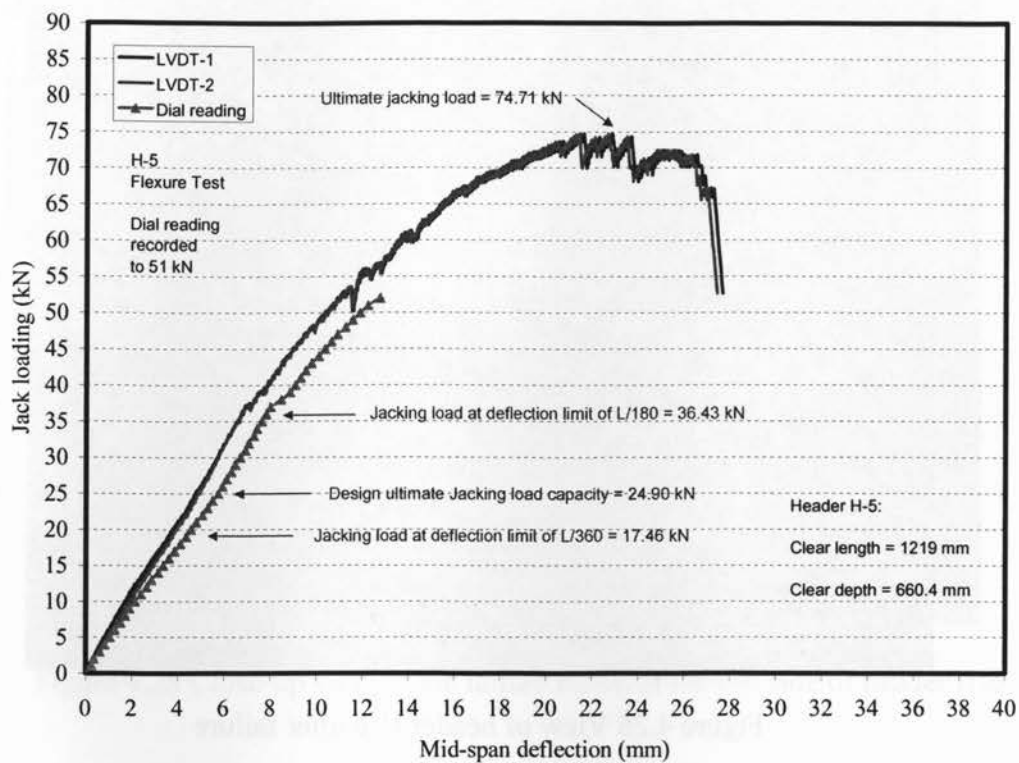


Figure 4.24 Jacking load-deflection relationship for header H-5

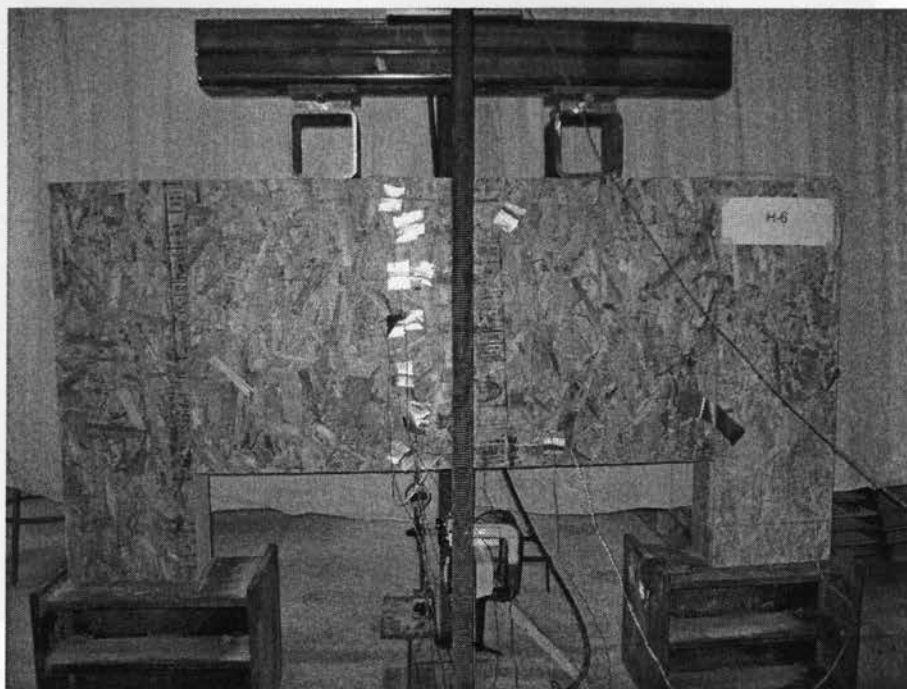


Figure 4.25 View of header H-6 before testing



Figure 4.26 View of header H-6 after failure



Figure 4.27 Close-up view of the failure mode of the right side of header H-6



Figure 4.28 Close-up view of the failure mode of the left side of header H-6

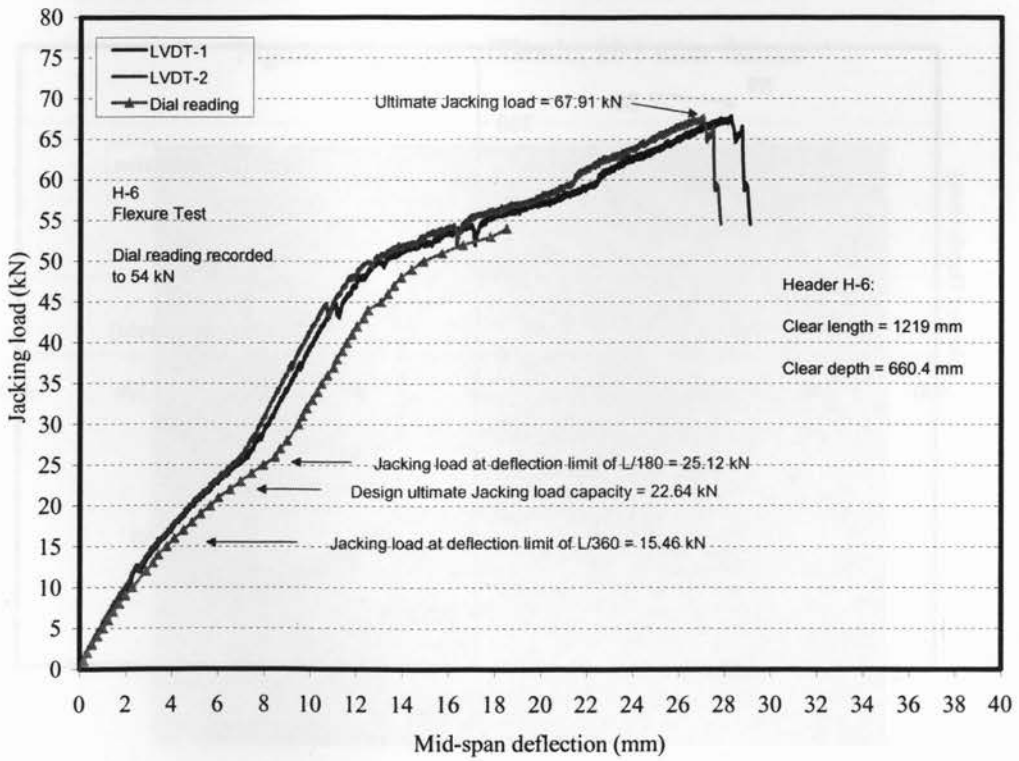


Figure 4.29 Jacking load-deflection relationship for header H-6

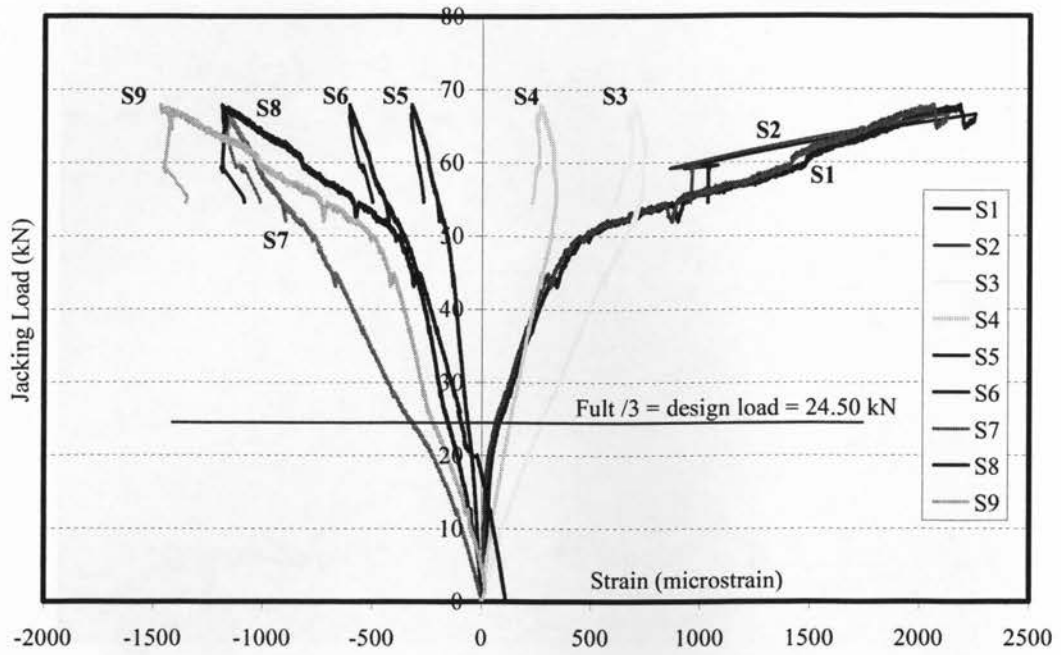


Figure 4.30 History of Jacking Load-Strain relationship for Header H-6

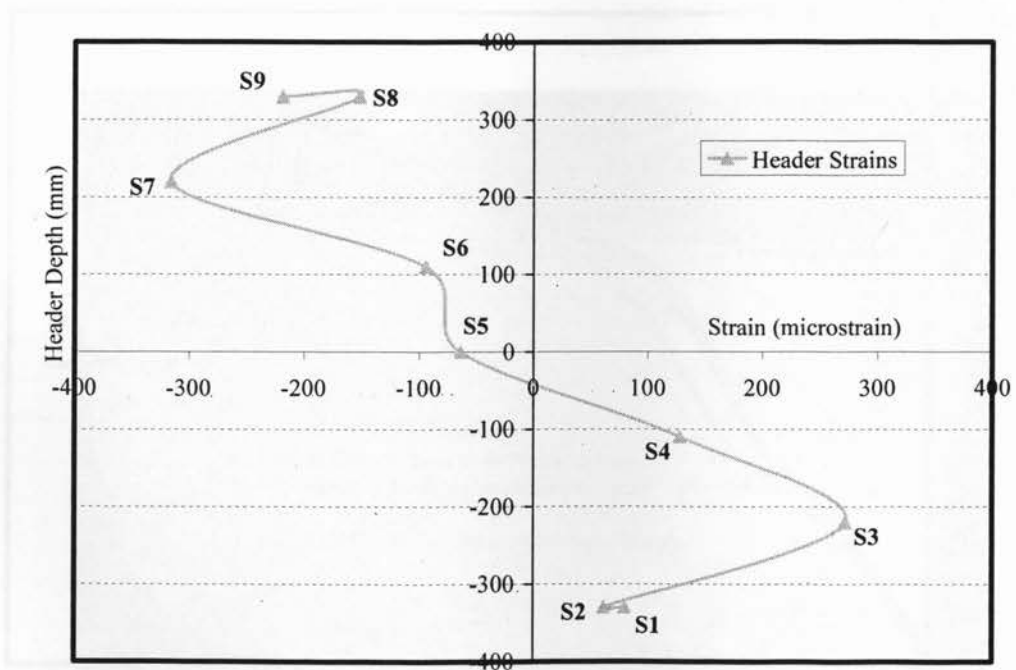


Figure 4.31 Strains across the header section for Header H-6 at $F_{ULT}/3$

4.4 Panel Group C

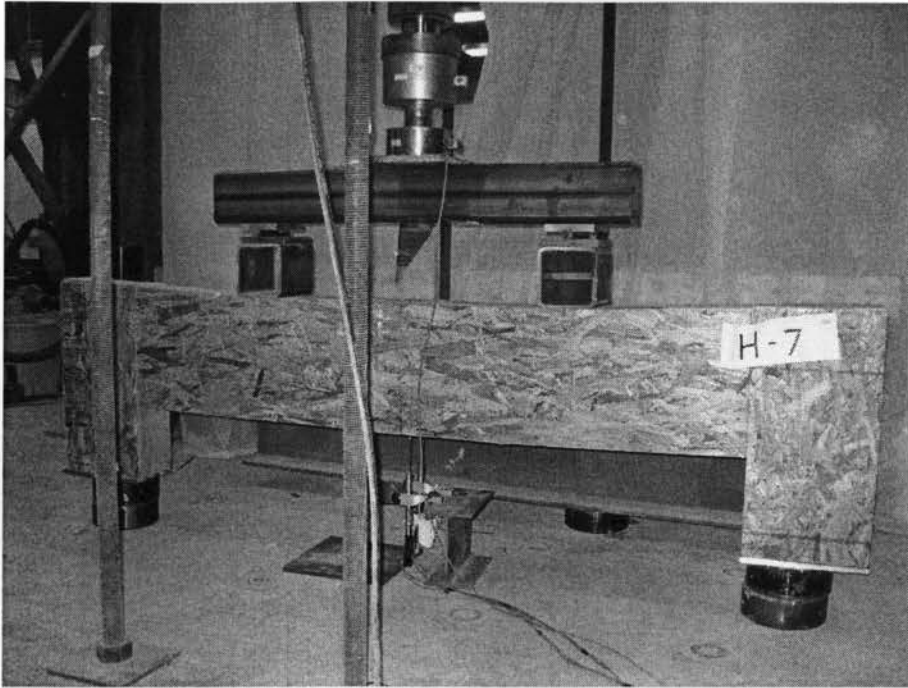


Figure 4.32 View of header H-7 after failure



Figure 4.33 Close-up view of the failure mode of the right side of header H-7



Figure 4.34 Close-up view of the failure mode of left side of header H-7

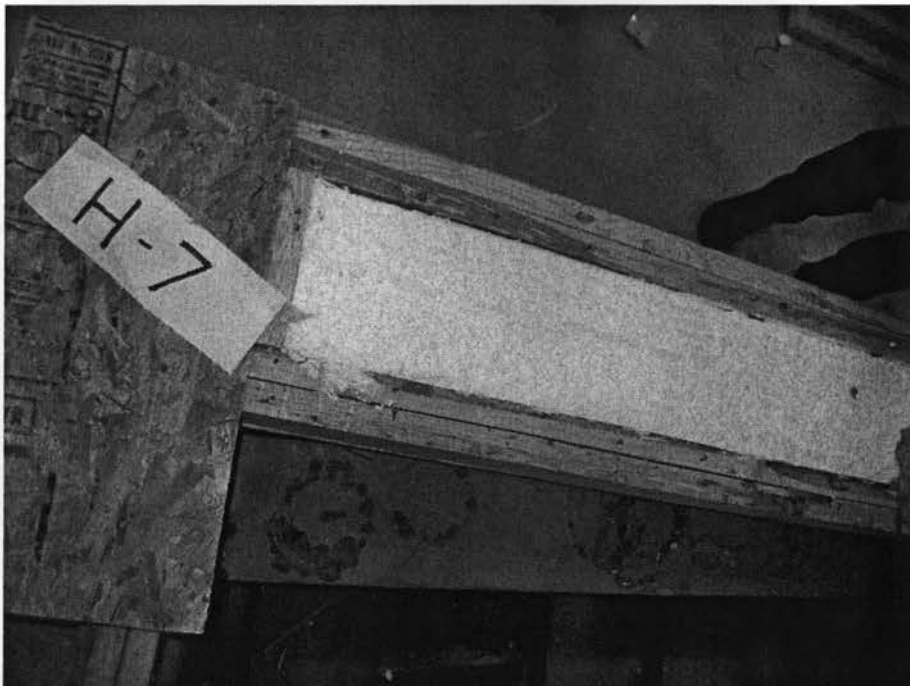


Figure 4.35 View of the foam at the location of failure of header H-7



Figure 4.36 Close-up view of the of the tensile fracture of the OSB web of header H-7

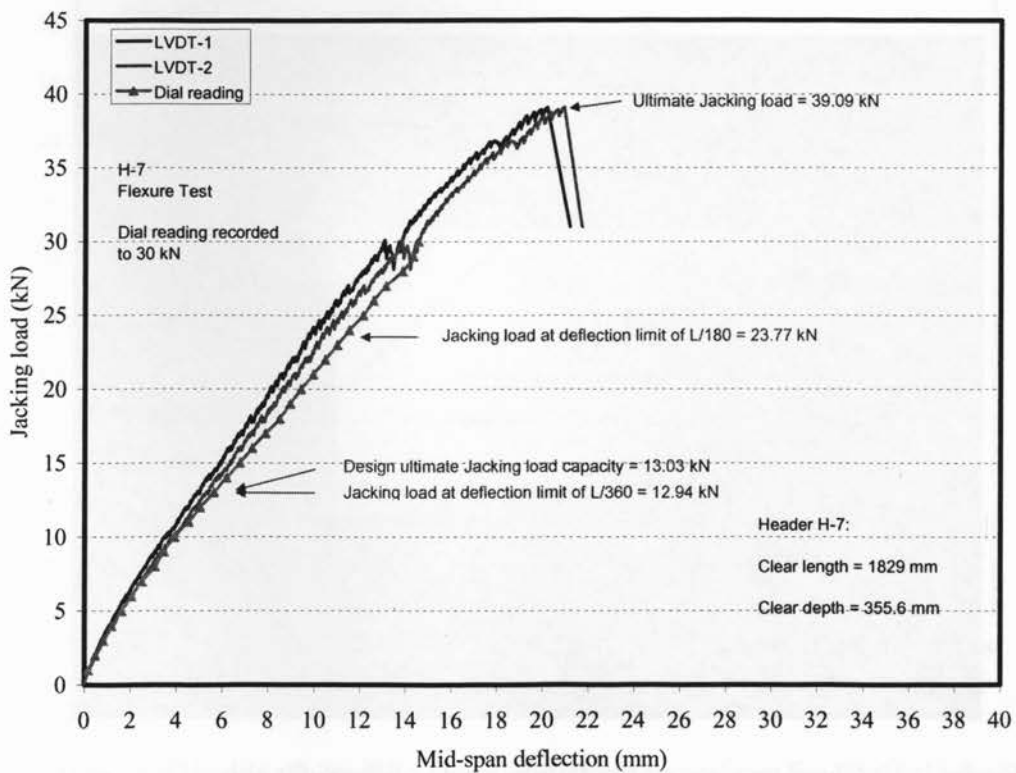


Figure 4.37 Jacking load-deflection relationship for header H-7

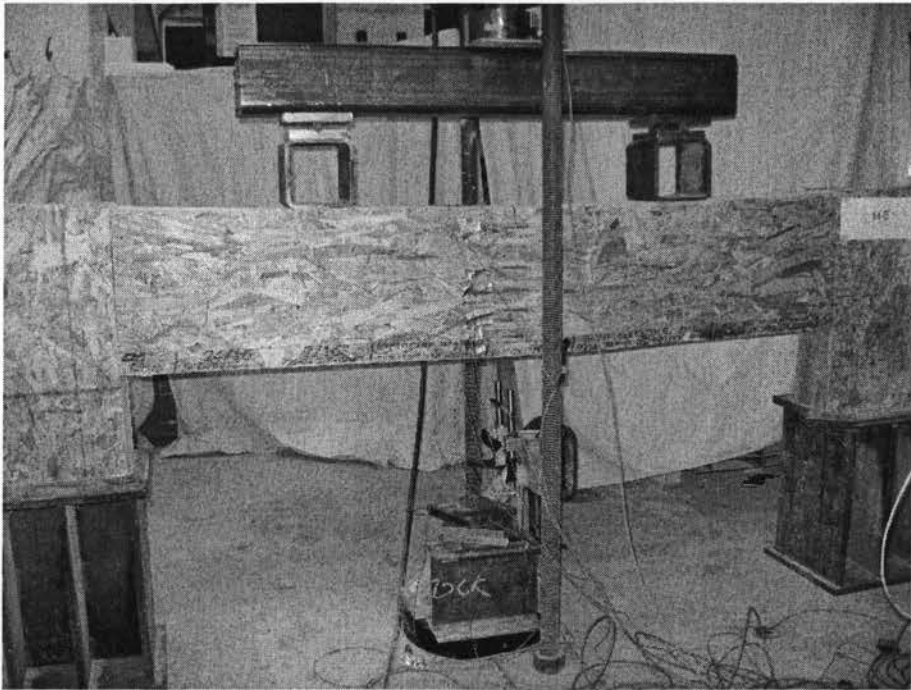


Figure 4.38 View of header H-8 after failure



Figure 4.39 Close-up view of the failure mode of the right side of header H-8



Figure 4.40 Close-up view of the failure mode of the left side of header H-8

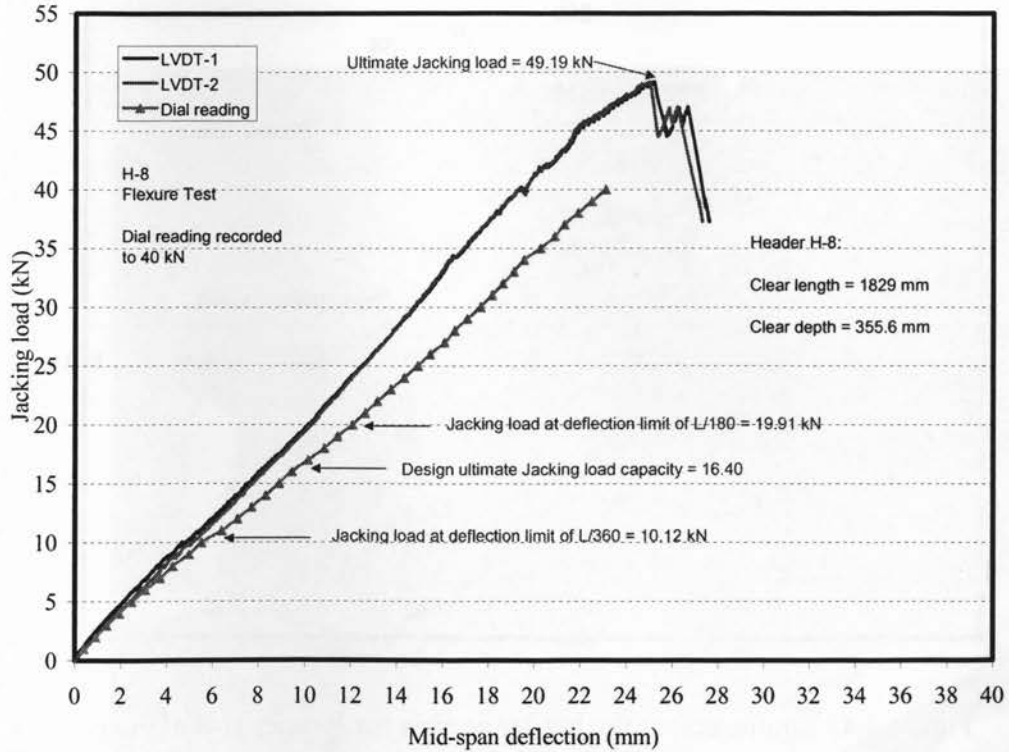


Figure 4.41 Jacking load-deflection relationship for header H-8

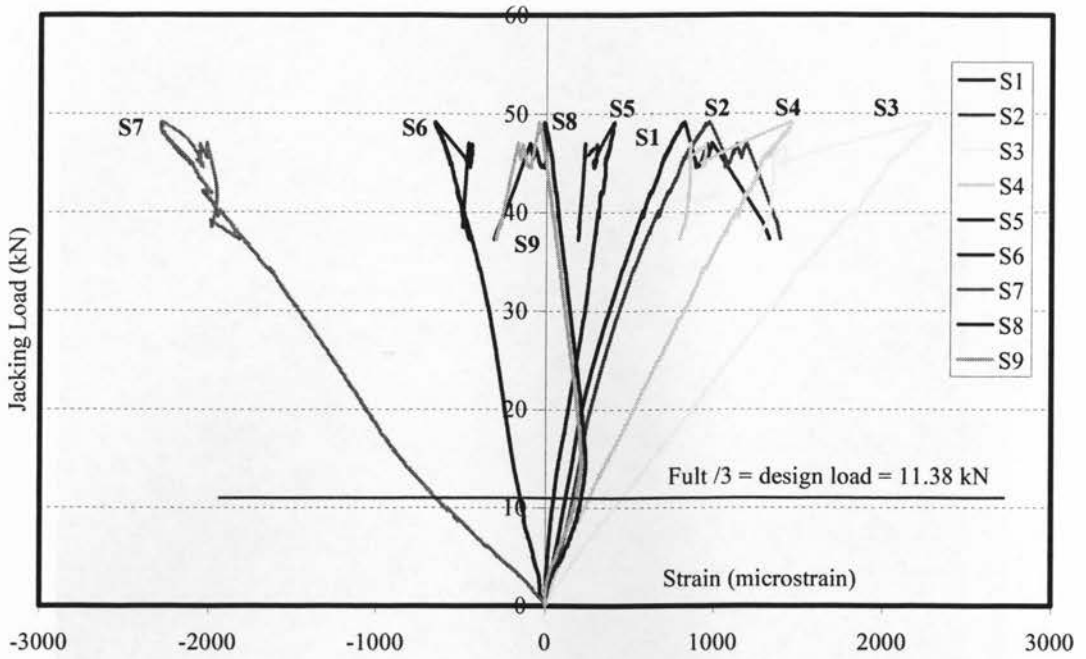


Figure 4.42 History of Jacking Load-Strain relationship for Header H-8

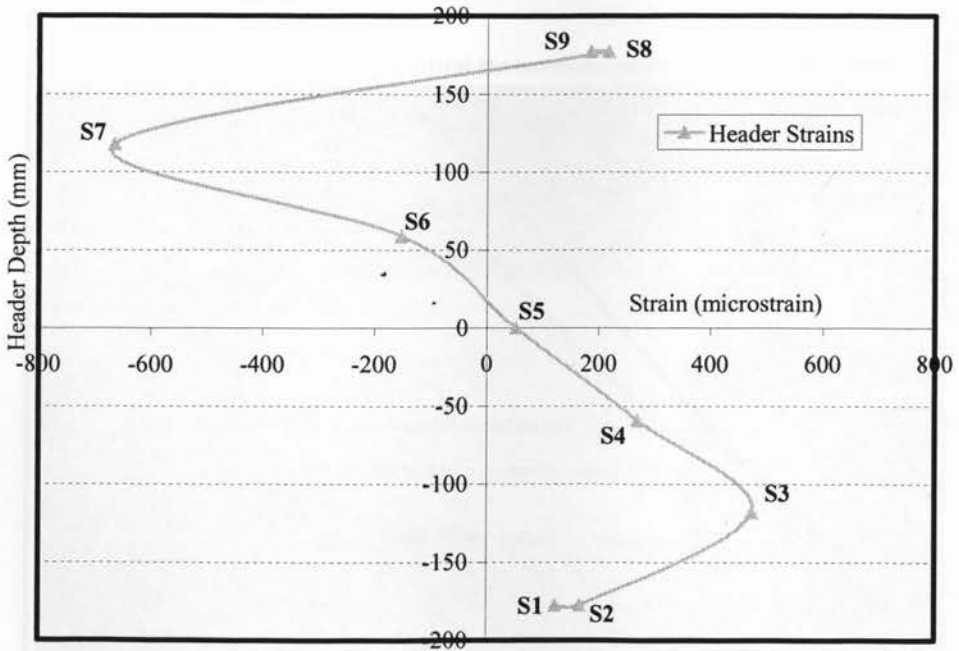


Figure 4.43 Strains across the header section for Header H-8 at $F_{ULT}/3$

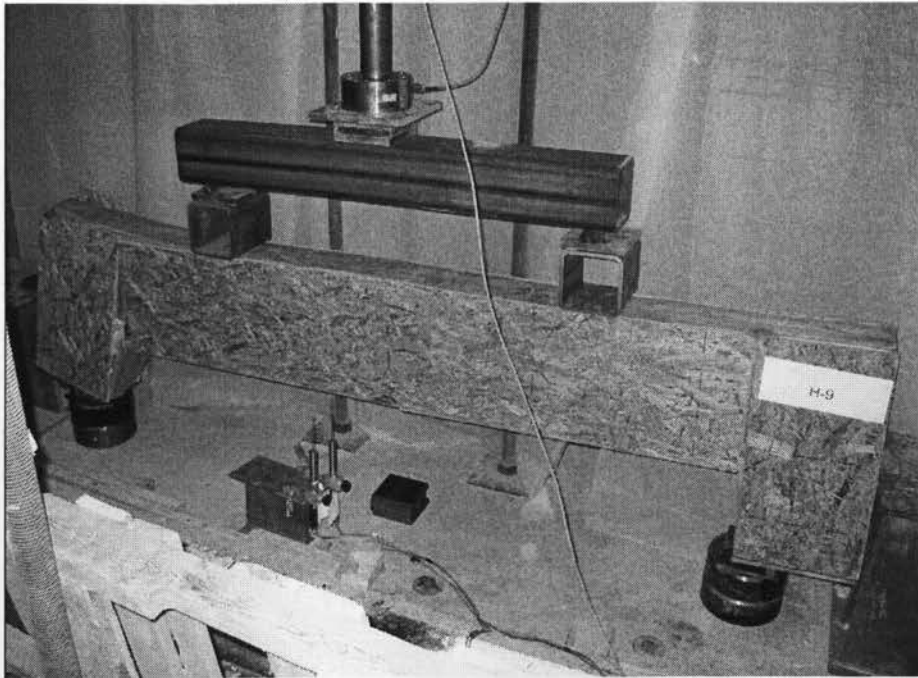


Figure 4.44 View of header H-9 after failure

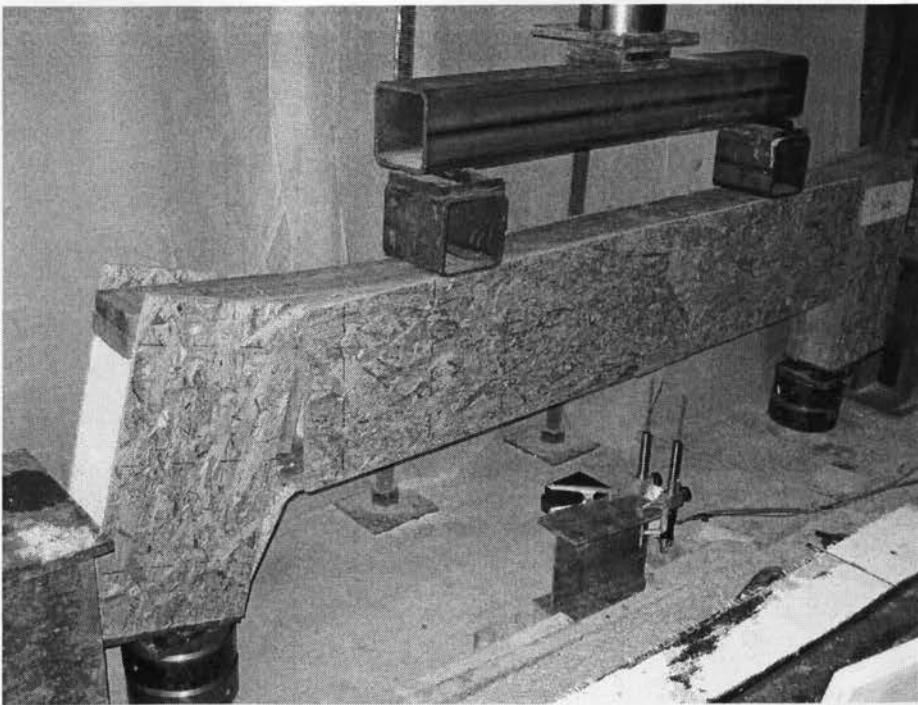


Figure 4.45 Other view of the failure mode of header H-9



Figure 4.46 Close up view of the failure mode of header H-9

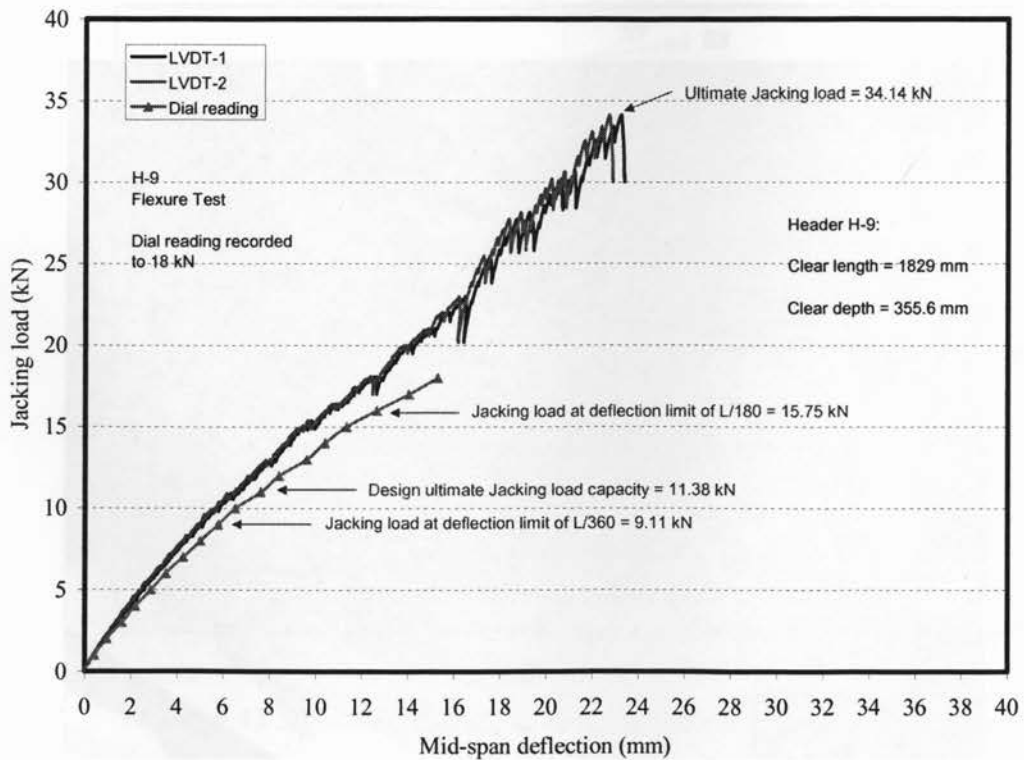


Figure 4.47 Jacking load-deflection relationship for header H-9

4.5 Panel Group D

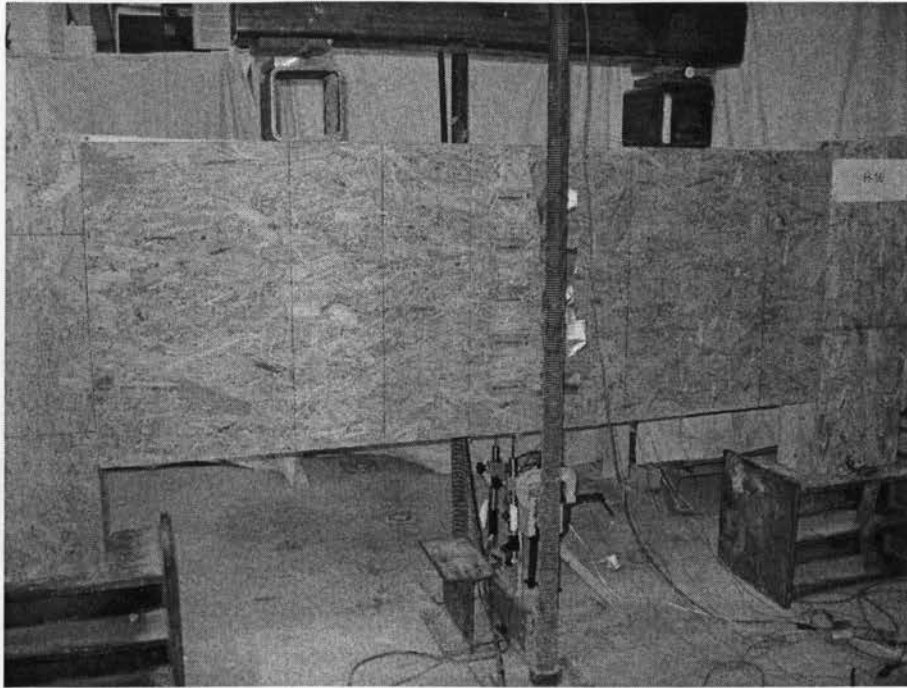


Figure 4.48 View of header H-10 after failure



Figure 4.49 Close-up view of the failure mode of the left side of header H-10

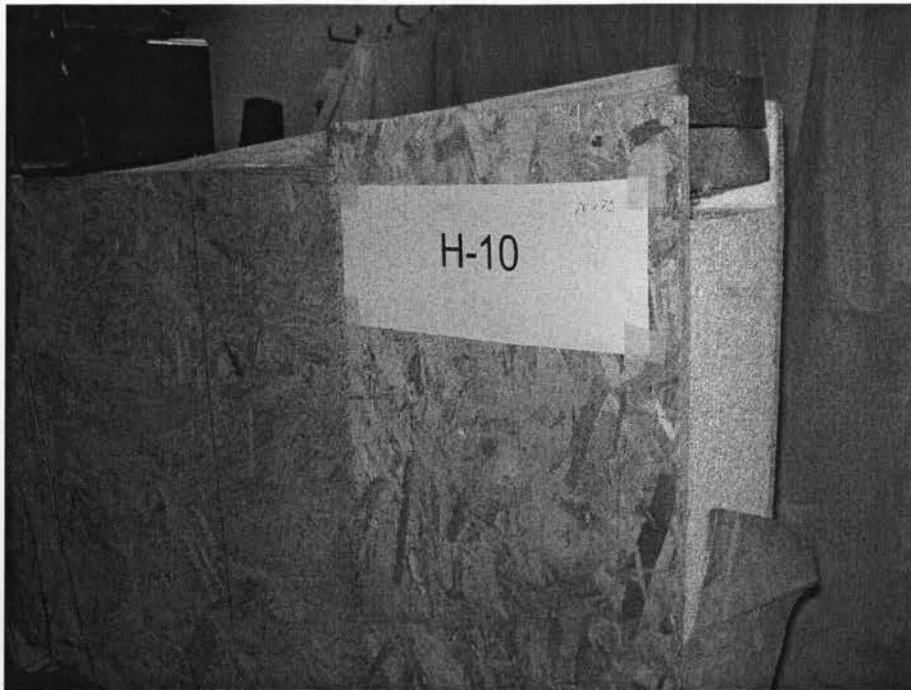


Figure 4.50 Close-up view of the failure mode of the right side of header H-10

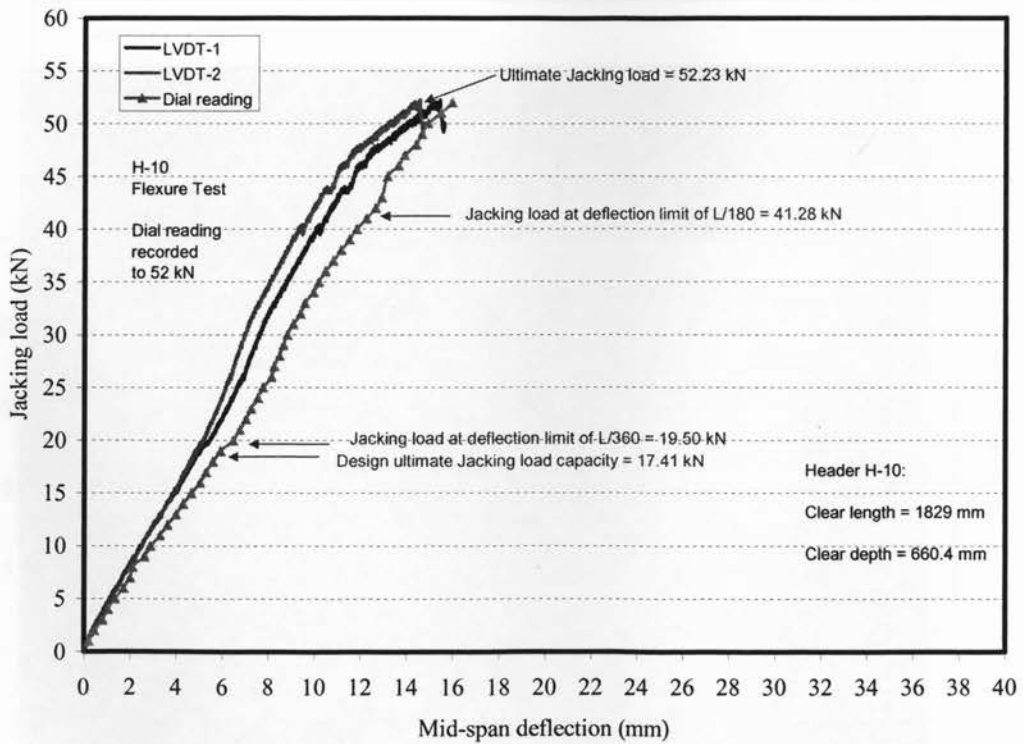


Figure 4.51 Jacking load-deflection relationship for header H-10

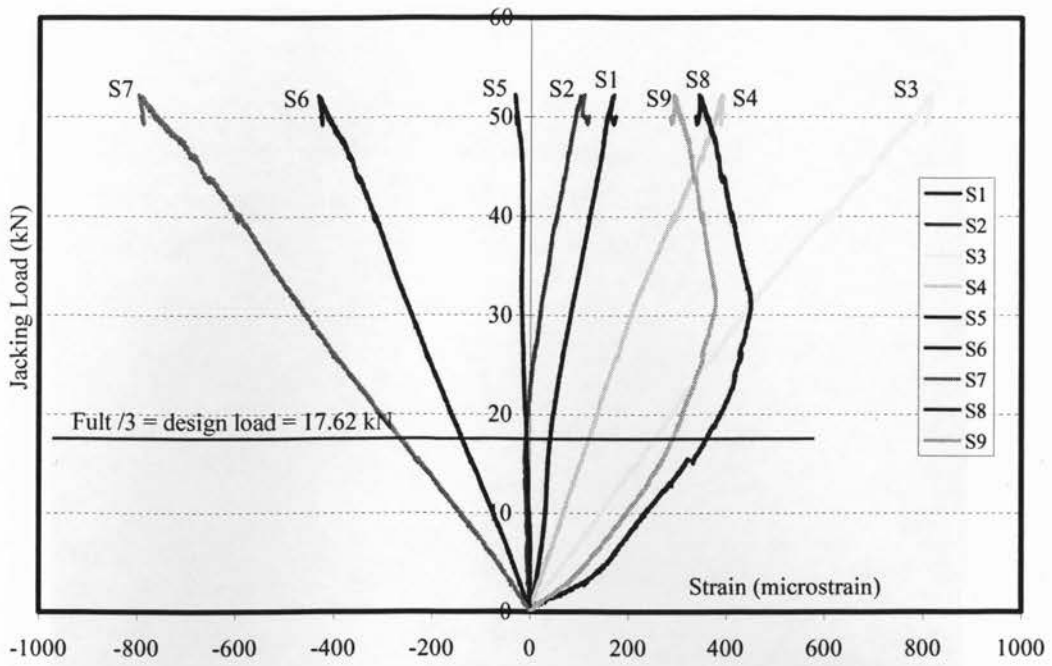


Figure 4.52 History of Jacking Load-Strain relationship for Header H-10

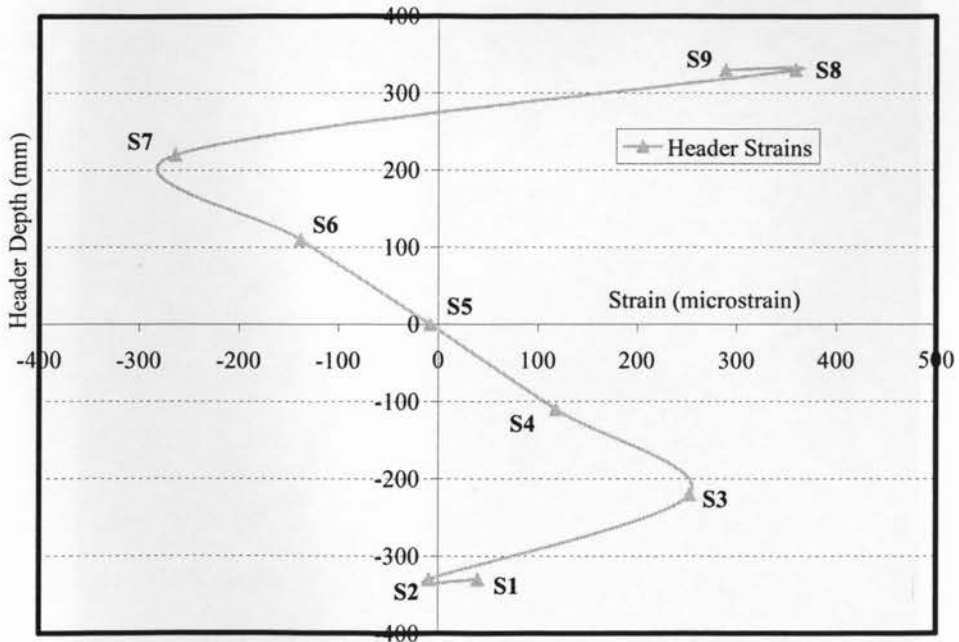


Figure 4.53 Strains across the header section for Header H-10 at $F_{ULT}/3$

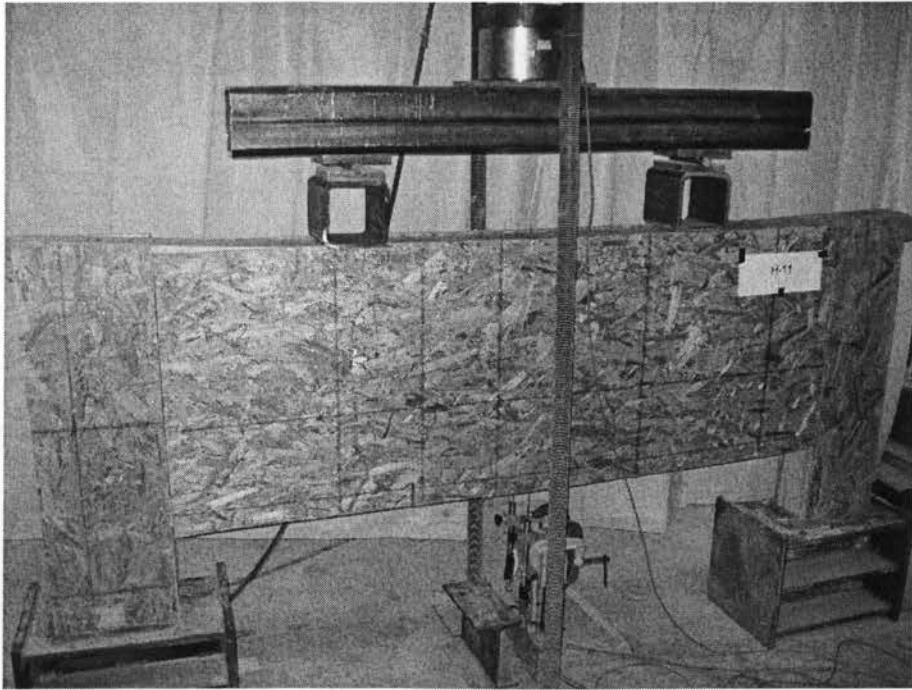
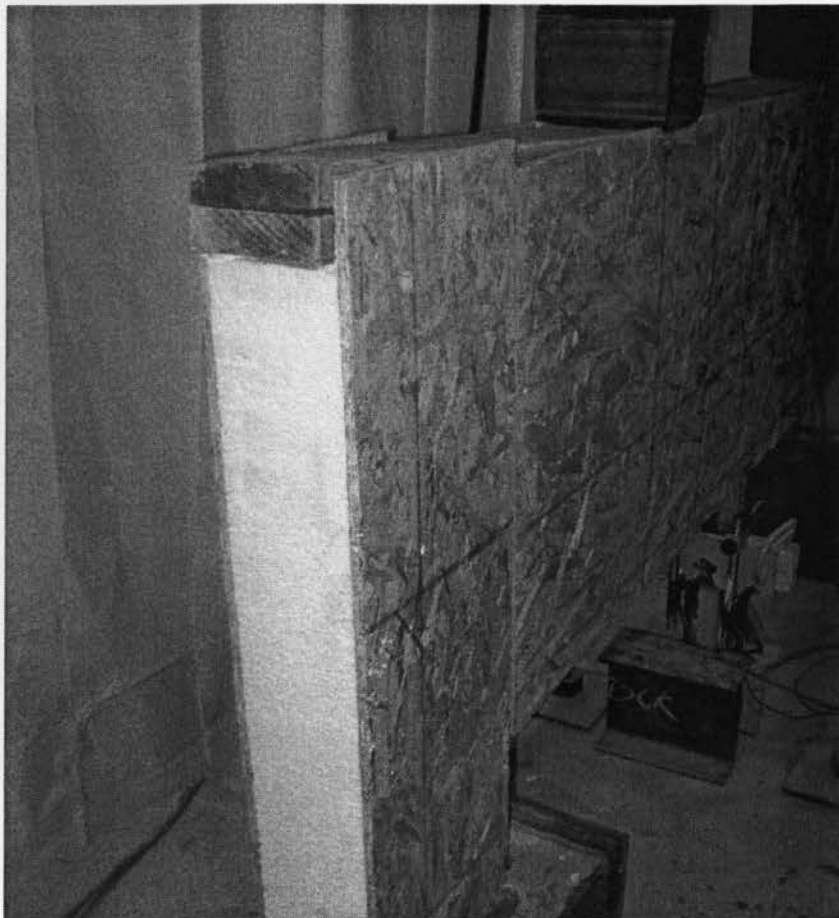


Figure 4.54 View of header H-11 after failure



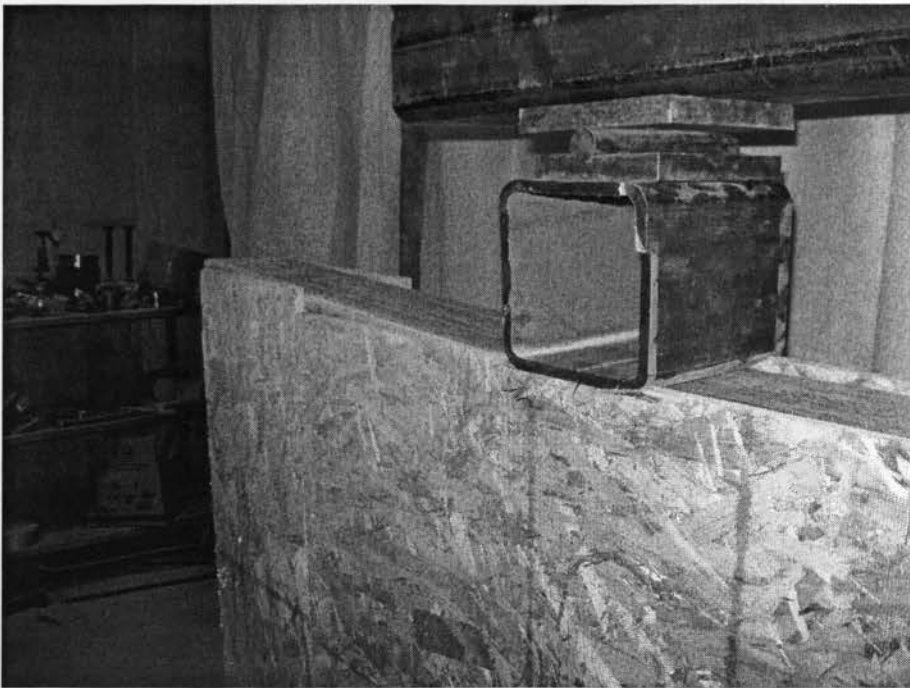
(a)



(b)



(c)



(d)

Figure 4.55 Views of the failure mode of header H-11

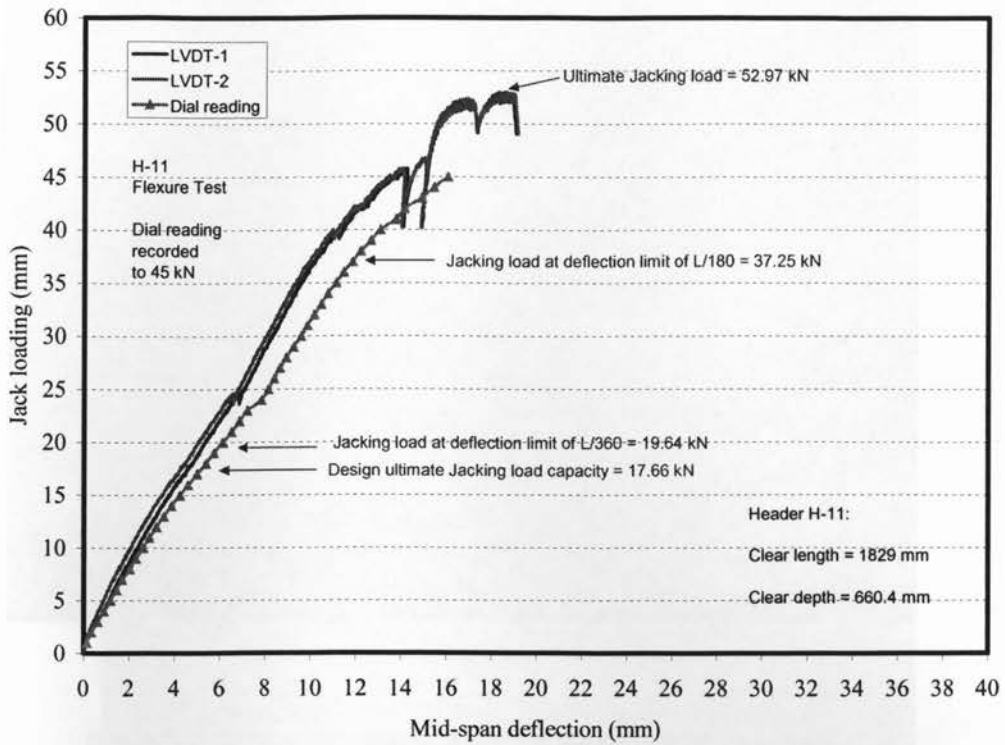


Figure 4.56 Jacking load-deflection relationship for header H-11

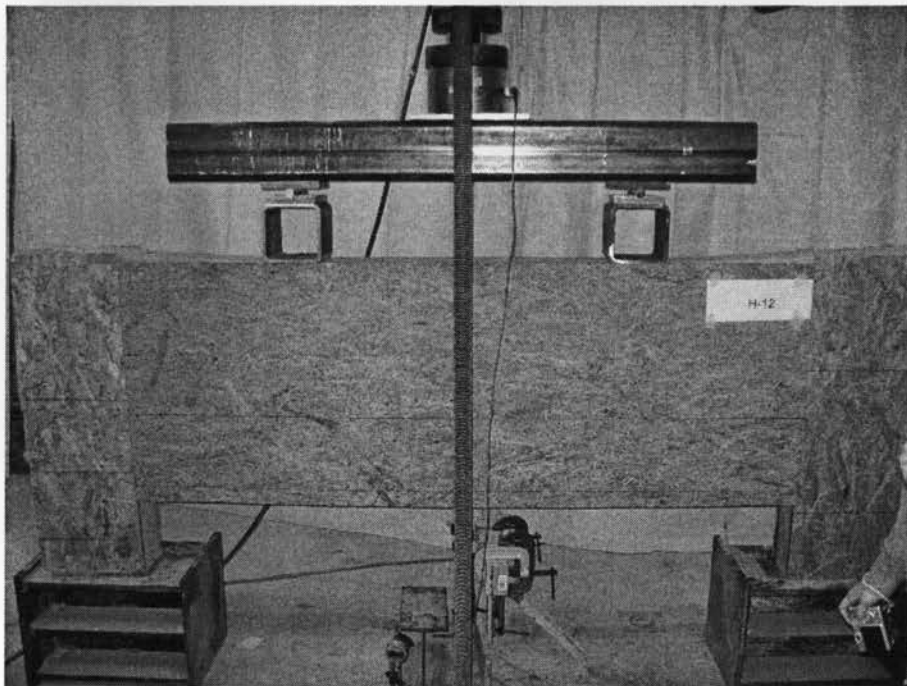


Figure 4.57 View of header H-12 after failure



(a)



(b)



(c)

Figure 4.58 Close-up views of the failure mode of header H-12

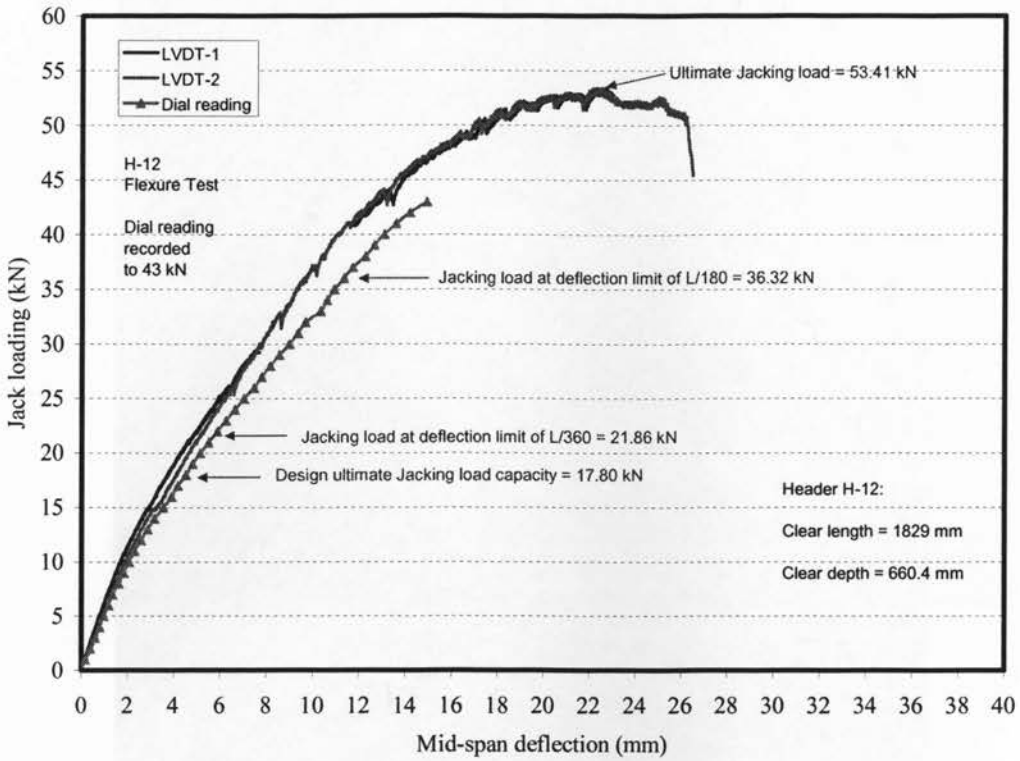


Figure 4.59 Jacking load-deflection relationship for header H-12

4.6 Panel Group E

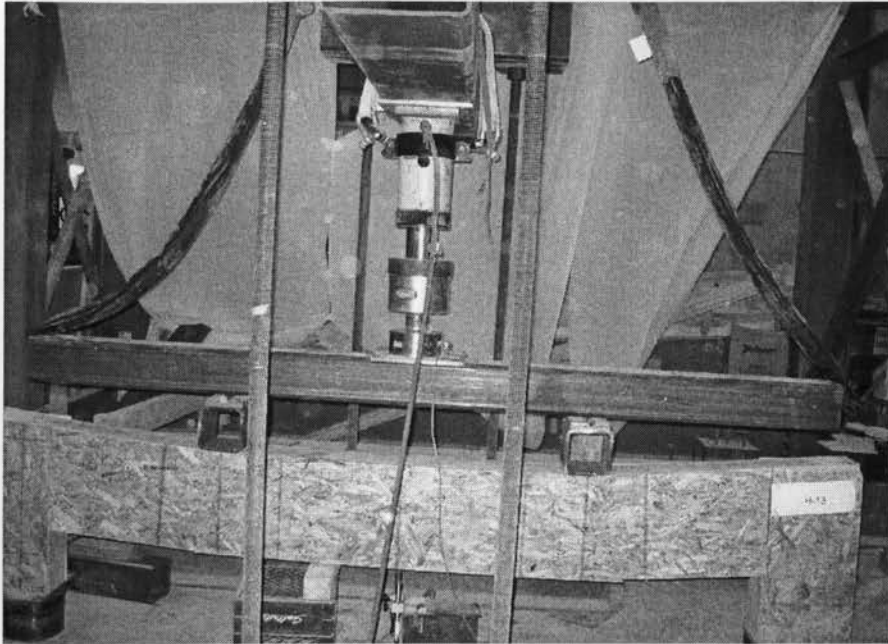


Figure 4.60 View of header H-13 after failure



Figure 4.61 View of header H-13 after failure



Figure 4.62 Close-up view of the failure mode at support of header H-13

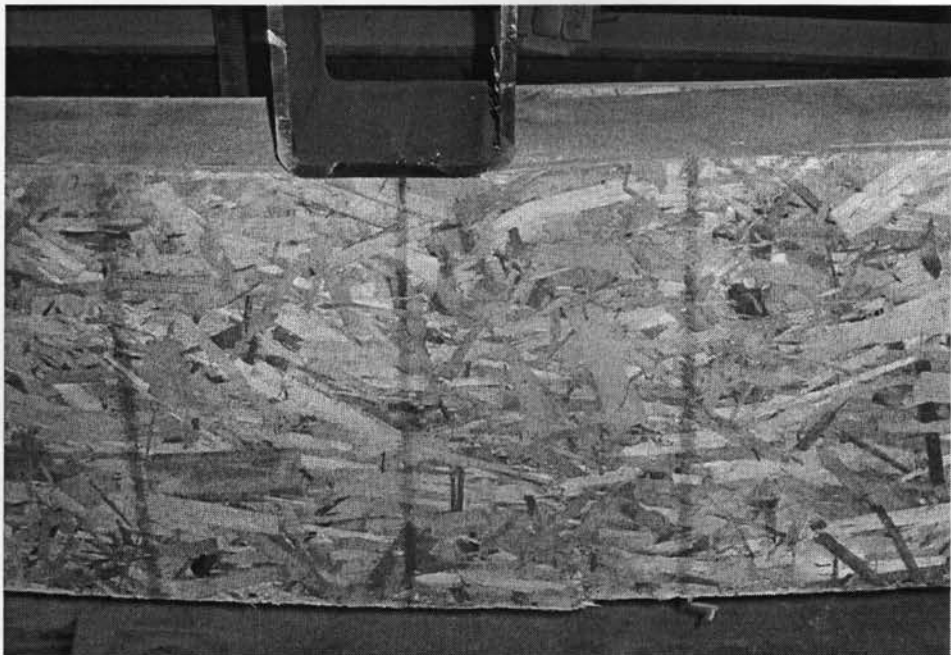


Figure 4.63 Close-up view of the flexure failure mode at quarter point of header H-13



Figure 4.64 Close-up view of the flexure failure mode at quarter point of header H-13



Figure 4.65 Close-up view of the flexure failure mode at quarter point of header H-13



Figure 4.66 Close-up view of the flexure failure mode at quarter point of header H-13



Figure 4.67 Close-up view of the flexure failure mode at quarter point of header H-13



Figure 4.68 Close-up view of the flexure failure mode at quarter point of header H-13

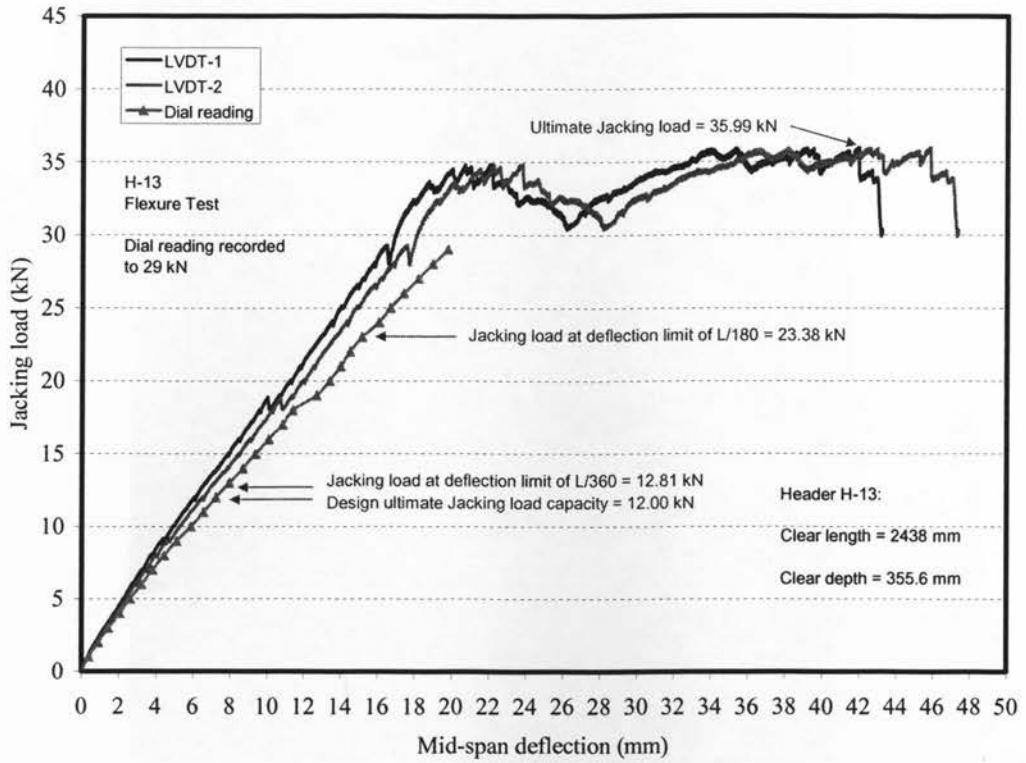


Figure 4.69 Jacking load-deflection relationship for header H-13

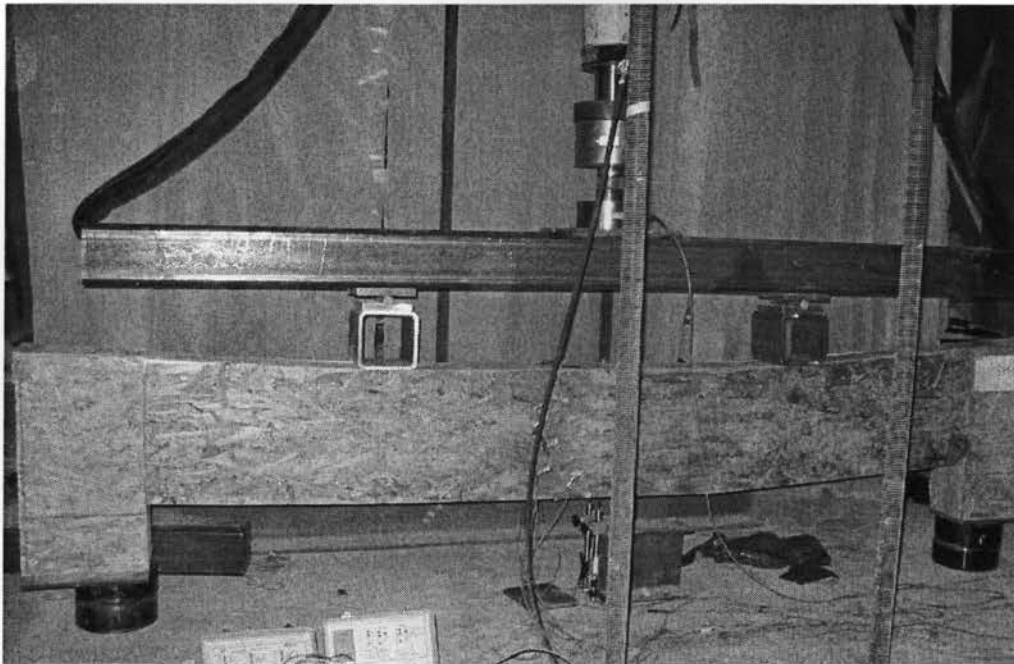


Figure 4.70 View of header H-14 after failure



Figure 4.71 Close-up view of the failure mode at support of header H-14

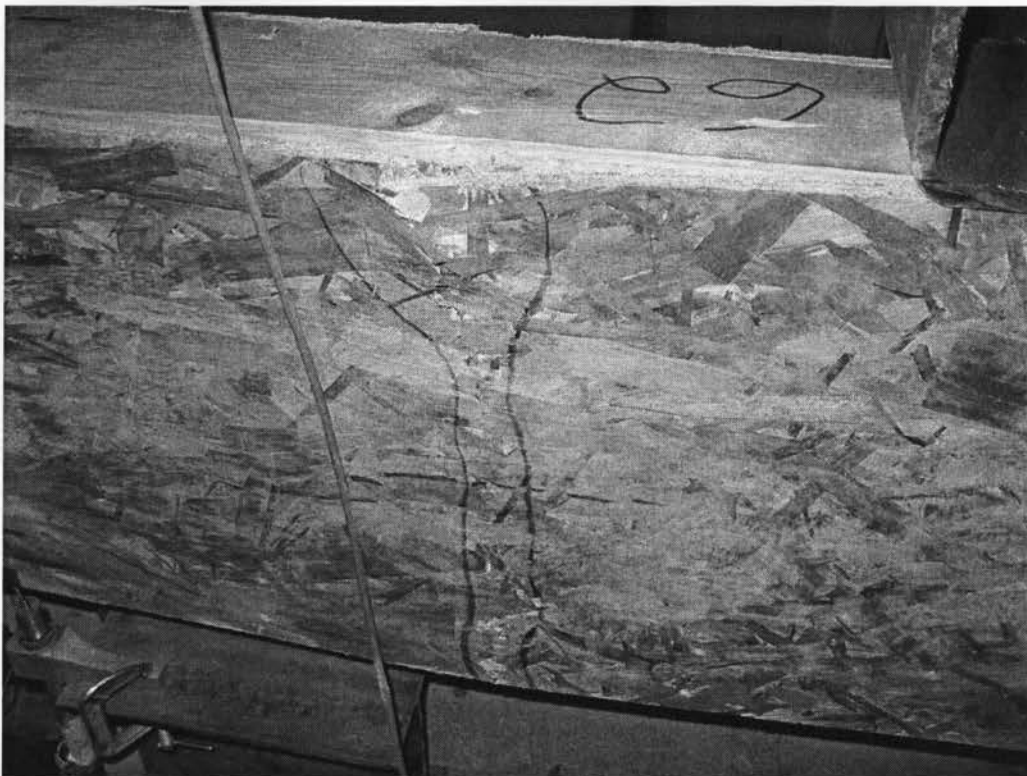


Figure 4.72 Close-up view of the flexure failure mode near mid-span of header H-14



Figure 4.73 Close-up view of the flexure failure mode between quarter point and mid-span of header H-14

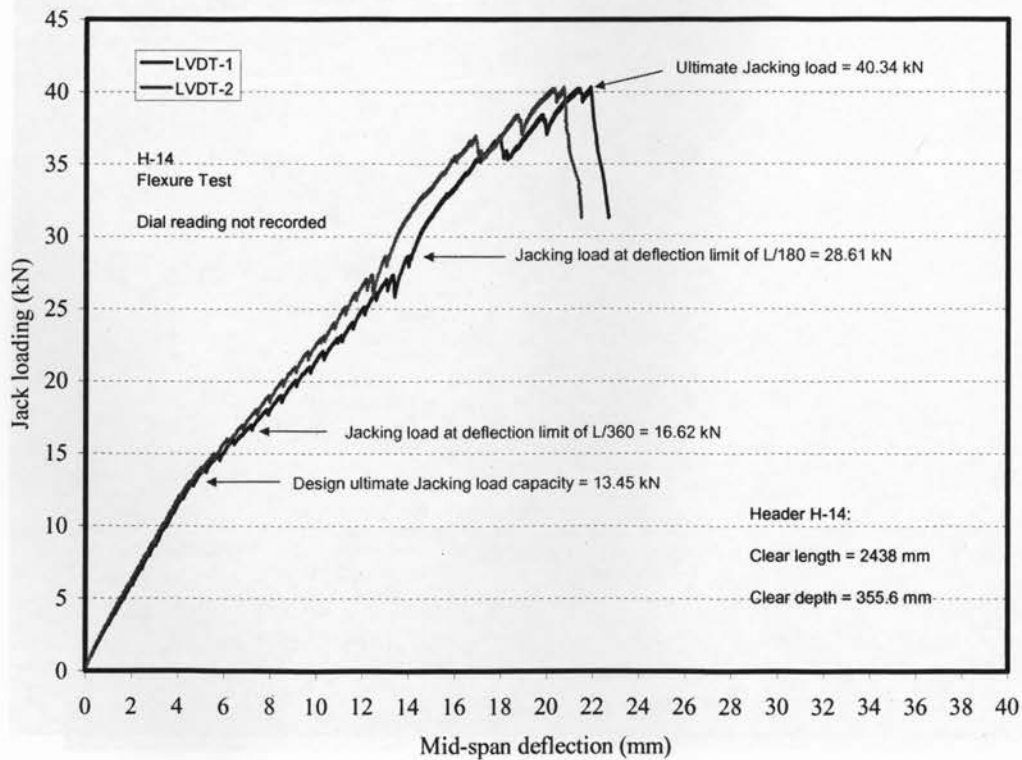


Figure 4.74 Jacking load-deflection relationship for header H-14

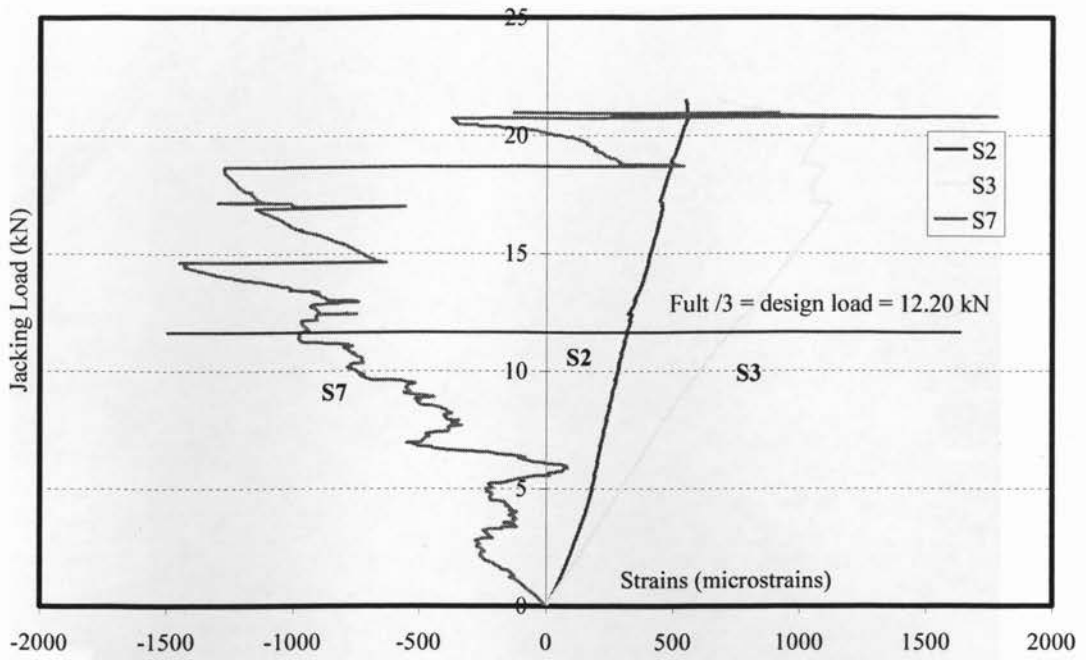


Figure 4.75 History of Jacking Load-Strain relationship for Header H-14

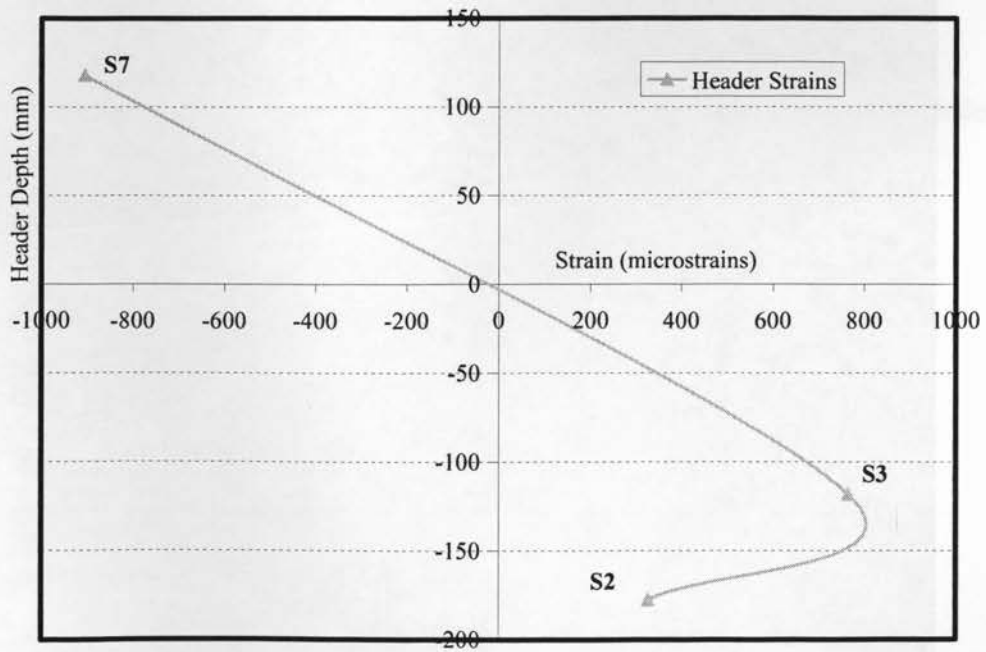


Figure 4.76 Strains across the header section for Header H-14 at $F_{ULT}/3$

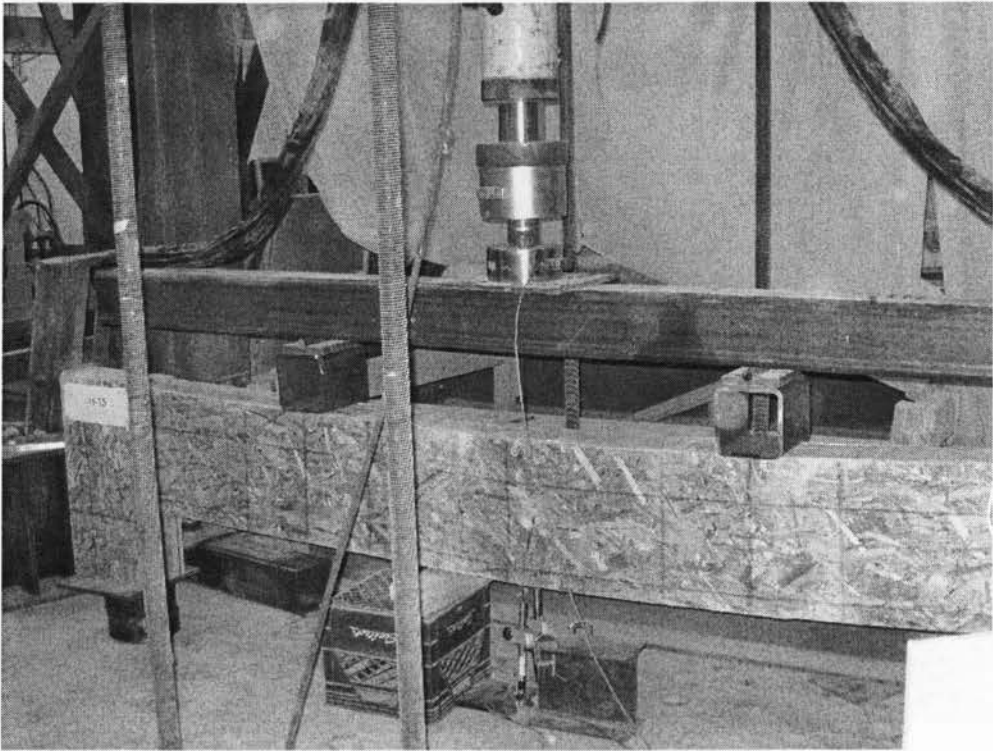


Figure 4.77 View of header H-15 after failure

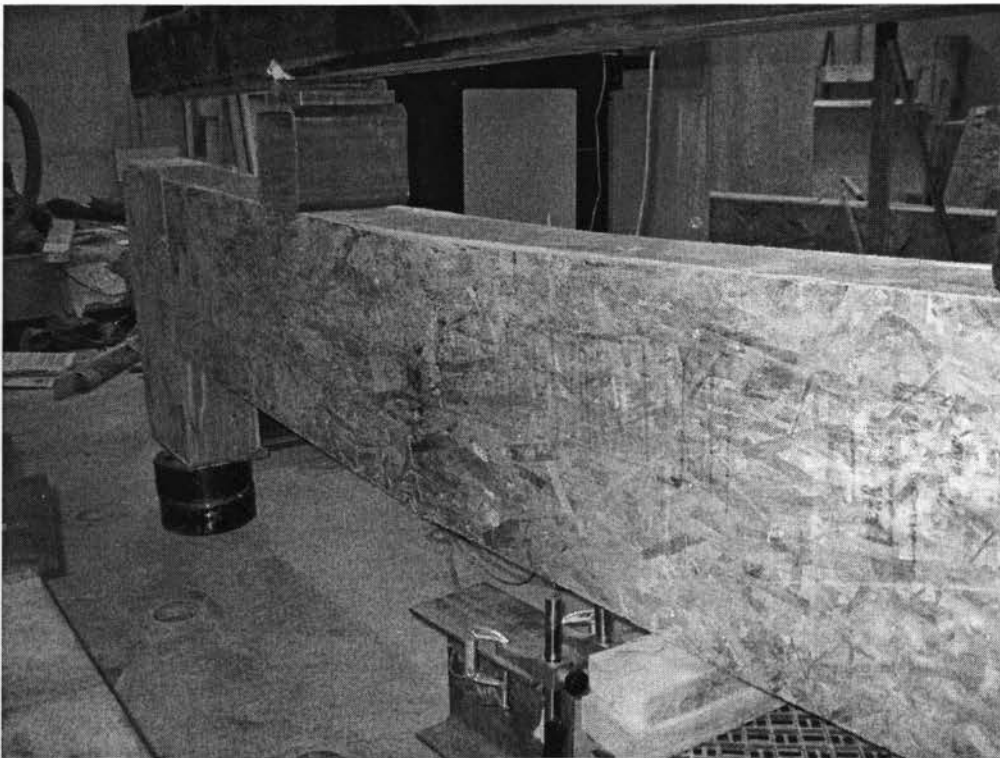


Figure 4.78 View of header H-15 showing flexure failure at mid-span



Figure 4.79 Close-up view of flexure failure mode at front side of mid-span of header H-15



(a)



(b)

Figure 4.80 Neutral axis after the flexure failure mode at back side of mid-span of header H-15



Figure 4.81 Neutral axis after the flexure failure mode of header H-15 at loading point



Figure 4.82 Close-up view of the failure mode at support of header H-15

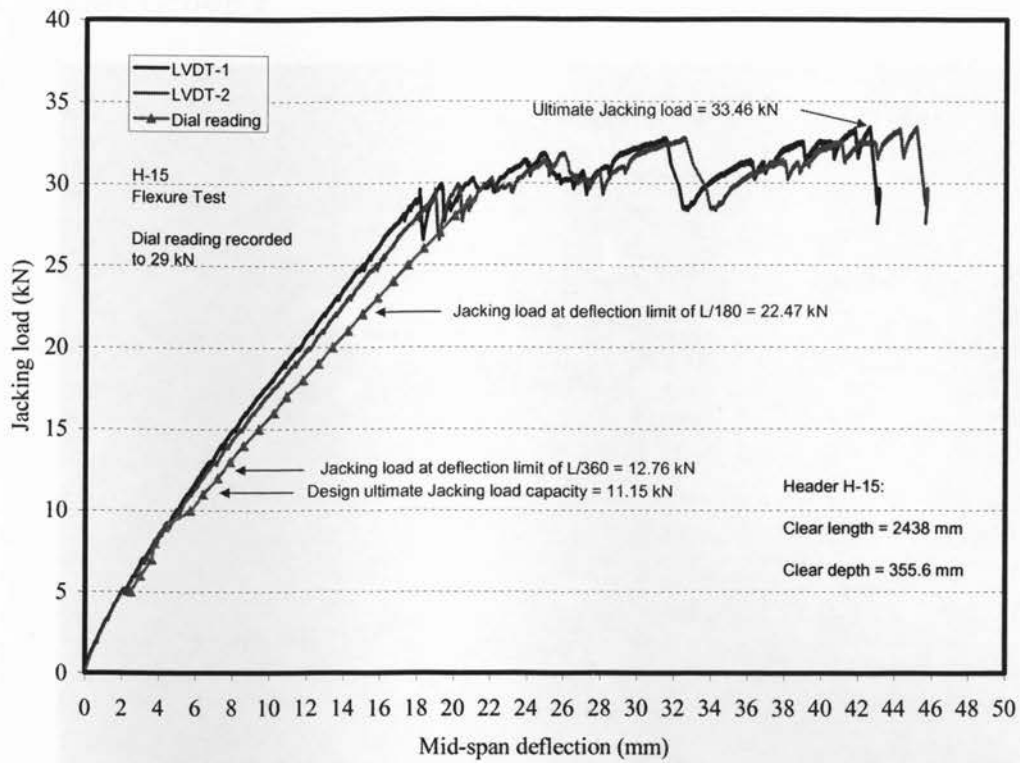


Figure 4.83 Jacking load-deflection relationship for header H-15

4.7 Panel Group F

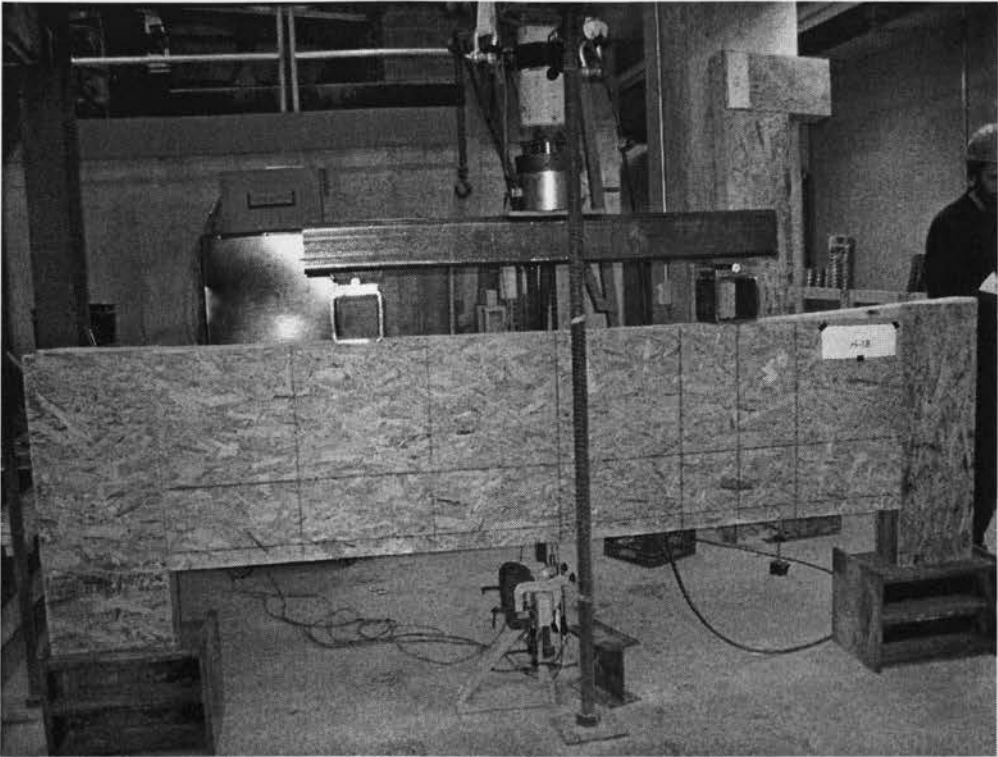


Figure 4.84 View of header H-16 after failure



(a)



(b)

Figure 4.85 Close-up views of the failure mode at supports of header H-16

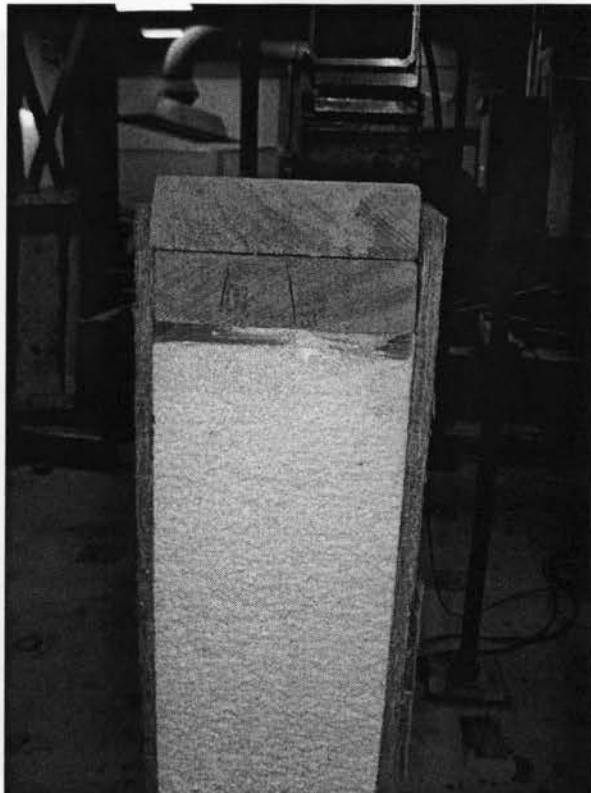


Figure 4.86 View of the foam at the location of failure of header H-16

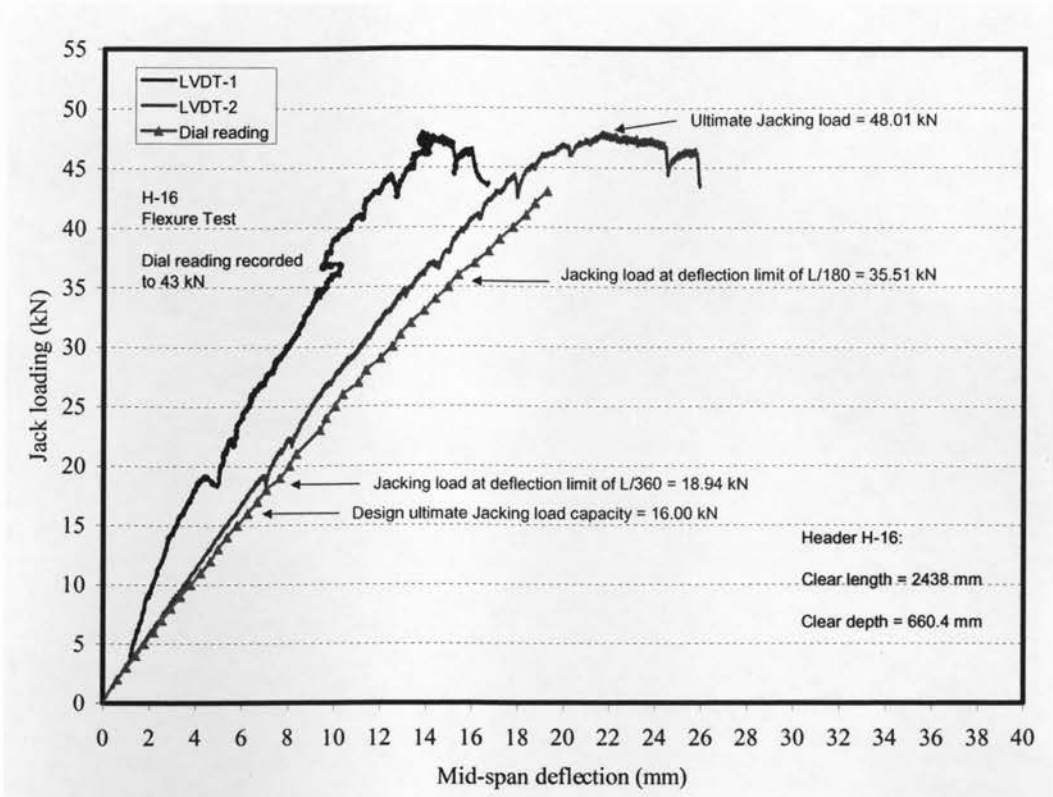


Figure 4.87 Jacking load-deflection relationship for header H-16

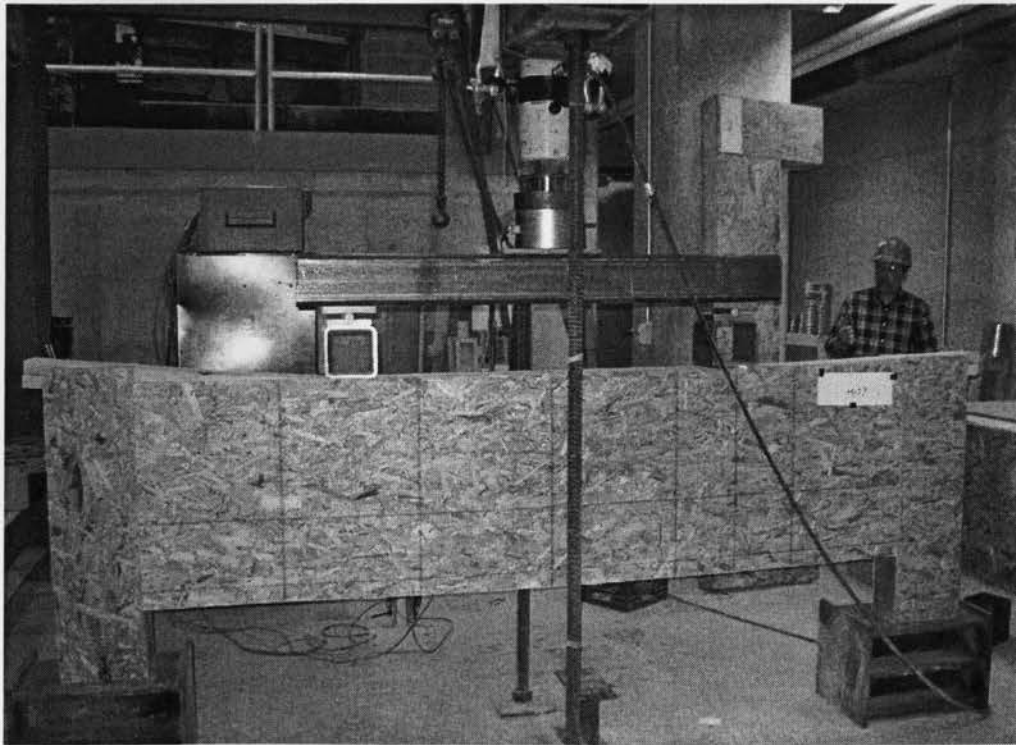


Figure 4.88 View of header H-17 after failure



(a)



Figure 4.89 Close-up views of the failure mode at right support of header H-17



Figure 4.90 Close-up view of the failure mode at left support of header H-17

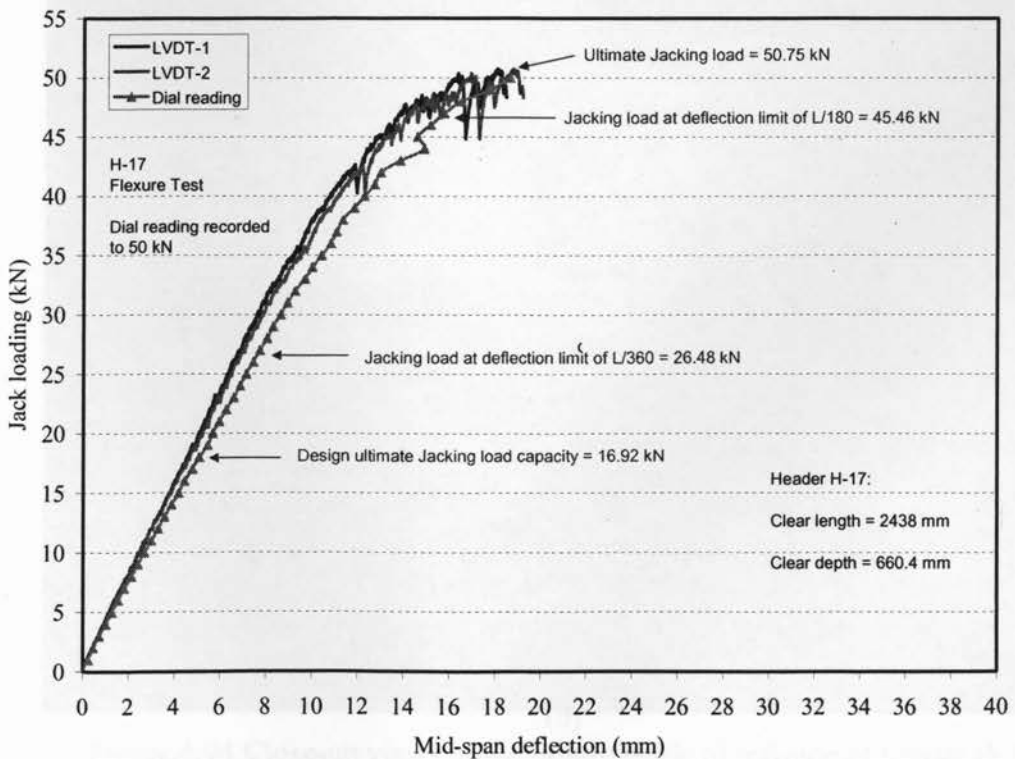


Figure 4.91 Jacking load-deflection relationship for header H-17

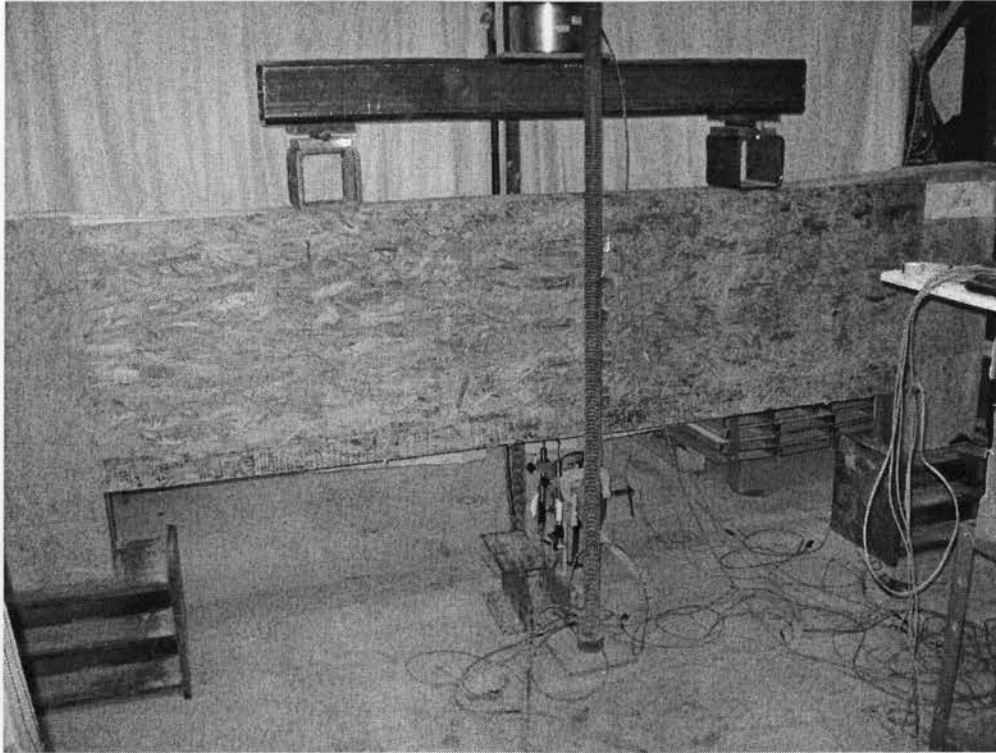


Figure 4.92 View of header H-18 after failure



Figure 4.93 Close-up view of the failure mode of header H-18



(a)



(b)

Figure 4.94 Close-up views of the failure mode of left side of header H-18

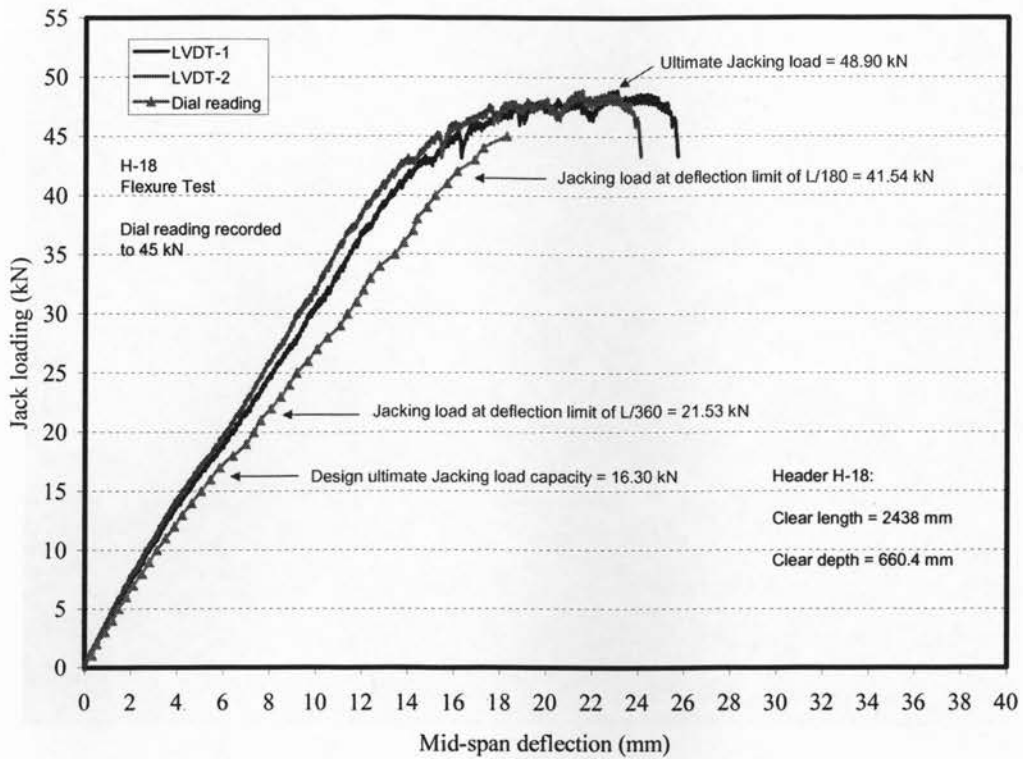


Figure 4.95 Jacking load-deflection relationship for header H-18

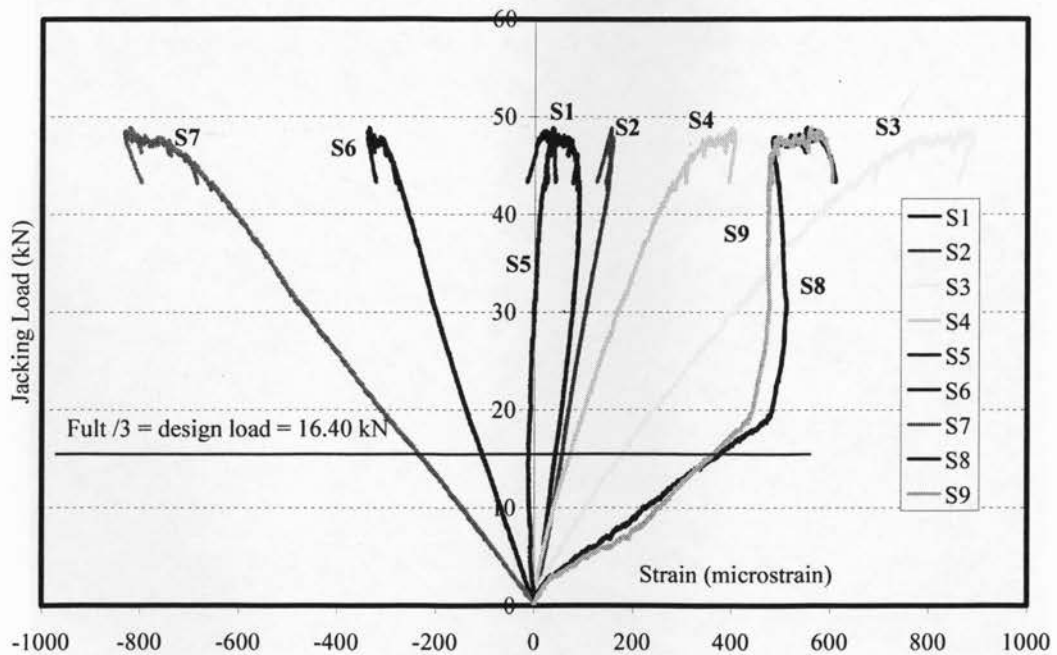


Figure 4.96 History of Jacking Load-Strain relationship for Header H-18

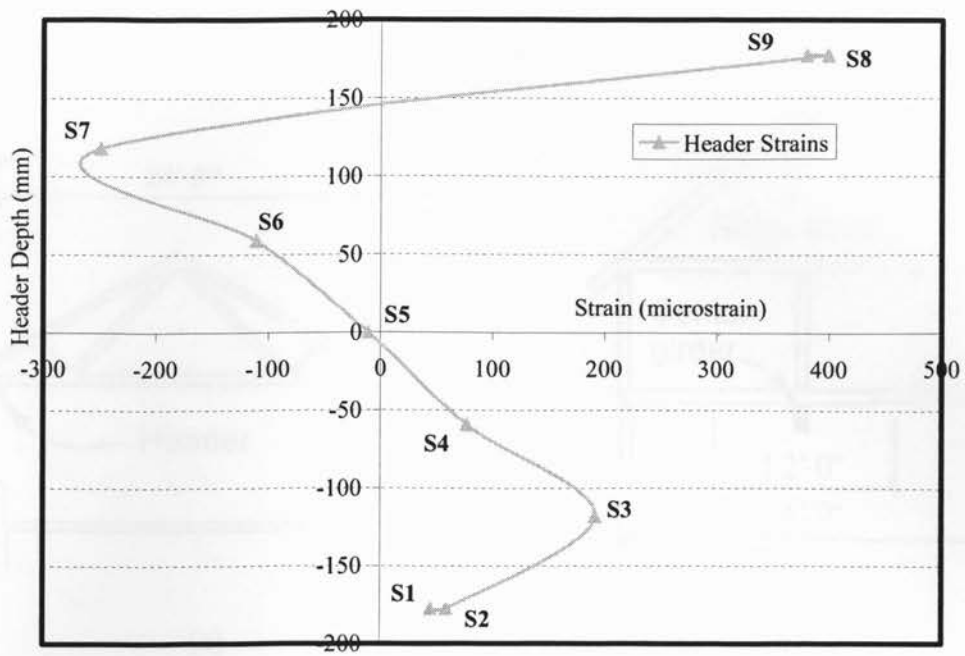


Figure 4.97 Strains across the header section for Header H-18 at $F_{ULT}/3$



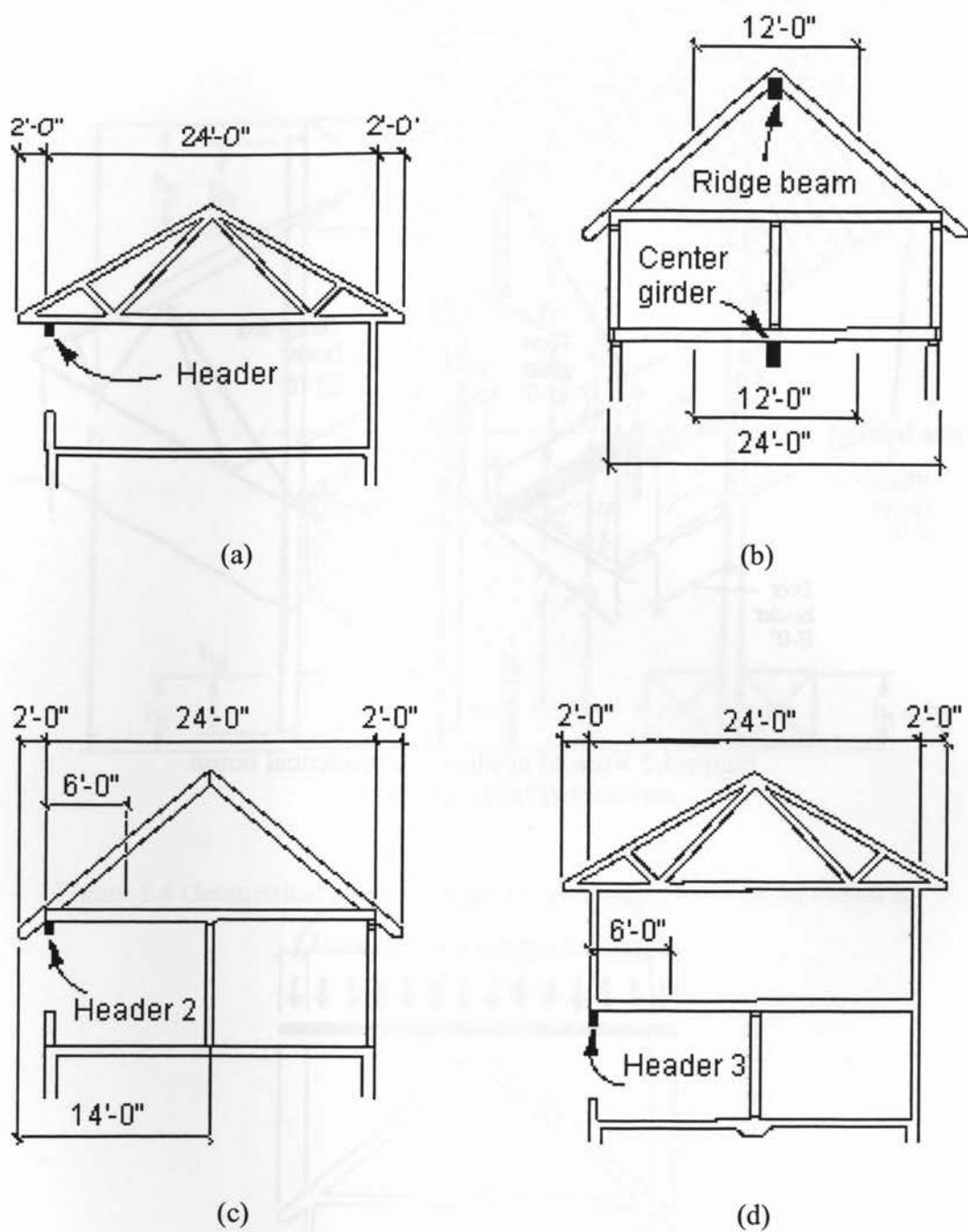


Figure 5.1 Views of headers in different locations in several house cross sections (Fisette, 2005)

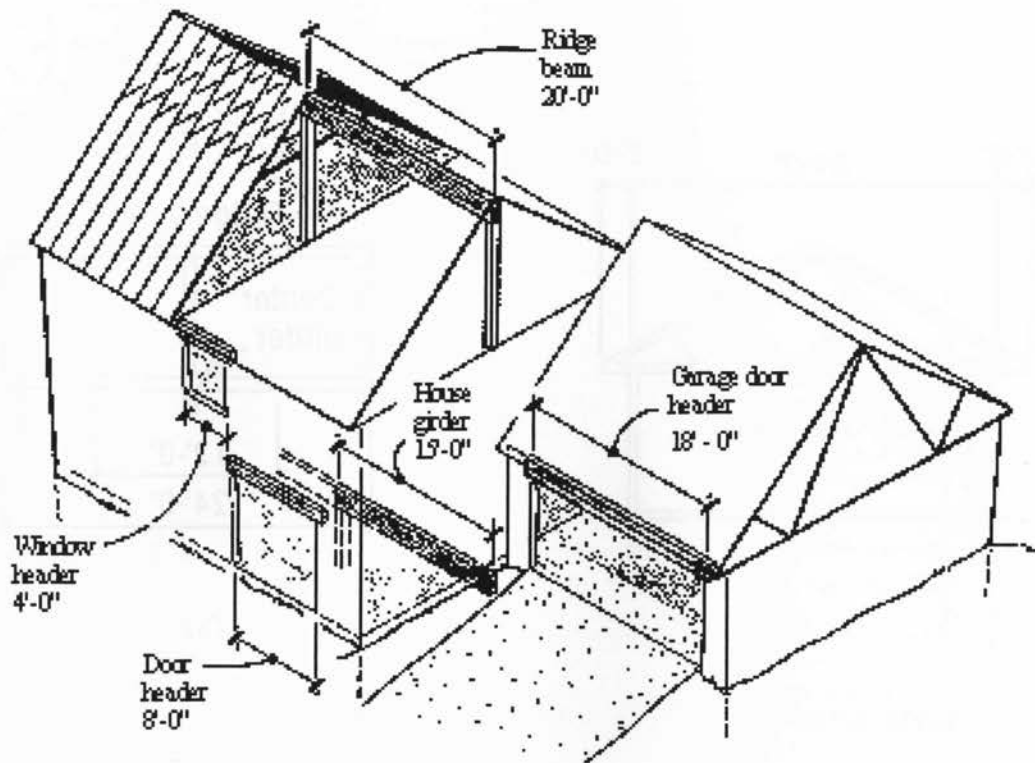


Figure 5.2 View of headers in a residential house
(Fisette, 2005)

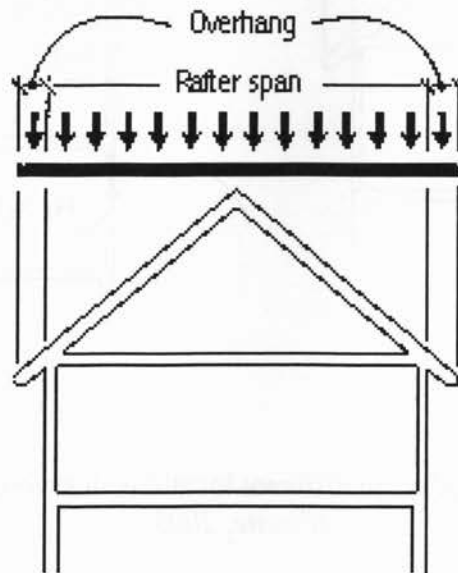


Figure 5.3 View of snow load on a roof of a residential house
(Fisette, 2005)

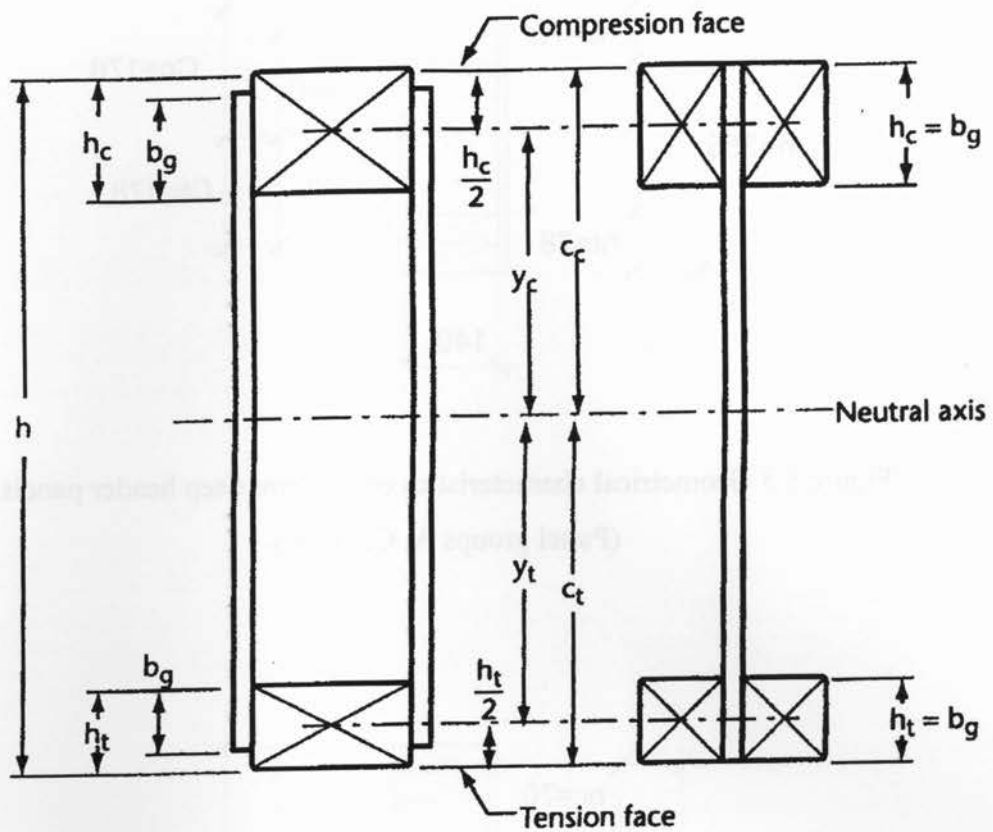


Figure 5.4 Geometrical characteristics of header panel section as shown in
 Clause 8.5 of CAN/CSA-O86-01
 (CWC, 2005)

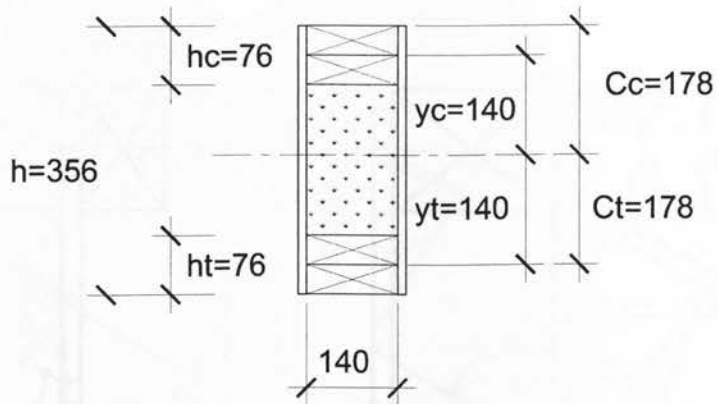


Figure 5.5 Geometrical characteristics of 356 mm deep header panels
(Panel groups A, C, and E)

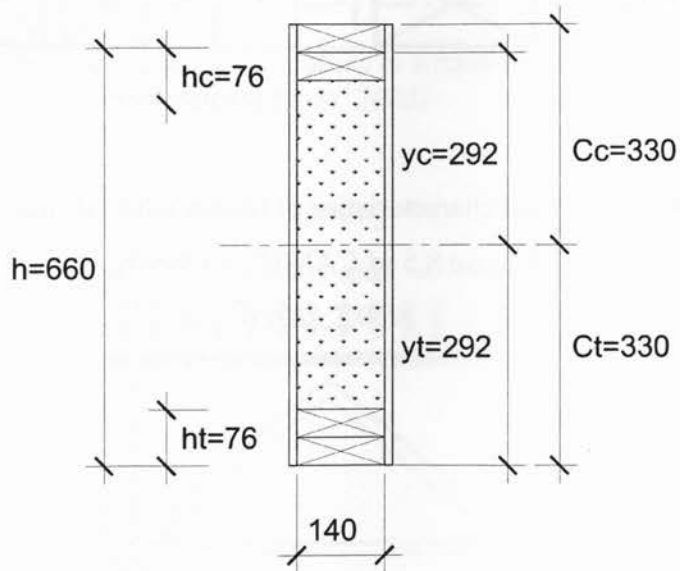


Figure 5.6 Geometrical characteristics of 660 mm deep header panels
(Panel groups B, D, and F)

Table 4.3.2.2
Load Duration Factor, K_D

Duration of loading	K_D	Explanatory notes
Short term	1.15	Short-term loading means that condition of loading where the duration of the specified loads is not expected to last more than 7 days continuously or cumulatively throughout the life of the structure. Examples include wind loads, earthquake loads, falsework, and formwork, as well as impact loads.
Standard term	1.00	Standard term means that condition of loading where the duration of specified loads exceeds that of short-term loading, but is less than permanent loading. Examples include snow loads, live loads due to occupancy, wheel loads on bridges, and dead loads in combination with all of the above.
Permanent	0.65	Permanent duration means that condition of loading under which a member is subjected to more or less continuous specified load. Examples include dead loads or dead loads plus live loads of such character that they are imposed on the member for as long a period of time as the dead loads themselves. Such loads include those usually occurring in tanks or bins containing fluids or granular material, loads on retaining walls subjected to lateral pressure such as earth, and floor loads where the specified load may be expected to be continuously applied, such as those in buildings for storage of bulk materials. Loads due to fixed machinery should be considered to be permanent.

Note: Duration of load may require professional judgment by the designer. Explanatory notes in this table provide guidance to designers about the types of loads and load combinations for which each modification factor should be applied.

Figure A1 - Table 4.3.2.2
(CWC, 2005)

Table 5.4.2
Service Condition Factors, K_S

K_S	Property	Dry service conditions	Wet service conditions: sawn lumber, piling, and poles of least dimension	
			89 mm or less	Over 89 mm
K_{Sb}	Bending at extreme fibre	1.00	0.84	1.00
K_{Sv}	Longitudinal shear	1.00	0.96	1.00
K_{Sc}	Compression parallel to grain	1.00	0.69	0.91
K_{Scp}	Compression perpendicular to grain	1.00	0.67	0.67
K_{St}	Tension parallel to grain	1.00	0.84	1.00
K_{SE}	Modulus of elasticity	1.00	0.94	1.00

Figure A2 - Table 5.4.2
(CWC, 2005)

**Table 5.4.3
Treatment Factor, K_T**

Product	Dry service conditions	Wet service conditions
Untreated lumber	1.00	1.00
Preservative-treated, unincised lumber	1.00	1.00
Preservative-treated, incised lumber of thickness 89 mm or less, for		
(a) modulus of elasticity	0.90	0.95
(b) other properties	0.75	0.85
Fire-retardant-treated lumber	<i>See Clause 5.4.3.2 for effects of fire-retardant treatment.</i>	

Figure A3 - Table 5.4.3 (CWC, 2005)

**Table 5.4.4
System Factor, K_B**

For specified strength in	Case 1*	Case 2†		
		Visually graded	MSR	Built-up beams
Bending	1.10	1.40	1.20	1.10
Longitudinal shear	1.10	1.40	1.20	1.10
Compression parallel to grain	1.10	1.10	1.10	1.00
Tension parallel to grain	1.10	N/A	N/A	1.00
All other properties	1.00	1.00	1.00	1.00

*See Clause 5.4.4.1 for conditions applying to Case 1.

†See Clause 5.4.4.2 for conditions applying to Case 2.

N/A = not applicable

Figure A4 - Table 5.4.4 (CWC, 2005)

**Table 5.4.5
Size Factor, K_Z , for Visually Stress-Graded Lumber**

Larger dimension (mm)	Bending and shear K_{Zb} K_{Zv}			Tension parallel to grain K_{Zt}	Compression perpendicular to grain K_{Zcp}	Compression parallel to grain K_{Zc}	All other properties
	Smaller dimension (mm)			All	All	All	
	38 to 64	89 to 102	114 or more				
38	1.7	—	—	1.5	<i>See Clause 5.5.7.5</i>	<i>Value computed using formula in Clause 5.5.6.2.2</i>	1.0
64	1.7	—	—	1.5			1.0
89	1.7	1.7	—	1.5			1.0
114	1.5	1.6	1.3	1.4			1.0
140	1.4	1.5	1.3	1.3			1.0
184 to 191	1.2	1.3	1.3	1.2			1.0
235 to 241	1.1	1.2	1.2	1.1			1.0
286 to 292	1.0	1.1	1.1	1.0			1.0
337 to 343	0.9	1.0	1.0	0.9			1.0
387 or larger	0.8	0.9	0.9	0.8			1.0

Figure A5 - Table 5.4.5 (CWC, 2005)

5.5.6.2.2 Factored Compressive Resistance Parallel to Grain

The factored compressive resistance parallel to grain, P_r , shall be taken as

$$P_r = \phi F_c A K_{zc} K_c$$

where

$$\phi = 0.8$$

$$F_c = f_c (K_D K_{DF} K_{SE} K_T)$$

f_c = specified strength in compression parallel to grain (Tables 5.3.1A to 5.3.1D, 5.3.2, and 5.3.3), MPa

$$K_{zc} = 6.3 (dL)^{-0.13} \leq 1.3$$

where

d = dimension in direction of buckling (depth or width), mm

L = length associated with member dimension, mm

Figure A6 - Table 5.5.6.2.2 (CWC, 2005)

Table 5.3.1C
Specified Strengths and Modulus of Elasticity
for Beam and Stringer Grades (MPa)

Species identification	Grade	Compression					Modulus of elasticity	
		Bending at extreme fibre,* f_b	Longitudinal shear, f_v	Parallel to grain, f_c	Perpendicular to grain, f_{cp}	Tension parallel to grain, f_t	E	E_{OS}
D Fir-L	SS	19.5		13.2		10.0	12 000	8 000
	No. 1	15.8	1.5	11.0	7.0	7.0	12 000	8 000
	No. 2	9.0		7.2		3.3	9 500	6 000
Hem-Fir	SS	14.5		10.8		7.4	10 000	7 000
	No. 1	11.7	1.2	9.0	4.6	5.2	10 000	7 000
	No. 2	6.7		5.9		2.4	8 000	5 500
S-P-F	SS	13.6		9.5		7.0	8 500	6 000
	No. 1	11.0	1.2	7.9	5.3	4.9	8 500	6 000
	No. 2	6.3		5.2		2.3	6 500	4 500
Northern	SS	12.8		7.2		6.5	8 000	5 500
	No. 1	10.8	1.0	6.0	3.5	4.6	8 000	5 500
	No. 2	5.9		3.9		2.2	6 000	4 000

* Specified strengths for beams and stringers are based on loads applied to the narrow face. When beams and stringers are subject to loads applied to the wide face, the specified strength for bending at the extreme fibre and the specified modulus of elasticity shall be multiplied by the following factors:

	f_b	E or E_{OS}
Select Structural	0.88	1.00
No. 1 or No. 2	0.77	0.90

Notes:

- (1) Beams and stringers have a smaller dimension of at least 114 mm, with a larger dimension more than 51 mm greater than the smaller dimension.
- (2) An approximate value for modulus of rigidity may be estimated at 0.065 times the modulus of elasticity.
- (3) With sawn members thicker than 89 mm that season slowly, care should be exercised to avoid overloading in compression before appreciable seasoning of the outer fibre has taken place; otherwise, compression strengths for wet service conditions shall be used.
- (4) Beam and stringer grades listed in this table are not graded for continuity (see Clause 5.5.3).
- (5) Tabulated values are based on the following standard conditions:
 - (a) 343 mm larger dimension for bending and shear, 292 mm larger dimension for tension and compression parallel to grain;
 - (b) dry service conditions; and
 - (c) standard-term duration of load.

Figure A7 - Table 5.3.1C (CWC, 2005)

Table 7.3C
Specified Strength, Stiffness, and Rigidity Capacities
for Type 1 (Standard) Design-Rated OSB*

Nominal thickness, mm	Rating grade	Planar shear								
		Bending, m_{ps} N•mm/mm		Axial tension, t_{ps} N/mm		Axial compression, p_{ps} N/mm		Shear-through-thickness, v_{ps} N/mm	Bending, v_{ps} N/mm	Shear in-plane, v_{sp} MPa
		Capacities relative to major axis*†								
		0°	90°	0°	90°	0°	90°	0° & 90°	0° & 90°	0° & 90°
9.5	A	290	90	79	38	79	38	30	4.1	0.64
9.5	B	240	90	63	38	63	38	30	4.1	0.64
9.5	C	190	90	47	38	47	38	30	4.1	0.64
11.0	A	390	120	91	44	91	44	35	4.7	0.64
11.0	B	320	120	73	44	73	44	35	4.7	0.64
11.0	C	260	120	55	44	55	44	35	4.7	0.64
12.5	A	500	160	100	50	100	50	40	5.3	0.64
12.5	B	420	160	83	50	83	50	40	5.3	0.64
12.5	C	330	160	62	50	62	50	40	5.3	0.64
15.5	A	770	240	130	62	130	62	50	6.6	0.64
15.5	B	640	240	100	62	100	62	50	6.6	0.64
15.5	C	510	240	77	62	77	62	50	6.6	0.64
18.5	A	1100	340	150	74	150	74	59	7.9	0.64
18.5	B	910	340	120	74	120	74	59	7.9	0.64
18.5	C	720	340	92	74	92	74	59	7.9	0.64
22.0	A	1600	480	180	88	180	88	70	9.4	0.64
22.0	B	1300	480	150	88	150	88	70	9.4	0.64
22.0	C	1000	480	110	88	110	88	70	9.4	0.64
28.5	A	2600	810	240	110	240	110	91	12.0	0.64
28.5	B	2200	810	190	110	190	110	91	12.0	0.64
28.5	C	1700	810	140	110	140	110	91	12.0	0.64

(Continued)

Figure A8 - Table 7.3C
(CWC, 2005)

Table 7.3C (Concluded)

Nominal thickness, mm	Rating grade	Bending stiffness, $B_y = EI_x$, N•mm ² /mm		Axial stiffness (in tension or compression), $B_x = EA$, N/mm		Shear-through-thickness rigidity, B_w , N/mm
		Capacities relative to major axis*†				
		0°	90°	0°	90°	0° & 90°
9.5	A	590 000	170 000	46 000	19 000	9 500
9.5	B	490 000	170 000	39 000	19 000	9 500
9.5	C	390 000	170 000	33 000	19 000	9 500
11.0	A	920 000	270 000	53 000	22 000	11 000
11.0	B	760 000	270 000	46 000	22 000	11 000
11.0	C	610 000	270 000	38 000	22 000	11 000
12.5	A	1 300 000	390 000	60 000	25 000	12 000
12.5	B	1 100 000	390 000	52 000	25 000	12 000
12.5	C	900 000	390 000	43 000	25 000	12 000
15.5	A	2 600 000	740 000	75 000	31 000	15 000
15.5	B	2 100 000	740 000	64 000	31 000	15 000
15.5	C	1 700 000	740 000	53 000	31 000	15 000
18.5	A	4 400 000	1 300 000	89 000	37 000	18 000
18.5	B	3 600 000	1 300 000	77 000	37 000	18 000
18.5	C	2 900 000	1 300 000	64 000	37 000	18 000
22.0	A	7 300 000	2 100 000	110 000	44 000	22 000
22.0	B	6 100 000	2 100 000	91 000	44 000	22 000
22.0	C	4 900 000	2 100 000	76 000	44 000	22 000
28.5	A	16 000 000	4 600 000	140 000	57 000	28 000
28.5	B	13 000 000	4 600 000	120 000	57 000	28 000
28.5	C	11 000 000	4 600 000	98 000	57 000	28 000

*For Type 2 Design-Rated OSB panels, tabulated specified capacities are increased by a percentage (see CSA Standard O452.0). For Type 3 Design-Rated OSB panels, specified capacities are proprietary (see Clause 13.3).

†Orientation of applied force relative to panel's long direction.

Notes:

- (1) For specified stiffness in bending on edge, use axial stiffness values.
- (2) Tabulated values are based on dry service conditions and standard-term duration of load.
- (3) Specified strength in bearing (normal to plane of panel) $q_p = 4.2$ MPa.

Figure A9 - Table 7.3C (Concluded)
(CWC, 2005)

**Table 7.4.4.1
Stress Joint Factor, X_j , for Scarf Joints**

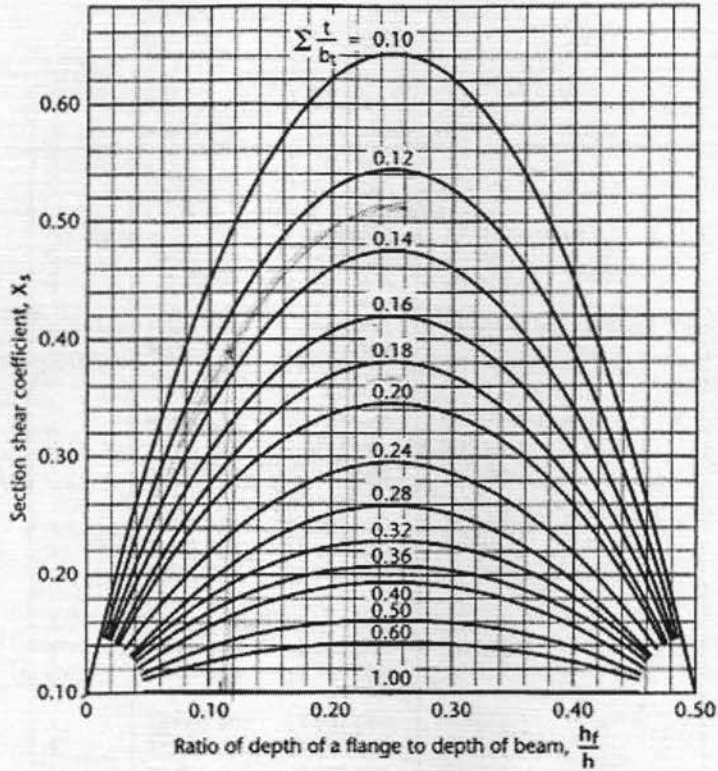
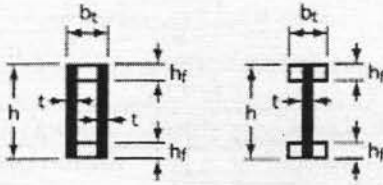
Panel type	Slope of scarf	Tension, bending	Compression	Shear
Plywood	1 in 12	0.85	1.00	1.00
	1 in 10	0.80	1.00	1.00
	1 in 8	0.75	1.00	1.00
	1 in 5	0.60	1.00	—
OSB	1 in 6	0.80	0.80	0.80
	1 in 5	0.70	0.70	0.70
	1 in 4	0.60	0.60	0.60

Figure A10 - Table 7.4.4.1
(CWC, 2005)

8.4.3.1 Scarf Joints in Shear

The slope of plywood scarf joints shall be not steeper than 1:8. The slope of OSB scarf joints shall not be steeper than 1:4.

Figure A11 - Table 8.4.3.1
(CWC, 2005)



Note:

The section shear coefficient is a geometrical property of a beam section that depends on the shape of the cross-section and arises because of nonuniform distribution of shearing stresses across the section. It can be derived using fundamental engineering theory and evaluated for any beam geometry from the formula.

$$X_s = \frac{1}{I h^2} \int_{y=0}^{y=h} \frac{Q^2 dy}{b_x}$$

where

X_s = section shear coefficient

I = moment of inertia (mm^4)

h = overall beam depth (mm)

Q = first moment of beam (mm^3)

b_x = width of beam carrying the shear associated with Q (mm)

This figure is valid only for box and I-beams symmetrical about 2 axes.

Figure 8.5.6
Section Shear Coefficient, X_s

Figure A12 – Figure 8.5.6
(CWC, 2005)

BC-31-47